CRANK ANGLE AND SPACE RESOLVED, SPECIATED SAMPLING OF ENGINE-OUT EXHAUST HYDROCARBONS

by

David J. Kayes

Bachelor of Science in Mechanical Engineering
University of California at Berkeley
(1994)

Submitted to the Department of Mechanical Engineering
in partial fulfillment of the requirements
for the Degree of

MASTER OF SCIENCE IN MECHANICAL ENGINEERING

at the

MASSACHUSETTS INSTITUTE OF TECHNOLOGY

May 1996

Signature of Author:_____
Department of Mechanical Engineering
May 10, 1996

Certified by:_____
Simone Hochgreb
Associate Professor, Department of Mechanical Engineering
Thesis Supervisor

Accepted by:_____
Ain A. Sonin
Chairman, Departmental Graduate Committee

CRANK ANGLE AND SPACE RESOLVED, SPECIATED SAMPLING OF ENGINE-OUT EXHAUST HYDROCARBONS

by

David J. Kayes

Submitted to the Department of Mechanical Engineering on May 10, 1996,
in partial fulfillment of the requirements for the Degree of Master of Science
in Mechanical Engineering

ABSTRACT

In order to understand how unburned hydrocarbons emerge from SI engines and, in particular, how non-fuel hydrocarbons are formed and oxidized, a new gas sampling technique has been developed. A sampling unit, based on a combination of techniques used in the Fast Flame Ionization Detector (FFID) and wall-mounted sampling valves, was designed and built to capture a sample of exhaust gas during a specific period of the exhaust process and from a specific location within the exhaust port. The sampling unit consists of a transfer tube with one end at a specifiable location in the port and the other connected to a three-way valve that leads, on one side, to a FFID and, on the other, to a vacuum chamber with a high-speed solenoid valve. Exhaust gas, drawn by the pressure drop into the vacuum chamber, impinges on the face of the solenoid valve and flows radially outward. Once per cycle during a specified crank angle interval, the valve opens and traps exhaust gas in a storage unit, from which gas chromatography (GC) measurements are made. The solenoid valve's actuation time can be adjusted to allow resolution of a crank angle interval as small as 15°CA.

Total HC concentrations measured by the FFID by the sampling unit are in good agreement, while the sampling unit goes one step further than the FFID by providing species concentrations. Spatial resolution of the exhaust port reveals that individual plugs of gas are well mixed; that is, there are not significant concentration gradients across the radius of the port. Moreover, spatial resolution reveals that significant oxidation occurs as the flow progresses along the length of the port. Specifically, 36 to 50% of the total HCs are oxidized in transit through the port, while non-fuel HC concentrations drop only 17 to 23% indicating significant amounts of partial oxidation. Crank angle resolution of speciated concentration trends shows that, as the exhaust process progresses, the ratio of non-fuel HC mass to fuel mass in the exhaust increases, which is consistent with increased quenching of oxidation reactions due to rapidly decreasing temperatures. Comparison with previous research suggests that the new sampling unit is fully capable of providing species concentration information as a function of engine speed, load, and air-fuel ratio at specific crank angles or on a mass weighted basis.

Thesis Advisor: Professor Simone Hochgreb
Associate Professor of Mechanical Engineering

ACKNOWLEDGMENTS

All too often, I forget to tell the people around me just how thankful I am for their help. And there is no denying that without that help, I would not be where I am today. I would like to use this medium to thank all of the people that helped me during my term as a master's student, but I realize that, no matter how hard I try, I will forget someone upon whom I rely heavily. If that is you, forgiving reader, I most heartily apologize.

I cannot say enough about the help I got from Professor Simone Hochgreb, without whom I could never have finished this project. I am grateful for our discussions, which always forced me to delve deeper into my results and to look at my research from a different perspective. I would also like to thank Professors Heywood, Cheng, and Keck for setting examples of academic excellence and for complementing the instruction of Professor Hochgreb.

If a successful professor is one whose work is cited in the references of numerous papers, then a successful student is one whose work is cited in the acknowledgments of numerous theses. I expect to see the following students cited frequently for their scholarly work, which often goes beyond the call of duty, sometimes even up until the last call: Bob Murry, Ted Trautman, Doug Whittington, Paige Mahaney, Greg Wakeham, and the rest of the chemists. In addition, I would like to thank all of the students, faculty, and staff of the Sloan Auto Lab, for each brings something different — different experiences, different perspectives, etc. — to the lab's collective intellect and consequently deserves my thanks. In particular, I would like to thank Mike Norris for his expert tutelage, Robert "Bobby Bondgraph" Meyer for many helpful discussions in preparation for the qualifiers, Jon Fox for unsurpassed practical knowledge, Pete Hinze whose love of the lambada (the forbidden dance) is only surpassed by his mastery of it, Brad Van Der Wege and Chris O'Brien for shedding a different light on the many problems we've worked on (although we'll all agree that, whenever there is a difference of opinion, it is I who is right), Younggy Shin and Kuo-Chiang Chen for invaluable help building and running the engine, Brian Corkum who has my undying gratitude, because without him I would still in the lab wondering why I cannot pound nails with a drill press and why I cannot drill holes with a hammer, and Nancy Cook upon whose able shoulders rests the entire lab and all of its occupants.

Of course, I would also like to thank my family who probably deserves the most of my thanks and, I am sorry to say, gets the least of it.

This work was funded by the National Science foundation and by the DOE/OTT. Invaluable help was lent by Jan Roger Linna and Dr. Nisbet at Volvo Corporation and by the industrial members of the Sloan Laboratory's Engine-Fuels Interactions Consortium.

David Kayes
3 May 1996

TABLE OF CONTENTS

LIST OF TABLES

LIST OF FIGURES

CHAPTER 1

INTRODUCTION

1.1 Motivation

Environmental and health concerns over the smog forming and toxic nature of certain hydrocarbons (HCs) have led to stringent regulations to control HC emissions from automobiles. Airborne HCs combine with nitrogen oxides to form ozone and, thus, lead to smog [1]. Not only does smog limit visibility and affect climatic changes (through increased fog formation and reduced solar radiation), but it also has deleterious effects on the human body. Although the effects of smog on the human body are not completely understood, it is believed that smog can lead to pulmonary difficulties and eye irritation [1]. Specifically, some of the non-fuel HCs (intermediate combustion products, or simply intermediates) formed during the combustion process have been found to be toxic*. In 1989, the EPA estimated that cancer caused by toxic air pollutants may result in 1500 to 3000 deaths per year in the United States, and that more than half of these cancers are caused by motor vehicle emissions [2]. In particular, benzene, one of the intermediates formed in gasoline combustion, has been linked to leukemia and cancer in humans [1], [3]. Consequently, it is imperative that reductions be made not only in the total amount of HCs emitted by automobiles, but also in the specific species emitted.

As a result of HCs' harmful effects, legislators are drastically reducing the amount of emissions permissible to vehicles. Specifically, California requires that a significant fraction of new cars meet the Ultra Low Emission Vehicle (ULEV) standard of 0.06 grams HC per mile [4], which calls for tremendous reduction over the 0.41 grams per mile permissible under the Clean Air Act Ammendment of 1990. Although a significant amount of the HC removal from automobiles' exhaust is achieved in the catalytic converter, limitations on the catalyst's performance (particularly at low temperatures encountered during cold starts) force researchers and engine designers to look to the engine itself for further improvement.

* Benzene, 1,3 butadiene, formaldehyde, and acetaldehyde are toxins as defined by the US EPA.

However, despite decades of HC emissions study, processes leading to engine-out emissions of unburned HCs and the formation of non-fuel HCs are still poorly understood [5].

In looking to the engine for HC emissions reductions, researchers must understand the pathways by which fuel HCs escape the combustion process and leave the engine unoxidized. Also, they must understand the processes by which fuel HCs are converted to the non-fuel HCs that subsequently leave the engine unoxidized. Methods by which researchers study these topics are varied: for example, the Fast Flame Ionization Detector (FFID) is used to measure the total HC concentration versus crank angle (CA) at various locations in the cylinder and exhaust manifold, and sampling valves are used to trap gas near the wall of the cylinder or exhaust manifold for speciation — measurement of each HC species concentration — via gas chromatography (GC). In order to give some background into and motivation for the author's experiment, these devices will be discussed.

1.2 Concentration Measurement Techniques

The two techniques most frequently used to resolve HC concentrations in the exhaust port as a function of CA are the FFID and wall-mounted sampling valves, notwithstanding inherent limitations of each. The FFID probe is able to spatially resolve total HC concentrations, and usual wall-mounted sampling valves can provide samples for speciated measurements, but neither technique can provide spatially resolved, speciated measurements as a function of crank angle degree (CAD) throughout the cycle. The FFID takes a stream of gas from an arbitrary location within the cylinder or port and, via a hydrogen flame and an ionization detector, supplies a signal proportional to the concentration of HC-bonded carbon atoms. The FFID signal however does not supply any information about the specific HC compounds sampled. On the other hand, wall-mounted sampling valves, which can be used to trap samples for speciation via gas chromatography, are constrained in the locations from which they can sample. Hence, spatial distributions of various HC species cannot be determined with such a method. Consequently, questions remain concerning the origin, stratification, transport, and oxidation of fuel and non-fuel HCs during the exhaust process. In order to answer some of these questions, a sampling unit was

designed to allow the time and space resolution of a FFID as well as the capability to store sampled gas for speciated measurements. This sampling unit will be discussed in detail in upcoming chapters.

1.3 HC Emissions from Engines

This section will give background into pertinent conclusions about HC emissions from engines reached in previous research: mechanisms by which HCs escape combustion, post-flame oxidation of those unburned HCs, cyclically-resolved exhaust port HC concentrations, speciated exhaust port concentrations, and effects of engine operating conditions on engine-out HC emissions.

1.3.1 Sources of Unburned HCs

The initial flame passage through the combustion chamber oxidizes approximately 90% of the HCs in the charge; the rest escapes oxidation in the flame through one of the following mechanisms. About 5% of the inducted fuel is packed into crevices too small for the flame to penetrate and is released after flame passage, when the cylinder pressure decreases [5]. The aforementioned crevices include those in the cylinder head (gaps in the spark plug thread, valves, and head gasket) and the topland crevice (the space above the top piston ring, between the piston and the cylinder wall). About 0.5% of the inducted fuel, which sits in a thin "quench layer" near the combustion chamber walls, escapes oxidation because the walls' relatively low temperature quench the flame before it can reach this layer [5]. Also, imperfect sealing between the exhaust valve(s) and seat(s) allows about 0.1% of the inducted HCs to be blown directly out of the cylinder when the pressure increases [5]. Up to 2% of the inducted charge (for gaseous fuels, this amount is significantly smaller) is absorbed into the oil layer and combustion chamber deposits during the compression stroke and released after flame passage as the pressure drops during the power stroke, thereby avoiding contact with the flame [5], [6], [7]. Lastly, about 1.2% of the liquid fuel (in steady state, mid-speed, mid-load operation) stays in liquid phase either by incompletely atomizing or by puddling on combustion chamber walls and escapes oxidation because of the flame's inability to completely burn liquid fuel [5].

1.3.2 Post-flame Oxidation

About half of the fuel escaping combustion through one of the above means is oxidized upon mixing with hot bulk gases [5]. Of the other half, about two-thirds is swept into the exhaust system (the other one-third remains in the cylinder's residual gas) and, of those HCs, about one-third to one-half is oxidized in the exhaust system prior to reaching the catalyst [5], [8]. Because oxidation rates are faster at higher temperatures, and because exhaust gas cools in transit through the exhaust system, port/runner HC oxidation is most rapid closest to the exhaust valve [9], [10]. The amount of HC oxidation in the port is increased most by optimizing engine operating conditions to increase exhaust gas temperature, port residence time, and exhaust oxygen concentration [9], [10].

1.3.3 Crank Angle Resolved HC Concentrations in the Port

Many researchers have used the FFID to observe CA-resolved trends in the port's total HC concentration in order to elucidate the pathways by which HCs escape the engine [7], [11], [12], [13]. The total HC concentrations observed in the exhaust port during the cycle and the pathways leading to those trends can be explained as follows. The beginning of the cycle finds the exhaust valve closing and a somewhat stagnant plug of gas trapped in the exhaust port, where it remains throughout the cycle until the exhaust valve opens and blowdown gas displaces it further along the exhaust runner [11]. Consequently, the total HC concentration measured by the FFID is relatively constant between the time that the exhaust valve closes in one cycle and the time that it opens in the next cycle (see figures 1.1 and 1.2). Blowdown gas contains quenched HCs from cylinder head quench layers and crevices and, hence, sometimes contains a higher HC concentration than the gas previously in the port, resulting in a small peak in HC concentration measured by the FFID at certain locations [11], [14]. After blowdown and through most of the exhaust process, burned gases, containing a low concentration of HCs, emerge from the cylinder. Therefore, the HC concentration observed by the FFID in the port is relatively low throughout most of the exhaust process. Under some engine operating conditions, a small peak in HC concentration occurs during the time in which the aforementioned burned gases escape the cylinder (as can be seen in figure

1.2). This peak is suspected to be either due to a flow reversal during which a plug of gas moves back and forth in the vicinity of the FFID sampling location [11] or due to the entrainment of a portion of the piston crevice HCs by bulk exhaust gas flow [7]. Toward the end of the exhaust process, HC-rich gases are scraped from wall quench layers, released from the piston topland crevice, and rolled into a vortex, which subsequently escapes the cylinder. Hence, just before the exhaust valve closes, the port HC concentration measured by the FFID increases [11]. Note that specific HC concentration trends become less resolveable as the sampling point is moved further from the exhaust valve due to mixing in the port [11].

Prior to the work that will be presented in this paper, it was hypothesized that the rolled-up vortex would more likely contain partial oxidation products than would the gases released from quench layers and crevices in the cylinder head and gasket; the rationale is as follows. The temperature of the environment into which quench layer and head crevice HCs are released is quite high (on the order of 2500 to 3000 K) [15], since the quench layer and crevice gases mix with bulk gases relatively early in the exhaust process. Hence, these gases should be oxidized rather completely. On the other hand, the temperature of the environment into which topland crevice gases are released is rather low and rapidly dropping, since these gases are released late in the expansion stroke. Plus, the HCs rolled into the vortex undergo only partial mixing with the hotter bulk gases. Thus, only a portion of the topland crevice HCs experience high temperatures and, then, only for a short time since the pressure and temperature are dropping; so the probability for incomplete oxidation should be relatively high. Although speciated measurements of exhaust gas have been made, this hypothesis has not been supported by firm evidence, due to limitations inherent in the use of the FFID and wall-mounted sampling valves to measure HC concentrations, as discussed in section 1.2.

1.3.4 Speciated HC Concentrations in the Port and Cylinder

Researchers have used wall-mounted sampling valves to examine the trends in species concentrations as a function of CAD at various locations in the engine. When firing the engine on propane fuel and sampling gas from the exhaust port, LoRusso *et al.* sampled propane, ethene, propene, ethyne, and methane (the former being most abundant, the latter least) [16]. Brown and Woods ran an

experiment using a rapid acting sampling valve to analyze the cyclically resolved species concentrations at various locations in the cylinder and exhaust port of an engine firing on propane during its warm-up period [17]. Although results of Brown and Woods' warm-up experiments are not directly comparable to results of the author's steady-state experiments, Brown and Woods' results do reveal some interesting features of crank angle resolved, speciated HC concentrations. At all times during the cycle, the fuel species made up 50 to 80% of the total HCs sampled from the exhaust port. Further, the non-fuel species made up the largest portion of the total HCs during the middle of the exhaust process, when the bulk gases escape from the cylinder.

1.3.5 Effect of Engine Operating Conditions on Engine-Out HCs

Engine operating conditions most strongly affect engine-out HC concentrations by affecting gas temperatures, the availability of oxygen, and residence times in the cylinder and port. In addition, the fuel species or blend can strongly affect HC emissions by virtue of various characteristics such as the fuel's absorptivity in the oil layer, the fuel's flame temperature, and the stoichiometric concentration of fuel in the unburned charge. This section summarizes the results of past research regarding the effect of certain engine operating conditions — speed, load, air-fuel ratio, and fuel type — on engine-out HC concentrations, both on cycle averaged and crank angle resolved bases.

Speed theoretically affects HC concentration in the following manner. Increased speed results in shorter residence time within the engine, and thus, results in a shorter time for heat transfer from gas to engine surfaces, ultimately resulting in higher gas temperatures. Because the amount of HCs oxidized decreases approximately linearly with residence time but increases exponentially with temperature, increased speed increases HC oxidation, thereby lowering HC concentrations. Studies of cycle averaged HC measurements, such as those by Thompson and Wallace, Drobot, and Kaiser *et al.*, have demonstrated this trend [7], [18], [19]. Moreover, the crank angle resolved trend tends to match the cycle averaged trend; at low speeds, lower rates of in-cylinder oxidation due to lower temperatures produce higher HC concentrations at almost all CAs [7]. In particular, peaks at exhaust valve open (EVO) and exhaust valve

close (EVC) corresponding to crevices and quench layers in the head and to the rolled-up vortex, respectively, are more pronounced (showing higher HC concentrations) at lower engine speeds [7].

Trends in HC concentration with respect to load are neither as strong nor as universal as those with respect to other engine operating conditions. In theory, one would expect HC concentration to decrease as load increases for the following reasons. Higher load results in higher cylinder pressure, thus higher cylinder temperatures [7], thus higher oxidation rates. Furthermore, as load increases, the amount of crevice HCs returning to the cylinder after peak pressure should, according to Namazian and Heywood, decrease (the rest should remain in the crevices or blow by the piston rings) [20]; thus, the relative amount of HCs from crevices that escape into the exhaust should decrease as load increases. Since crevice gases are the largest contributors to exhaust HCs [5], the above trend should theoretically reduce cycle averaged engine-out HCs as load increases. In practice, however, this is not always the case. For instance, when firing an engine on propane, Drobot measured that cycle averaged HC concentrations increase when load increases, but when firing on gasoline and isooctane, she found the opposite [18]. Thompson and Wallace found that, when firing on natural gas, cycle averaged HC concentrations decrease when load increases [7]. Regarding crank angle resolved trends, at low loads, HC concentration is more uniform throughout the cycle; that is, the HC concentration is low during the exhaust valve closed portion of the cycle and drops only slightly during the exhaust process. On the other hand, at high loads, HC concentration varies significantly from the high levels during the exhaust valve closed period to the low levels during the exhaust process [7]. The differences between CA resolved trends can be explained in terms of both the fraction of mass forced into and escaping from the crevices and in terms of the degree of exhaust flow reversion during the valve overlap. Regarding the mass forced into and escaping from the crevices, more HC-rich gases from the crevices return to the cylinder and mix with the bulk gas during the power stroke under low load operation than return under high load operation [20], resulting in higher HC concentrations during the bulk gas emission phase of the exhaust process under low loads. Regarding exhaust reversion, at low loads, a lot of the HC-rich gas escaping from the cylinder at the end of the exhaust process is blown back into the cylinder when the intake valve opens, while at wide open throttle,

there is effectively no reversion, so more of the rolled-up vortex escapes into the exhaust port, resulting in a higher plateau HC concentration from EVC until the subsequent EVO at high load [7].

Air-fuel ratio affects exhaust HC concentration by affecting temperature and oxygen availability. Gas temperatures are maximized quite near stoichiometric operation [7]. But, the leaner the mixture, the more oxygen is available for oxidation reactions. Since HC oxidation depends on both temperature (exponentially) and oxygen availability (to a power on the order of one), minimum unburned HC concentrations should theoretically be observed at slightly lean air-fuel ratios (ϕ from 0.9 to 0.95). In practice, measurements of cycle averaged unburned HC concentrations support this theory quite well [7], [12], [18]. As with speed, the trend in HC concentration with respect to air-fuel ratio displays direct correlation on cycle averaged and CA resolved bases. Specifically, Thompson and Wallace's comparison of FFID traces from operation under a variety of air-fuel ratios show the above trends at essentially all CAs. At $\phi = 0.91$, the HC concentration is lowest throughout the entire cycle, and either increasing or decreasing ϕ from 0.91 monotonically increases HC concentration at all CAs [7].

Although fuel effects on HC emissions have been widely studied, it is beyond the scope of this paper to detail all of the results, so this paragraph will describe only results pertinent to the experiments performed by the author. Kaiser *et al.* found that, in paraffin combustion, the total HC emission levels decrease monotonically as fuel molecular weight increases [21]. These findings are related in part to Gatellier *et al.*'s finding that fuels' solubility in oil (and thus absorption and desorption from oil layers) is a positive function of molecular weight [6]. By chromatographically analyzing exhaust gas, Kaiser *et al.* found that the percentage contribution of unburned paraffin fuels to total HC emissions (on a ppmC1 basis) decreases with increasing molecular weight; they measured roughly 60% for propane and 50% for isooctane at mid-speed, mid-load conditions [21]. For propane combustion, Kaiser *et al.* found that the major non-fuel species formed are methane, ethene, propene, and ethyne [21]. In a similar experiment using toluene fuel, they found that unburned fuel contributes roughly 83% to total HC emissions, with the remainder coming from benzene, methane, ethyne, ethene, ethylbenzene, and benzaldehyde [21]. For isooctane combustion, Ninomiya and Golovoy [22] as well as Demster and Shore [23] found that the

major non-fuel species formed are methane, ethene, propene, ethyne, and isobutene. As a final note, Kaiser *et al.* noted exhaust emissions are approximately "additive" [24]; that is, for the blended fuels they studied, the mole fractions of product species could be predicted reasonably accurately given data on the individual fuels' emissions and the concentrations of each fuel in the blend (thereby justifying studies of single component fuels' emissions).

1.4 Objectives

The primary objective of this project was to study how the composition of unburned HCs varies during the cycle at different locations of the exhaust port/runner and at different engine operating conditions, using both gaseous and liquid fuels. Specifically, the objective was to compare the relative proportion of fuel and non-fuel HCs at different CAs — particularly near EVO, at a number of CAs in the middle of the exhaust process, and near EVC — at different locations, as well as to relate the findings to existing models of post-flame oxidation. Moreover, an objective was to measure any possible species concentration gradients across the radius of the port in order to verify whether, in fact, wall-mounted sampling valves adequately measure the concentrations in the port by sampling gases near the walls or whether there are significant concentration gradients across the radius. Fulfillment of this objective required the design of a sampling unit with the combined advantages of the FFID and wall-mounted sampling valves; that is, the device must be capable of sampling gases from arbitrary locations within the exhaust port during small CA intervals, and the device must be capable of storing those gases for speciation.

In order to verify that this sampling unit works as desired, an objective of these experiments was to relate data taken with the sampling unit to that taken by a FFID under the same conditions and by wall-mounted sampling valves in similar experiments. Specifically, an objective in verifying that the sampling unit works as desired was to demonstrate that it measures the same trends in total HC concentration as does the FFID. A further objective was to compare data taken by this sampling unit to data taken by other

researchers in terms of both concentrations of the various species and concentration trends with respect to engine operating conditions and fuel type.

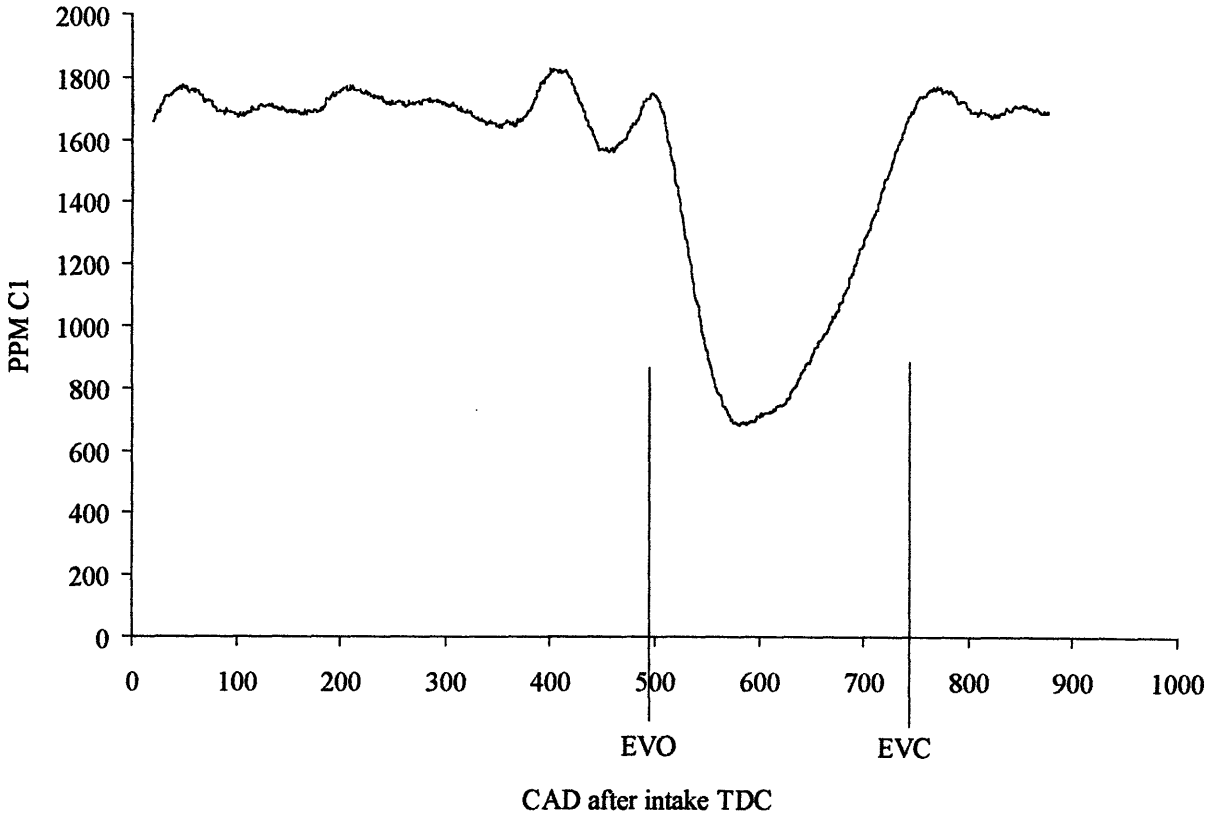

Figure 1.1 Total HC concentration measured by FFID.
Conditions: 1500 rpm, relative air-fuel ratio λ = 1.10, load = 3.75 bar IMEP.

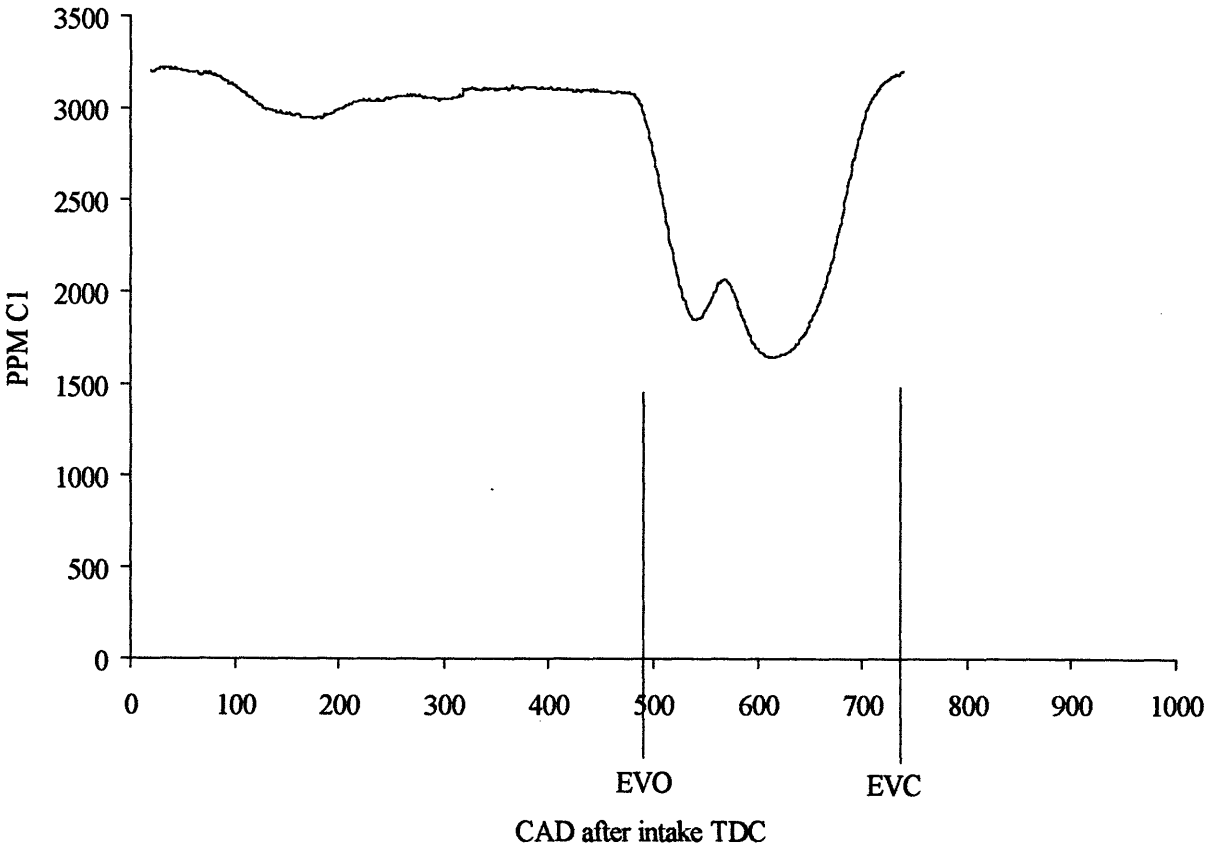

Figure 1.2 Total HC concentration measured by FFID.
Conditions: 900 rpm, relative air-fuel ratio λ = 1.10, load = 3.75 bar IMEP.

CHAPTER 2

EXPERIMENTAL DESIGN

2.1 Design Criteria

The main criteria directing the design of the sampling unit were:

1. the ability to resolve concentrations over a short time window
2. the ability to move the sampling unit's inlet to different locations in the port
3. the ability to store a number of samples for subsequent GC analysis in order to speed the sample-taking and analyzing processes
4. the ability to compare data taken by the sampling unit to that taken by a FFID in order to validate the sampling unit's output.

In meeting the first two criteria, certain features of the FFID and wall-mounted sampling valves were used, thereby reaping the benefits of each device's design. GC analysis requires the storage of samples, which is most easily done via a valve (as opposed to a rotary system like that used by Rhee *et al.* [25]). Further, the ability to resolve a time window on the order of crank angle degrees requires a very fast acting valve. In order to give the sampling unit the ability to probe the port, a transfer tube similar to that used in the FFID was needed. But, the combination of flow through a transfer tube and discrete sampling by a valve (as opposed to the continuous sampling in the FFID) requires some method of purging the transfer tube so that, each time the valve fires, the sample would consist of gas from the desired time window rather than gas trapped in the tube during the entire cycle. For the sampling unit, purging is achieved via a vacuum chamber setup: the valve sits in a vacuum chamber into which flow is continuously drawn. The flow impinges on the face of the valve and is drawn past so that, when the valve fires, only the gas passing by during that short window of time is drawn into the valve.

The third criterion required the use of a storage unit with a number of storage loops that can be triggered by a computer. The reason that the ability to store a number of samples is a necessary criterion is as follows. Getting the engine to a certain fully warmed-up operating condition is very time

consuming; therefore, if only one sample could be obtained and analyzed each time the engine were run, the time required to take a test matrix worth of data would be overburdening. Furthermore, data analysis is not labor intensive, but is time consuming; therefore, tremendous time savings can be achieved by automating the analysis of numerous samples.

The fourth criterion influenced the design of the transfer tube from the exhaust port to the solenoid valve. This criterion and the design are discussed in the Apparatus section, 2.2.

2.2 Apparatus

As mentioned above, the sampling unit combines certain features of the FFID with those of wall-mounted sampling valves. It consists of a transfer tube with one end located in the exhaust port at an arbitrary position — much like that of the FFID — and the other end connected to a three-way valve (Fig. 2.1). One side of the three-way valve is connected to a Cambustion HFR400 FFID (the use of which is described later), the other to a vacuum chamber containing a General Valve Series 9 high-speed solenoid valve. Exhaust gas is drawn continuously through the transfer tube to the vacuum chamber, where it impinges on the face of the solenoid valve and is then drawn past the valve and out of the vacuum chamber by a vacuum pump. The level of vacuum in the vacuum chamber is controlled by a bleed flow and measured by a Validyne DP15 pressure transducer. The solenoid valve is controlled by the General Valve Iota One pulse driver, which receives a TTL signal from the engine control circuit once per cycle at a specified but arbitrary crank angle, at which time the controller opens the solenoid valve for 0.6 milliseconds. During this time, flow is drawn through the open valve into a storage unit consisting of a 350 ml reservoir with a Validyne DP15 pressure transducer (the reservoir improves the transducer's accuracy) and a 10 ml storage loop, separated from the reservoir by a valve. After a number of cycles, when a enough exhaust gas for a GC analysis is trapped in the reservoir (typically resulting in a pressure of 0.25 bar absolute, which is below the exhaust mixture's condensate saturation pressure), the controller stops opening the high-speed solenoid valve, and the stored gas is diluted with nitrogen to atmospheric pressure for subsequent analysis. A sample of this stored gas is then drawn into a storage loop. A Valco

AST16P 16-port valve contains the storage loops and allows a number of samples to be taken and later analyzed in rapid succession (as will be discussed shortly). Once samples are collected in each of the different storage loops, the 16-port valve is connected to a Hewlett Packard HP5890A gas chromatograph with a flame ionization detector (FID).

The sixteen-port valve is hooked to the GC such that the GC can turn the valve to load samples into the column and analyze each sample automatically. Extra actuator lines on the GC (for switching the inlet valves) are routed instead to the sixteen port valve, allowing the GC to pulse the valve and advance the sampling loops in order to step through the analysis procedure. The GC method used to analyze samples is similar to a method described by Jensen *et al.* [26]. The column temperature is kept at -50°C until the light species (C1 and C2) elute so as to allow good separation. Afterwards, the temperature is ramped up at 6°C/minute so as to quickly elute the heavier species. Analysis took 17 minutes for samples consisting of species C1 to C3 (~4 hours for a full test of 15 samples) and 35 minutes for samples consisting of species C1 to C8 (~9 hours for a full test of 15 samples).

The storage unit is outfitted with a heating unit in order to keep samples from condensing in the storage loops. The heating unit consists of an insulated box (Valco HVEC-3 Heated Valve Enclosure) outfitted with a thermocouple and could be maintained at a nominal temperature of 100°C by a Watlow Series 965 temperature controller, which powered a Valco HA1 valve heating assembly and Thermolyne Brisk Heat heater tape. The heating unit was not used during tests in which the engine was fired on propane. The reason is these samples have no components that could condense at room temperature because all HCs (C1 to C3) are gaseous and because the partial pressure of water is below its condensation pressure. On the other hand, the heating unit was used during tests in which the engine was fired on a liquid fuel. The reason is that, if the storage unit were at room temperature, the unburned fuel could condense in the storage loops and not be drawn into the GC. In addition, the inlet to the GC was heated during these tests to avoid condensation.

As alluded to above, a FFID is connected to the transfer tube in parallel with the sampling unit via a three-way valve for two reasons: first, it provides immediate feedback on the HC level at the desired

sampling location and, second, it serves as a comparison for sampling unit data. Since the parallel connection assures that the sampling unit and the FFID obtain samples from exactly the same location, any problems with the transfer tube location can quickly be detected via the FFID. In addition, FFID data were taken prior to the use of the sampling unit once the engine reached steady-state operation. The FFID signals, taken once per crank angle degree for twenty-two cycles using the *Global Lab*® software, are averaged and compared to the sampling unit output (i.e., the total HC concentration measured by the GC at each crank angle, properly scaled to account for nitrogen dilution). It should be noted that, because the sampling unit requires approximately 1000 cycles to capture a significant volume for chromatographic analysis, the only relevant comparison is that between the sampling unit output and the FFID output *averaged* over a large number of cycles. (All FFID data shown in this thesis are averaged over twenty-two cycles.) Further, while the three-way valve is a source of some mixing within the transfer tube, the resulting slight loss of time resolution was found to be insignificant when compared to the inherent resolution of the sampling unit.

All tests were performed on a Volvo B5254 FS four valve, single cylinder, spark ignition engine connected to a dynamometer. Engine specifications are listed in Table 2.1. Propane fuel was introduced into the intake air flow well upstream of the intake valve. Liquid fuels were injected onto the closed intake valves via a standard fuel injector.

Feedback necessary for adjustment of engine load and for finding MBT spark timing was obtained from cylinder pressure data. Cylinder pressure data were taken once per crank angle degree for thirty cycles by using the *Global Lab*® software; a simple program uses the *Global Lab* output to calculate the IMEP and the crank angle corresponding to maximum cylinder pressure. MBT timing was assumed to be the timing that resulted in peak pressure at 16 ± 2 °CA after top dead center [15].

Table 2.1 Summary of Engine Specifications

Model	Volvo B5254 FS head and base in a Ricardo Hydra crank case
Type	Single-cylinder, 4-stroke engine, 4-valve head
Bore	83 mm
Stroke	90 mm
Displacement	0.5 liter
Compression Ratio	10.1 : 1
Intake Valve Open by 0.1 mm	4° CA BTDC
Intake Valve Closed to within 0.1 mm	236° CA ATDC
Exhaust Valve Open by 0.1 mm	492° CA ATDC
Exhaust Valve Closed to within 0.1 mm	12° CA ATDC (labeled as 732° CA in following text)

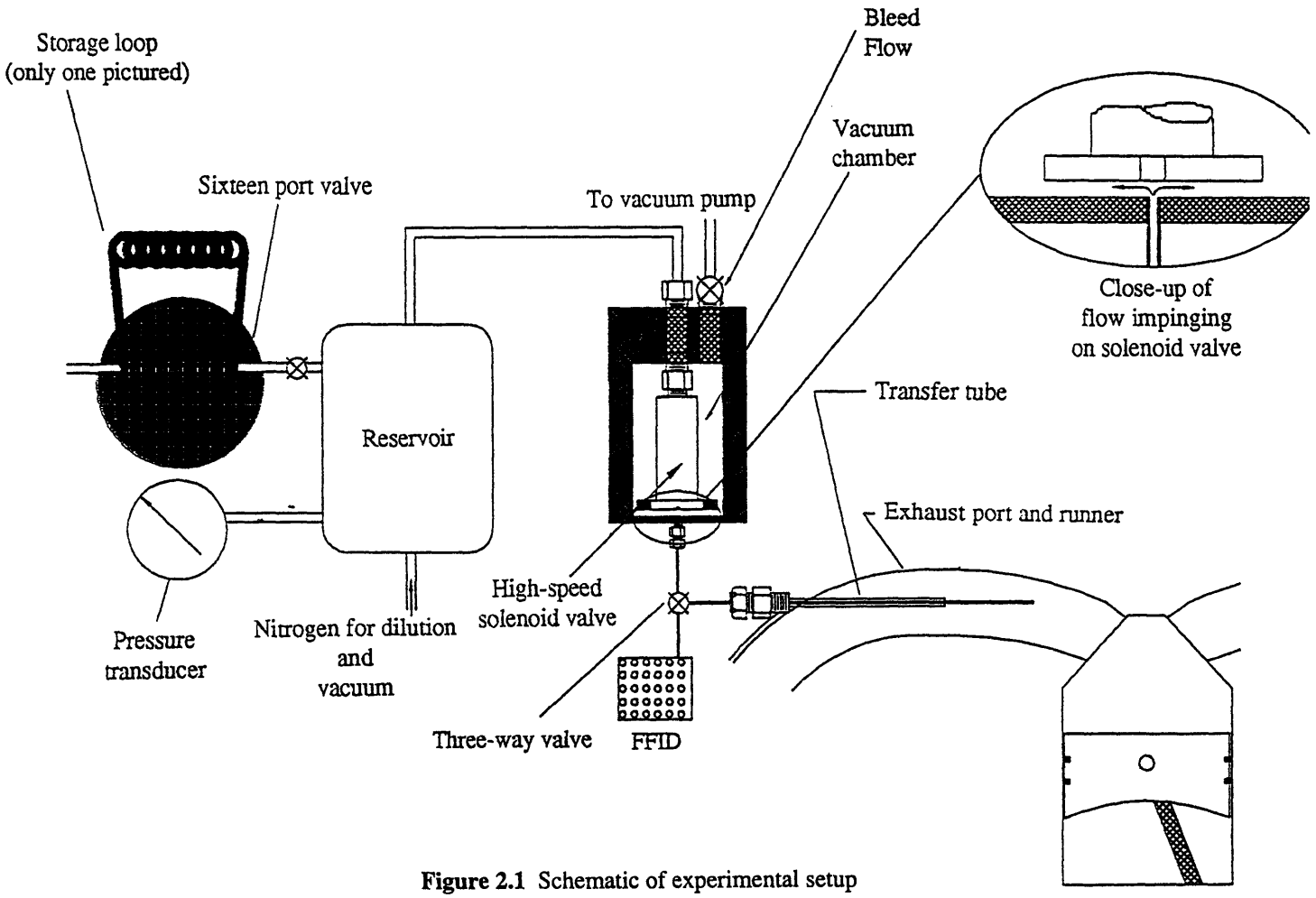

Figure 2.1 Schematic of experimental setup

CHAPTER 3

EXPERIMENTAL PROCEDURE

3.1 Test Matrices

Two experimental matrices were developed to test the effect of (a) engine operating conditions plus sampling location and (b) fuel type on speciated, CA resolved HC concentrations. Both matrices were centered about the "baseline conditions" listed in Table 3.1; conditions for those matrices are listed in Tables 3.2 and 3.3. The baseline engine operating condition is called by Ford the World Wide Mapping Point and, except for air-fuel, ratio is representative of a mid-speed, mid-load cruise condition used during the FTP cycle [18], [21]. The baseline air-fuel ratio of $\lambda = 1.10$ was chosen because at this air-fuel ratio, engine-out HC concentrations are not sensitive to small changes in air-fuel ratio.

All tests consisted of a number of CAs; those CAs and the corresponding points during the cycle are listed in Table 3.4. For tests at an air fuel ratio of $\lambda = 1.10$, samples were collected at thirteen to fifteen CAs, while at air-fuel ratios of $\lambda = 1.00$ and 0.90, samples were collected at only four CAs.

3.1.1 Engine Operating Condition Test Matrix Using Propane Fuel

The following is a brief description of the tests run using propane fuel. For all tests, the spark timing was set to MBT timing and the coolant and oil temperatures were set to their fully warmed conditions (85° $\pm$ 5°C). The following parameters were varied: speed, load, and air-fuel ratio. Engine speeds used were 900 rpm and 1500 rpm; the dynamometer is not capable of speeds much below 900 rpm, and at speeds above about 1500 rpm, the sampling unit's crank angle resolution becomes poor (see discussion of sampling unit resolution in section 4.1.1). Loads used were 2.15 and 3.75 $\pm$ 0.05 bar IMEP; higher loads were not permissible at low speeds because the dynamometer is not capable of high load / low speed operation for the length of time necessary to complete one test. Air-fuel ratios used were $\lambda =$ 1.10 (fuel lean), 1.00 (stoichiometric), and 0.90 (fuel rich). Samples were taken at a number of locations

in the port in order to spatially resolve the concentration differences axially along the flow path and radially across the port. Locations from which samples were taken are shown in Figure 3.1: the center point (B) is the sampling location for the baseline condition, and samples were taken from locations 8 and 16 mm above that position (points B_{inter} and B_{top} respectively), which correspond to 10 mm and 2 mm below the top of the port, 16 mm below that position (point B_{bottom}), which corresponds to 2 mm above the port bottom, and approximately 5 to 6 cm ahead of and behind that position (points A and C respectively), which correspond to points 1 to 2 cm ahead of the exhaust valve and behind the port/runner interface, respectively.

3.1.2 Fuel Composition Test Matrix

The three fuels tested at the baseline conditions were propane, toluene, and isooctane. Propane was tested extensively because of its ease of use. One reason is that propane and all of the intermediates formed during propane combustion are gaseous, so tests could be run before the implementation of a heating unit for the storage loops without worry of condensation problems. Second, propane and its combustion products elute from the GC quickly [26], allowing a number of samples to be analyzed in a short period of time. Toluene was chosen as the second fuel because it is representative of aromatics found in commercial gasoline. Moreover, toluene has the interesting characteristic that it produces a small amount of non-fuel combustion products [21], [22]. Isooctane was chosen as the third fuel because it is representative of a paraffin component found in commercial gasoline. Isooctane, on the other hand, is known to produce a wide variety of non-fuel combustion products [21], [22].

Because of the fact that the tests in the fuels matrix did not show significant differences between the proportion of fuel to non-fuel HCs emitted at different times during the cycle (see results in chapter 7), it was not deemed necessary to use toluene and isooctane in the engine operating conditions test matrix. That is, because the propane test results are quite similar to the toluene and isooctane results, there did not seem a lot to gain from repeating the engine operating condition test matrix for the liquid fuels.

3.2 Optimization of Sampling Unit Parameters

Optimal resolution was obtained only after careful choice of sampling unit parameters such as solenoid-valve open time and vacuum chamber pressure. One might expect that the shorter the valve open time, the better the sampling unit's crank angle resolution. To check that this was the case, an abbreviated crank angle sweep was run using two different valve actuation durations, the idea being that the optimal open time will correspond to the test with the best resolution. As expected, the shorter valve open duration corresponded to the best resolution, so for all subsequent tests, the solenoid valve actuation time was set as small as possible: 0.6 milliseconds. In order to find the optimal vacuum chamber pressure, an abbreviated crank angle sweep was run using three different vacuum chamber pressures, again with the optimal vacuum chamber pressure corresponding to the test with the best resolution. As might be expected, the lower the vacuum chamber pressure, the better the resolution because lower pressure induces faster flow through the transfer tube and decreases mixing in the vacuum chamber. Note that the sample pressure before dilution is constrained to be below the vacuum chamber pressure; thus, the dilution ratio increases as vacuum chamber pressure decreases. Since the sampling unit's uncertainty scales directly in proportion to the dilution ratio, there is a lower limit to the useable vacuum chamber pressures, which was found to be approximately 0.3 bar, absolute.

3.3 Integrity Checks

Integrity of the sampling unit data corresponds to the ability to correctly and repeatably measure port HC concentrations. In order to test the sampling unit's ability to correctly measure port concentrations, the exhaust port was filled with gas of a known HC concentration and a number of samples were taken by the sampling unit for GC analysis. The samples were treated exactly as samples taken in a real test with the engine firing; that is, they were diluted and stored for the same length of time and subsequently analyzed by the GC using the same technique. Comparison between the GC output and the known input showed that the sampling unit and GC correctly measure port concentrations to within

the GC's uncertainty. In order to verify the repeatability of the sampling unit data, 15 samples were taken at the same engine operating conditions and at the same crank angle for subsequent GC analysis. Again, samples were treated exactly as those from a real test. Results of this test show that the sampling unit output has a standard deviation of 80 ppmC1. Note that, because this entire test was performed on one day, the above result does not include the effects of day-to-day variability in engine operation.

3.4 Test Procedure

The following is the test procedure. Before beginning a test, the transfer tube was located in the exhaust port. The first few times a particular transfer tube was used, the location process required measurement of the actual location and adjustment so that the transfer tube inlet was in the desired position. However, after those first few times, when the transfer tube was inserted into the port and tightened down, it would return to the desired location to within the desired margin of error. (Note that Finlay *et al.* showed that the HC concentrations are not very sensitive to transfer tube location [11].) Also before beginning a test, the vacuum chamber and solenoid valve face were cleaned, and all of the storage loops were purged by high pressure nitrogen. Next, the pressure transducer for the sample reservoir was calibrated using a two-point linear calibration (as suggested by the manufacturer). Plus, each storage loop was tested to insure that the leakage rate was negligible (unless a storage loop had a significant leak, the leakage rate was too small to measure using the Validyne DP15 Pressure Transducer). Then, the engine was started and brought to the desired steady state operating condition; specifically the engine was brought to the desired IMEP, with MBT timing, and with coolant and oil temperatures at 85° $\pm$ 5°C. Once these conditions were met, FFID data was taken for a period of twenty-two cycles. After this, samples were taken by using the sampling unit. Periodically during the sampling process, the vacuum chamber pressure was adjusted to insure that drift was not significant (so that transit times stayed constant). During the sampling process, the GC was started and calibrated, and immediately after taking the last sample, the storage unit was moved to the GC and the analysis process was begun.

Table 3.1 Baseline operating conditions

Parameter	Value
Engine speed	1500 ± 20 rpm
Load	3.75 ± 0.05 bar IMEP
Relative air-fuel ratio (λ)	1.10 ± 0.01
Spark Timing	MBT ± 2°CA
Coolant and oil temperatures	85° ± 5°C
Transfer tube location	4.5 cm from the exhaust valve at port midplane

Table 3.2 Parameters swept about the baseline condition for operation on propane fuel

Parameter	Value
Engine speed	900 and 1500 (± 20) rpm
Load	2.15 and 3.75 (± 0.05) bar IMEP
Relative air-fuel ratio (λ)	0.90, 1.00, 1.10 (± 0.01)
Sampling locations (also see Figure 3.1)	1.5 cm above valve at port midplane, 4.5 cm behind valve at port midplane, 4.5 cm behind valve, 16 mm above port midplane, 4.5 cm behind valve, 8 mm above port midplane, 4.5 cm behind valve, 16 mm below port midplane, 10 cm behind valve (1.7 past port/runner interface) at port midplane

Table 3.3 Fuels tested at the baseline operating conditions

Fuel	Formula (Phase)
Propane	C_3H_8 (g)
Toluene	$C_6H_5CH_3$ (l)
Isooctane (2,2,4-trimethylpentane)	C_8H_{18} (l)

Table 3.4 CAs at which samples were collected

Crank angle after intake TDC (in degrees)	
177	
327	
477	
492	Exhaust Valve Open (EVO)
522	
522	
582	
612	Exhaust process
642	
672	
702	
732	Exhaust Valve Close (EVC)
747	

Note that 732° and 747° correspond to 12° and 27°, respectively, but are labeled as such in subsequent graphs so that the entire exhaust process is located in one continuous region of the graph.

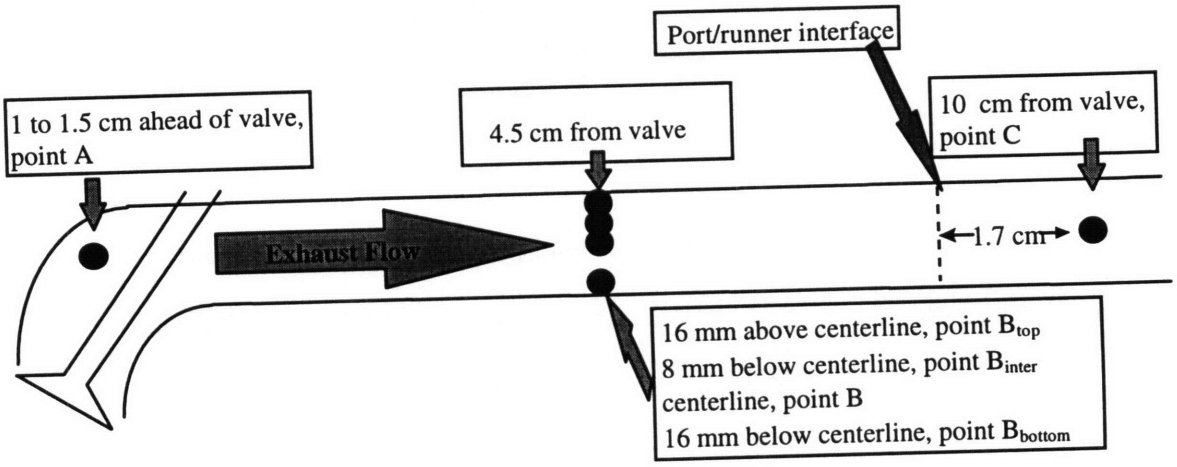

Figure 3.1 Sampling locations. Note that point B_{top} is approximately 2 mm below the top of the port, and point B_{bottom} is approximately 2 mm above the bottom of the port.

CHAPTER 4

DISCUSSION OF SAMPLING UNIT CHARACTERISTICS

4.1 Resolution

4.1.1 Sampling Unit Time Resolution

The goal of optimum operation was to minimize the crank angle interval sampled by the solenoid valve, thereby collecting samples during the smallest possible portion of the exhaust process. The sampling unit's optimum crank angle resolution (minimum crank angle sampling interval) was estimated as a function of the sampling unit parameters such as the pressure drop along the transfer tube, the pressure drop through the solenoid valve, the tube diameters and temperatures, and the solenoid valve open-time. (Note that sampling unit time resolution is essentially independent of engine parameters such as speed and load since, most importantly, the exhaust port pressure only fluctuates within a small range. However, the crank angle resolution is dependent upon engine speed in that the time resolution is fixed with respect to speed, but the time per crank angle degree varies inversely with speed.) Estimates of the resolution were made based upon measurements of the mass trapped by the solenoid valve as well as approximations of the sampled volume and flow velocity within the vacuum chamber. That is, knowing the mass trapped by the solenoid valve during one opening, one can estimate the shape and size of the volume trapped. One can then superimpose that sampled volume on the flow pattern within the vacuum chamber; the difference in crank angle degrees represented within the sampled volume is the sampling unit's crank angle resolution. Such estimates suggest that the unit is capable of differentiating concentrations over a crank angle interval as small as 18 to 30° CA at an engine speed of 900 rpm. This number compares well to the observed resolution — defined as the smallest CA interval over which the sampling unit measures the same time rate of concentration changes as does the FFID — of approximately 15 degrees (see figures in subsequent sections). Estimates using the above method show that, as the vacuum chamber pressure is decreased relative to that in the exhaust port, and as the solenoid valve's

open time is decreased, the sampling unit resolution should improve. Calculation of the sampling unit's resolution is more thoroughly detailed in Appendix 1.

In reality, limitations upon the sampling unit's resolution result from sample mixing during transit from the exhaust port to the solenoid valve. Consequently, the resolution will improve only with decreased sample mixing. Mixing within the transfer tube is assumed to be as little as that in any FFID transfer tube, and mixing in the three-way valve was demonstrated to be very small by virtue of the fact that little loss of resolution was observed in the FFID trace due to the introduction of the three-way valve. Since steady mixing and entrainment within the vacuum chamber would diminish as the vacuum chamber pressure is decreased relative to the port pressure due to larger flow velocities in the vacuum chamber, and since resolution does not get significantly better as the vacuum chamber pressure is changed, it is believed that steady mixing is not what limits resolution. By elimination, the unsteady mixing caused by the rapid opening and closing of the solenoid valve must then be the limiting factor on the sampling unit's resolution. Despite the fact that the cause is known, no simple cure exists: resolution of a small number of crank angle degrees relies upon use of a fast-acting sampling valve, yet that fast action inherently causes a certain amount of mixing and therefore decreases resolution.

Note that the first design of the sampling unit, a replica of the FFID with the ionization detector replaced by a high speed solenoid valve, failed to give sufficient time resolution. This sampling unit consisted of a transfer tube, T-top tube, and a third tube from which samples were drawn, as well as a constant pressure (CP) chamber, much like the FFID. The sizes of the various tubes, however, were different from those of the corresponding parts in the FFID in order to achieve different flowrates. Significant mixing in the T-top tube and the third tube resulted in poor time resolution, so to solve the problem, the newer design (that described in Chapter 2) was built.

4.1.2 Sampling Unit Spatial Resolution

The sampling unit achieves spatial resolution the same way that the FFID does: it has a transfer tube that the operator can locate as desired. Consequently, the sampling unit's accuracy at resolving spatial concentration differences is, as in the case of the FFID, only as good as the operator's accuracy at

locating the transfer tube. However, it is useful to check that the sampling unit's output from different locations matches (a) FFID output at the same location and (b) trends measured in previous research. This will be done in Chapter 6 (Comparison Between the Sampling Unit and the FFID).

4.2 Oxidation Within the Transfer Tube and Storage Unit

Uncertainty in sampling unit data arises from the possibility of HC oxidation after samples are taken from the port. Places in which oxidation is most likely are within the transfer tube (because the temperature is rather high) and within the storage unit (because the residence time is long). Note that oxidation in these locations should be far more significant a problem than that in places like the reservoir or vacuum chamber where (a) temperatures are relatively low *and* (b) residence times are relatively short.

Like a FFID, the sampling unit's transfer tube is not cooled, although it sits in the hot exhaust stream; hence, HCs in the transfer tube may undergo oxidation. However, this problem is faced by any instrument that samples gas from the port via an uncooled transfer tube, be it the sampling unit or the FFIDs used by other researchers. Worst case estimations of the extent of HC oxidation in the transfer tube using two-step rate expressions [27] evaluated at the prevailing temperatures indicate a total oxidation of the order of 1%, owing to the relatively short residence time (about 4 ms) in the tube. This indicates that the HC concentrations leaving the transfer tube are a good representation of those entering it. See Appendix 2 for details of the calculations.

Estimates of the amount of oxidation within the storage unit were made in a similar manner to those of transfer tube oxidation. Results suggest that less than 1% of the HCs oxidize in storage due to the low temperature. Experiments were performed to demonstrate that negligible reaction occurs within the storage unit. Specifically, in experiments where samples of propane and its non-fuel products were stored and analyzed repeatedly over time periods equal to or greater than the duration of a normal test, the amount of HC oxidation within the storage unit was found to be between 1% and 9% of the total HCs per four and a half hours (the duration of a test using propane fuel). It should be pointed out that the amount of reaction is so small that it is difficult measure without incurring other errors, so the 1% to 9% quoted

above are upper bounds on the fractions oxidized. For instance, in tests where samples are analyzed over long periods of time (some tests ran up to two days in length) in order to find the amount of oxidation, small leaks in the storage loops may become significant compared to the fractional oxidation. On the other hand, a small variation in the samples stored in each loop can mask the amount of oxidation taking place if too little time is allowed to elapse. (In the experiment where 9% oxidation per 4.5 hours was measured, samples were taken from the engine exhaust over a period of about an hour, so sample-to-sample variability may have overwhelmed the oxidation.) Note that 1% to 9% error is on the same order of magnitude as the GC's inherent uncertainty. Hence, the concentrations measured by the GC are a good representation of those entering the sampling unit's transfer tube; i.e., the sampling unit does not seem to introduce artifacts into the concentration measurements. Because oxidation rates for the liquid fuel species and their combustion products are on the same order of magnitude as those of propane [27], the amount reacted in storage is assumed negligible for the liquid fuel tests as well as the propane tests. See Appendix 3 for further details of the calculations and the experimental verification.

CHAPTER 5

DATA ANALYSIS

5.1 Calculation of Concentrations

The steps taken to calculate the HC species concentrations from the raw gas chromatography signals are as follows. Before each day of experiments, a calibration gas was chromatographically analyzed. Jensen *et al.* found and tabulated the order in which HC species elute under similar conditions to those used; pairing Jensen's results with the resulting chromatogram yields both retention times and FID area counts per ppmC1 for species in the calibration gas. The retention times for the calibrated species remained nearly constant from the initial calibration gas test through a full sequence of sample analyses, with only slight but predictable changes. Species not present in the calibration gas could be identified by comparing Jensen's tabulated retention indices to the measured retention indices calculated from the following linear interpolation of retention time, as suggested by Jensen *et al.* [26]:

$$\frac{RI}{100} = n + \left[\frac{t_{unk} - t_n}{t_{n+1} - t_n}\right] \tag{5.1}$$

where RI is the retention index for the unknown species, t_{unk} is the retention time of the unknown species, n is the carbon number of the last n-paraffin that elutes prior to the unknown species, t_n is the retention time of that paraffin, and t_{n+1} is the retention time of the next n-paraffin to elute.

Although the GC's FID should theoretically give output with a constant ratio of area counts to ppmC1 (called the response factor) for all species, in practice there were slight differences in the response factor from species to species. Measurements made on a calibration gas with known concentrations of C1 to C5 hydrocarbons showed that the GC's response factor for different HC species differs no more than 6 to 10% between different species. This compares well to Jensen's *et al.* measurement that the response factor differs by 6 to 8% for all HC species except methane, which they found to have a significantly different response factor [26]. Consequently, it is believed that at most 10% error is incurred by using the

following formula for the concentration of each species in the exhaust gas from the GC area counts and the sampling unit's reservoir pressure data:

$$X_i = \left(\frac{A_i}{A_{ref}}\right)\left(\frac{p}{p_o}\right)X_{ref} \tag{5.2}$$

where X_i is the mole fraction of species i, A_i is the area of the peak corresponding to species i measured by the GC, A_{ref} is the area of the peak corresponding to a HC with mole fraction X_{ref} measured by the GC in the calibration test, and the pressure ratio corresponds to the dilution ratio of the sample. The calibration or reference species for the above calculation was chosen in the following manner: if the species whose concentration was to be calculated was C1 to C5, then the calibration species chosen was the species in the calibration gas with the same carbon number; if the species whose concentration was to be calculated was C6 or higher, then the calibration species chosen was methane. (Although researchers such as Jensen *et al.* and Kaiser *et al.* measured a difference in response factor between methane and other species [24], [26], the author did not measure such a difference, and thus believes that the choice of methane is as good as the choice of any other species.)

5.2 Transit Times

Since there is naturally a finite transit time through the transfer tube and vacuum chamber, the measured concentrations as a function of the crank angle degree become shifted in time from the actual concentrations. In order to correct for this transit time from the transfer tube inlet to the high-speed solenoid valve in the sampling unit, the following method was applied. The time in transit through the transfer tube was approximated using Cambustion's *SATFLAP1* program [28], assuming that the entire transfer tube (i.e., the length before and after the three-way valve as well as that within the valve) is of uniform diameter and at a uniform temperature, which is taken to be the average of the tube's maximum and minimum temperatures. The transit time from the outlet of the transfer tube to the inlet of the high-speed solenoid valve is calculated from conservation of mass and geometric considerations, using the transfer tube outlet velocity given by *SATFLAP1*. In addition, it is useful to further correct the data for the

cycle-averaged time in transit from the cylinder exit to the transfer tube inlet so that events during the cycle are shown at the same crank angle degree, regardless where the transfer tube is located. The time in transit from the exhaust valve to the transfer tube inlet was estimated from the distance between the transfer tube inlet and the center of the exhaust valve seat and an average velocity, approximated from results of CFD calculations using the FIRE code [29]. More detailed calculations of the transit time are presented in Appendix 4.

In order to compare FFID data to sampling unit data, the FFID data must also be corrected for the transit time from the exhaust valve to the transfer tube inlet and through the FFID to the ionization detector. Because the FFID's transit tube has a nonuniform diameter (i.e., tube diameters are different upstream, within, and downstream of the three-way valve), and because transit times approximated by Cambustion's *SATFLAP1* [28] and *SATFLAP3* [30] are very sensitive to tube diameter, *SATFLAP3* did not give good estimates of the actual transit times. (*SATFLAP3* is the program for the FFID's three tubes, as opposed to the single tube program *SATFLAP1*.) Consequently, the following correction was applied to all FFID data. Since it is known that the FFID registers a sharp drop in HC concentration after the exhaust valve opens [11], FFID data measured in the course of these experiments were simply shifted so that the drop occurs accordingly. This procedure has an uncertainty no greater than that of the transit time through the sampling unit.

The results shown in all of the following figures were shifted by transit times calculated as described above. Therefore, the crank angles from 492° to 732° CA on the abscissas correspond to those at which the gas emerges from the cylinder; other CAs, which correspond to gas that sits stagnant in the exhaust port, represent the CA at which the gas entered the sampling unit minus an offset approximately equal to the average port residence time.

5.3 Mass Weighting of CA Resolved Data

Comparison of CA-resolved data taken by the sampling unit with cycle averaged data from previous research (for example, tests where exhaust gas was sampled from a mixing tank at the end of the runner or where the exhaust gas was quenched once per cycle) requires that each sampling unit datum be weighted by the fraction of mass passing through the port during the corresponding CA interval. The following model was used in order to estimate the mass flowrate through the exhaust port as a function of CA.

A first law analysis of the control volume enclosing the burned gases contained in the cylinder yields the following governing equation:

$$\frac{\dot{m}}{m} = \frac{1}{\gamma}\left(\frac{\dot{p}}{p}\right) + \left(\frac{\dot{V}}{V}\right) - \frac{\gamma - 1}{\gamma}\frac{\dot{Q}}{pV} \tag{5.3}$$

where m is the instantaneous mass, p is the pressure, V is the volume, γ is the ratio of specific heats, $\dot{Q}$ is the heat transfer rate to the cylinder gas. Consequently, the mass flowrate into or out of the cylinder can be calculated based upon a knowledge of the instantaneous volume, pressure, an estimate of the instantaneous cylinder heat transfer rate, and a correlation for γ. The cylinder volume is calculated from the following equation:

$$V(\theta) = V_C \cdot \left[1 + \left(\tfrac{1}{2}\right)(r_C - 1)\left(R + 1 - \cos\theta - \sqrt{R^2 - \sin^2\theta}\right)\right] \tag{5.4}$$

where R is the ratio of connecting rod length to crank radius, r_c is the compression ratio, V_c is the clearance volume, and θ is the crank angle. The cylinder pressure was obtained in the following manner: a Kistler pressure transducer mounted in the cylinder head recorded the pressure once per CAD for twenty-two cycles, then data were cycle averaged. (Note that the pressure data has some noise that, upon differentiation, results in noise in the mass flowrate data.) The instantaneous cylinder heat transfer rate is given by the Woschni correlation [15], [31]:

$$h_c = 3.26B^{-0.2}p^{0.8}T^{-0.55}w^{0.8} \tag{5.5}$$

where h_c is the convective heat transfer coefficient to the gas from the cylinder walls in W/m^2K, B is the cylinder bore in meters, p is the pressure in kPa, T is the gas temperature in K, w is the average cylinder gas velocity equal to 6.18 times the mean piston speed in meters per second.

The correlation used for γ is [12], [32]:

$$\gamma = 1.35 - 5 \cdot 10^{-5} T(K). \tag{5.6}$$

Using this information, estimates of the mass flowrate through the exhaust port as a function of θ were obtained; for example, figure 5.1 shows the mass flowrate for the baseline engine operating conditions. Further, the cycle was broken down into intervals around the crank angles at which samples were taken, and the fraction of exhaust gas passing through the exhaust valves during each interval was calculated from the mass flowrate information. Figure 5.2 shows the intervals and fractional mass flows corresponding to the baseline engine operating conditions.

The cycle- or mass-averaged HC mole fraction (on a ppmC1 basis) is given by the following equation:

$$X_{tot} = \sum_{\theta_i} f_i \cdot X_i \tag{5.7}$$

where f_i is the fractional mass flow through the port during interval i, X_i is the mole fraction measured during interval i, and the sum is made over all crank angle intervals.

5.4 Uncertainty Analysis

Because of the large number of parameters that affect the species concentrations measured in these experiments, and because many of those parameters affect concentrations in ways that are difficult to quantify, the following technique was used to approximate the uncertainty in the sampling unit data. An experiment was run in which 15 samples were taken during the same crank angle interval under the same engine operating conditions and were chromatographically analyzed in order to compare the variation (or, more precisely, the standard deviation) in measured concentrations. The crank angle interval chosen was

from 597 to 603°CA, which approximately corresponds to the occasional peak in HC concentration during the middle of the exhaust process, the assumption being that this erratic peak would result in the worst concentration variations. The standard deviation and resulting 95% confidence interval size, as estimated from this test, are as follow:

Table 5.1 Standard deviation and total uncertainty in concentration measurements

Concentration measurement	Standard deviation, σ (ppmC1)	Total uncertainty, $\pm$ 1.96 σ (ppmC1)
total HC	80	$\pm$ 160
propane	30	$\pm$ 60
toluene	70	$\pm$ 140
isooctane	80	$\pm$ 160
total non-fuel	70	$\pm$ 140

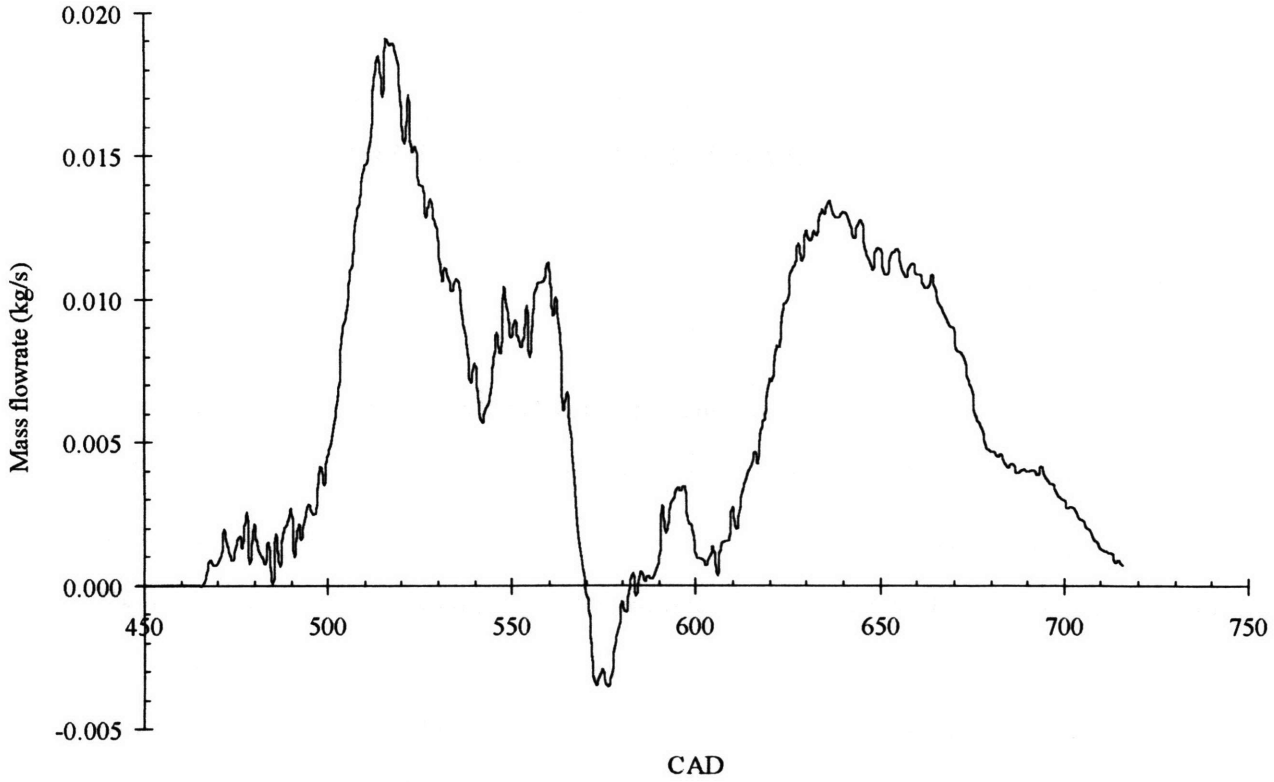

Figure 5.1 Exhaust mass flowrate as a function of crank angle degree at baseline engine operating conditions. (Noise in data is a result of time differentiation of unsmoothed pressure data.)

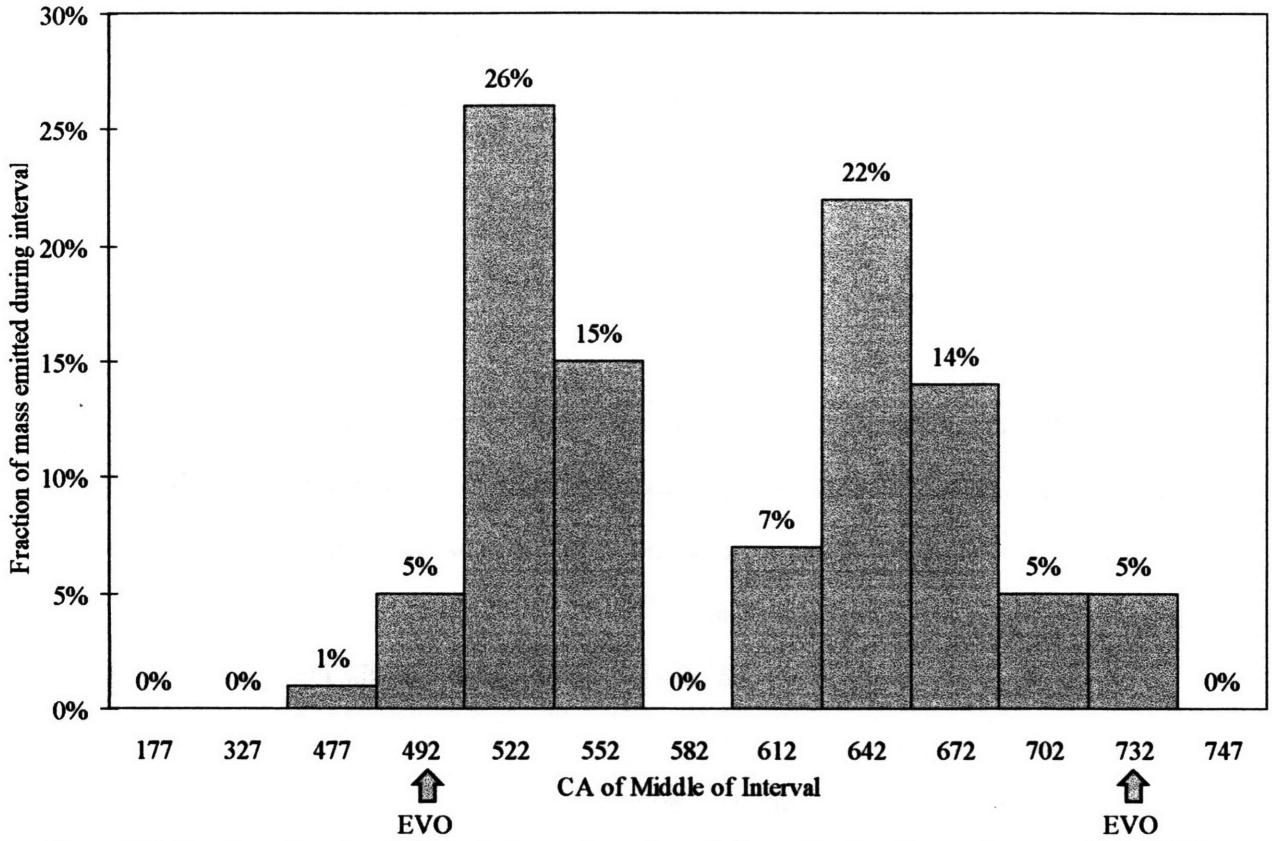

Figure 5.2 Fraction of total mass flow during each crank angle interval at baseline engine operating conditions. (EVO and EVC indicate CAs at which exhaust valve is open or closed to within 0.1 mm.)

CHAPTER 6

COMPARISON BETWEEN SAMPLING UNIT AND FFID

6.1 Introduction

Comparison between data taken by the sampling unit and by the FFID in parallel with the unit is useful in verifying that the unit works correctly. A quick means of comparison might have been to collect the sample through the operating solenoid valve and connect a FFID downstream of the valve to analyze the total HC concentration. However, practical limitations on the minimum pressure required for FFID operation made such a procedure impractical. The following test was used in order to verify the effectiveness of the sampling unit. Samples were collected at different crank angles throughout the cycle and analyzed chromatographically to produce a total HC concentration profile as a function of crank angle. This profile was compared to the averaged FFID signal, obtained prior to collecting samples, as shown in Figs. 6.1 through 6.6. The FFID signal shows the same pattern as the sampling unit results; however, the two differ by a multiplicative scaling factor, which varies from test to test and will be explained in the next section, 6.2.

6.2 FFID Calibration Issues

The FFID was calibrated in the following manner. Before starting the engine, when the exhaust port was filled with only air, the FFID signal was recorded. Next, the static engine's exhaust port was filled with a mixture containing 4500 ppmC1, and the FFID signal was recorded. All FFID data were then scaled linearly according to these two points.

After scaling (as discussed above) and adjusting for the transit time, the FFID signal shows the same pattern as the sampling unit results; however, the two differ by a multiplicative scaling factor, which varies from test to test. Similar behavior was described by Woods *et al.* [13]. However, tests were performed in order to be certain that the FFID was in error, and not the sampling unit. In order to test the

sampling unit's accuracy, the unit was used to collect gas from a tank of gas with a known HC concentration; the GC results gave evidence that the sampling unit correctly measures that concentration. In order to test the FFID's accuracy, the FFID was tested using the following method. First, the FFID was calibrated using the method described above. Then the engine was motored, with enough propane injected per cycle to give a steady concentration of about 4500 ppmC1 as measured by a Rosemount Model 402 HC Analyzer. The FFID output often did not correspond to 4500 ppmC1, indicating some problem translating a static calibration to a tests on a motoring engine. Consequently, tests indicate that FFID data from the static calibration are in error, a conclusion which has been acknowledged by Cambustion, makers of the FFID [33]. For lack of a better calibration technique, all FFID data shown in this paper are based upon the static calibration described above, despite its evident introduction of a multiplicative scaling factor. (Table 6.1 lists scaling factor errors for some tests in order to demonstrate that there is no systematic error. The tabulated scaling factor error is the FFID output divided by the sampling unit output at the same crank angle.)

6.3 Cyclic Port HC Trends Measured by FFID and Sampling Unit

Tests involving the sampling unit have allowed for greater understanding of the cyclic HC trends in the exhaust port than were allowed by tests involving the FFID alone. This section will take the discussion from the introduction section, which related engine events to concentration trends in the port, one step further by incorporating the species information gleaned by the sampling unit with the cyclic trends noted in previous research via the FFID.

From the time that the exhaust valve closes at the beginning of one cycle to the time when it next opens, a stagnant plug of gas is trapped in the port. Consequently, when FFID and sampling unit data are shifted in time to account for finite transit times (see discussion in the Data Analysis section, 5.2), the resulting data show a relatively constant total HC concentration between the time that the exhaust valve closes and the time that it next opens. Little oxidation of the stagnant HCs is observed during this time (observe how all FFID traces stay relatively flat from the beginning of the cycle through EVO), perhaps

due to the relatively low temperatures (thus low oxidation rates) of the gas trapped in the port at this time [14]. However, when the same specimens of gas (i.e., gas correpsonding to the same CA) are analyzed at different points along the port/runner, it is seen that the total HC concentration drops; that is, the level of the plateau region is lower at points further from the exhaust valve. Specifically, the plateau total HC concentration drops approximately 40% to 50% from sampling point A to point B and 20% to 40% from point B to point C (see figure 3.1 for names of points). These decreases are perhaps due to mixing between the bulk gas and the previously stagnant gas along the length of the port/runner; that is, mixing becomes more thorough further along the port and thus decreases the plateau level. Note that the non-fuel concentrations and the total HC concentration change in different proportions, and non-fuel HC concentrations actually tend to increase toward the port exit possibly indicating the occurance of partial or quenched oxidation along the length of the port (see figure 6.7 for mass averaged concentrations along the length of the port).

Under mid to high load conditions (for instance, 3.75 bar IMEP), blowdown causes a rapid expulsion of gas from the cylinder, some of which can contain quenched HCs from cylinder head quench layers and crevices; hence, blowdown can contain a higher HC concentration than the gas previously in the port and can result in a small peak in HC concentration measured by both the FFID and the sampling unit at certain sampling locations and operating conditions (see figures 6.1 and 6.2). Note that, in some mid to high load tests near EVO (for example, figures 6.2 and 6.3), the FFID picks up high frequency signals while the sampling unit only shows a gradual increase from the plateau HC concentration. These signals could either be artifacts of the flame ionization technique, or the signals could show real HC concentration fluctuations that are at a frequency too high for the sampling unit to resolve. The high frequency fluctuations have a characteristic frequency approximately equal to that of the measured characteristic frequency of pressure oscillations in the exhaust port, suggesting that the FFID output may be sensitive to pressure fluctuations, despite the manufacturer's extensive attempts to eliminate pressure dependence. (Note that the sampling unit's larger constant pressure vacuum chamber inherently damps pressure oscillations better that the FFID's.) Alternatively, it has been suggested that the fluctuations near EVO are not the fault of pressure oscillations but rather show actual HC concentration trends [33]. That

is, when the exhaust valve opens, plugs of gas each with a different HC concentration can circulate back-and-forth in front of the transfer tube inlet because of the port's pressure oscillations, giving rise to the fluctuations in the FFID data. Another possibility is that the first peak is due to HCs in crevices near the exhaust valve, followed by a dip due to burned gas followed by a second peak due to gases initially in a quench layer or crevice located further away from the exhaust valve. If one of the latter possibilities were the actual explanation of the difference between the sampling unit data and the FFID, then it would mean that the FFID is indeed capable of resolving trends that the sampling valve cannot.

Under low load conditions (for instance, 2.15 bar IMEP), the cylinder pressure is low enough at EVO that the blowdown event causes a relatively small expulsion of gas. Consequently, the amount of HCs stripped from head quench layers and crevices is relatively small, and the HC concentration measured by the FFID and the sampling unit is essentially the same as was measured during the exhaust valve closed period (see figure 6.4). That is, just after EVO, the stagnant plug of gas that sat in the port is not pushed far along the runner, so the inlet of the transfer tube often remains in that stagnant gas; therefore, the FFID and sampling unit read the plateau HC concentration for a short time after EVO.

Under any load, blowdown gas (i.e., the gas emitted immediately after EVO) is found, with 95% certainty, to contain a larger ratio of fuel to non-fuel than the cycle average. This seems to indicate that the HC-rich gases stripped from crevices and quench layers during blowdown are either so hot that they fully oxidize or do not have enough time to oxidize at all. (Figures 6.8 and 6.9 show statistical distributions over ten tests of the non-fuel to fuel HC concentration ratio plotted as the number of standard deviations of that ratio at each CA from the cycle- and mass-averaged ratios, respectively.)

After blowdown and through most of the exhaust process, burned gases, containing a low concentration of HCs, emerge from the cylinder. Therefore, the FFID and the sampling unit register relatively low concentrations of HC throughout most of the exhaust process. Under some engine operating conditions, a small peak in HC concentration is measured by the FFID and the sampling unit during the period in which the burned gases escape the cylinder. It has been suggested that this peak is the result of either a flow reversal during which a plug of gas moves back and forth in the vicinity of the transfer tube [11] or the entrainment of a portion of the piston crevice HCs by bulk exhaust gas flow [7]. One can

conjecture that the peak is more likely due to flow recirculation in the vicinity of the transfer tube. That is, if the flow reversal resulting from the piston's downward motion (see figure 5.1 for the exhaust mass flowrate as a function of CA) caused a peak to move passed the transfer tube at one location, then at a location further downstream, the sampling unit and FFID should pick up two peaks (i.e., the high HC gas passes the transfer tube, then gets sucked backwards, leaving gas with a lower HC concentration in its place, then the high HC gas gets pushed back passed the transfer tube again). This in fact is the case: figure 6.2 shows that the sampling unit and FFID register a slight peak in HC concentration at location B during the flow reversal at 540°CA, while figure 6.5 shows two peaks further downstream at location C under the same engine operating conditions.

Trends in speciated HC concentration during the middle of the exhaust process, when bulk gases escape the cylinder, can be explained as follows. Between the time that the blowdown gas escapes the cylinder to the time that the rolled-up vortex escapes the cylinder, the ratio of non-fuel to fuel concentrations consistently increases. (Refer again to figures 6.8 and 6.9). The increase in the non-fuel to fuel concentration with increasing CA is consistent with the fact that the cylinder temperatures are rapidly dropping, thus causing oxidation reactions to be quenched.

Toward the end of the exhaust process, HC-rich gases are scraped from wall quench layers, released from the piston topland crevice, and rolled into a vortex, which subsequently escapes the cylinder [11]. Hence, just before the exhaust valve closes, the FFID and the sampling unit register a higher concentration of HCs, which persists until the next time the exhaust valve opens. These gases contain the highest ratio of non-fuel to fuel that is observed throughout the cycle (with 95% certainty). This is consistent with the explanation that the HC rich gases released from quench layers along the cylinder wall and from the topland crevice are mixed in the vortex with the hotter bulk gases and begin to undergo oxidation, but as temperatures continue to drop, the oxidation reactions are quenched, leaving intermediates.

6.4 Spatial Trends in Port HC Concentrations

One of the main questions to be answered is: is there a difference in species concentrations between the center of the flow stream and the edges of the port? Specifically, one might expect the edges of the port to be cooler than the center, which would result in a reaction rate gradient across the radius of the port and thus a difference in species concentrations across the port radius. Alternatively, one might expect that the vigorous mixing in the exhaust port would evenly mix the gases so that small or negligible concentration gradients exist across the port radius. By comparing graphs in figures 6.3 and 6.10, which show the speciated concentrations at the top, intermediate top, middle, and bottom of the port (locations B_{top}, B_{inter}, B, and B_{bottom} shown in figure 3.1), one can see that, with the exception of the center location, all traces show roughly the same trends. The center point shows a sharper decrease in HC concentrations during the middle of the exhaust process than the other traces. Despite this difference, however, there is not strong enough evidence to conclude that significant concentration gradients exist across the port radius.

Another question to be answered is: how do species concentrations change axially along the port? Comparison of species concentrations measured at points A, B, and C (as shown in figures 6.7 and 6.11) shows the following trends. As the flow progresses along the port, oxidation results in a 30% to 50% decrease in the total HC concentration as well as a 17% to 23% decrease in the non-fuel HC concentration (fig. 6.7). The fact that the intermediate HCs exhibit a lesser amount of oxidation suggests that some of the fuel oxidized in transit through the port is partially oxidized, and ends up as a non-fuel species upon entering the runner. In fact, comparisons of ethene and propene concentrations at locations A, B, and C in figure 6.7 show that the concentrations can decrease between points A and B (perhaps due to oxidation at high temperatures prevalent between these locations) and can increase between points B and C (perhaps because fuel is being partially oxidized to olefins, which then cannot be oxidized as quickly at the lower temperatures prevalent between these locations). In addition, as the flow progresses along the port, mixing causes the HC versus CA trace to change shape (fig. 6.11). A similar effect was

noted by Finlay *et al.* who demonstrated via a plug flow model that axial mixing is indeed capable of causing the shape change that the FFID measures [11].

Table 6.1 Scaling factor error (FFID output divided by sampling unit output) for various tests

Engine speed (rpm)	IMEP (bar)	Sampling location	Scaling factor error
1500	2.1	B	1.5
1500	3.75	B	0.8
900	3.75	A	0.4
1500	3.75	A	1.0
1500	3.75	B_{inter}	1.3
1500	3.75	B_{top}	0.9
1500	3.75	B_{bottom}	0.7

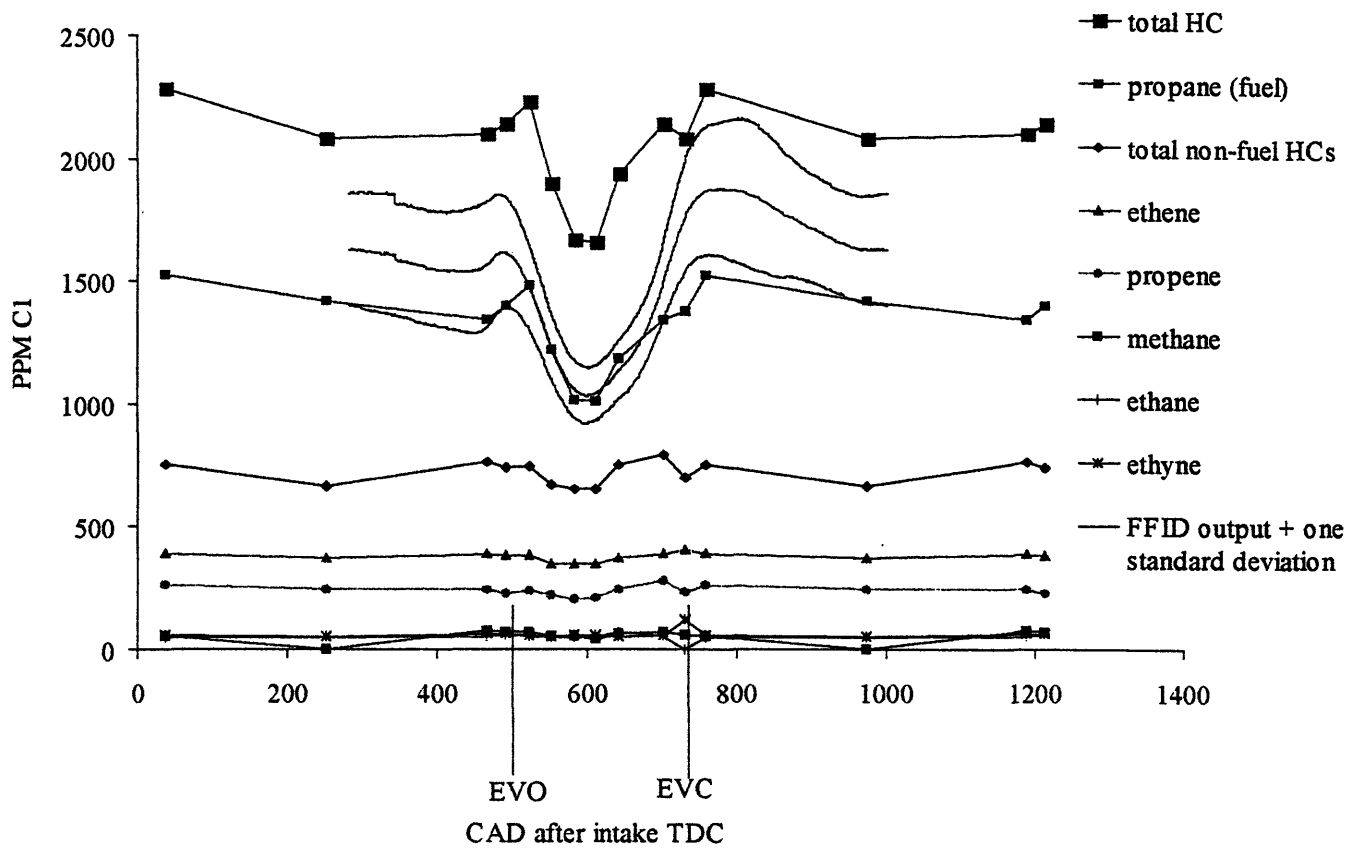

Figure 6.1 HC concentration versus crank angle degree after intake TDC, as measured by sampling unit and FFID. Conditions: 1500 rpm, relative air/fuel ratio λ = 1.10, load = 3.75 bar IMEP. Sampling location B_{top}.

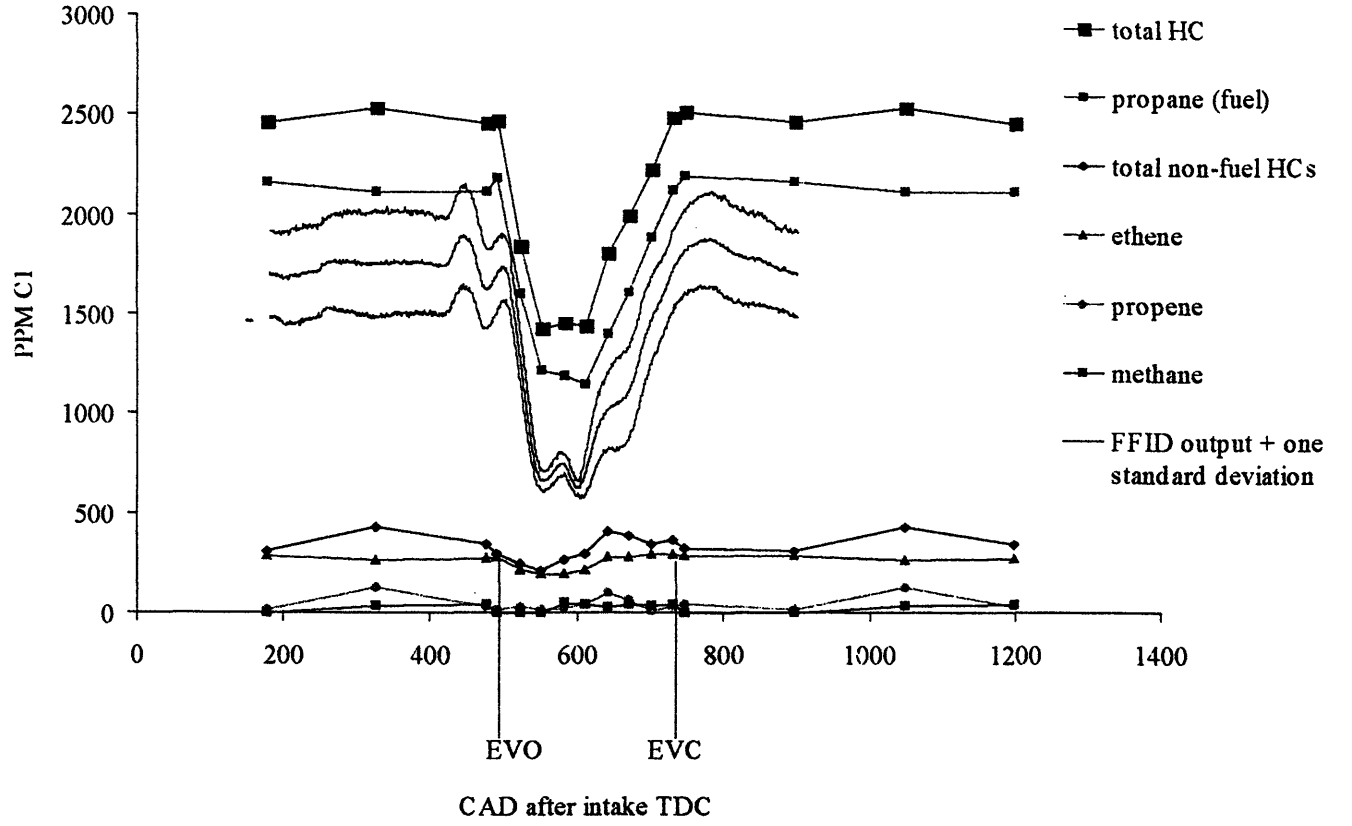

Figure 6.2 HC concentration versus crank angle degree after intake TDC, as measured by sampling unit and FFID. Conditions: 900 rpm, relative air/fuel ratio λ = 1.10, load = 3.75 bar IMEP. Sampling location B.

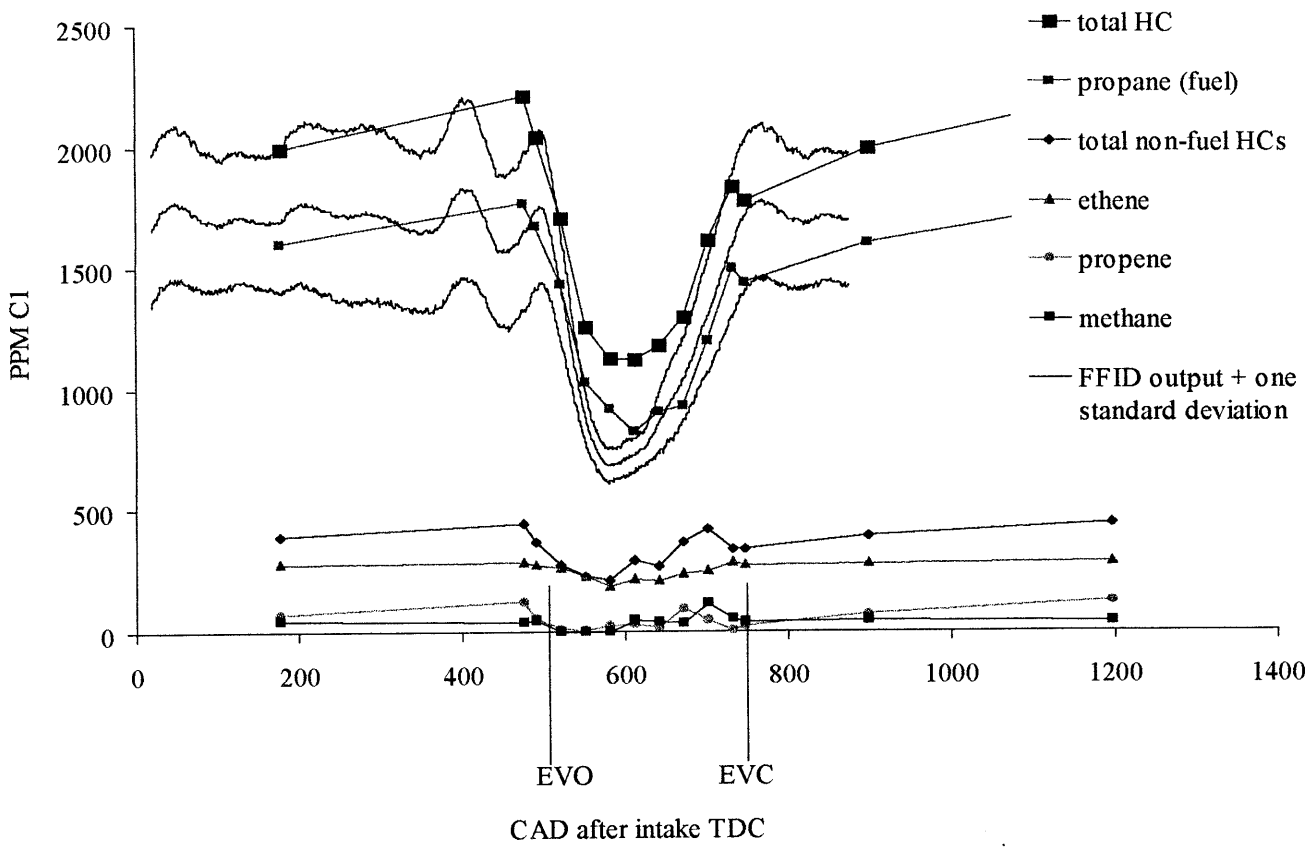

Figure 6.3 HC concentration versus crank angle degree after intake TDC, as measured by sampling unit and FFID. Conditions: 1500 rpm, relative air/fuel ratio λ = 1.10, load = 3.75 bar IMEP. Sampling location B. Baseline conditions.

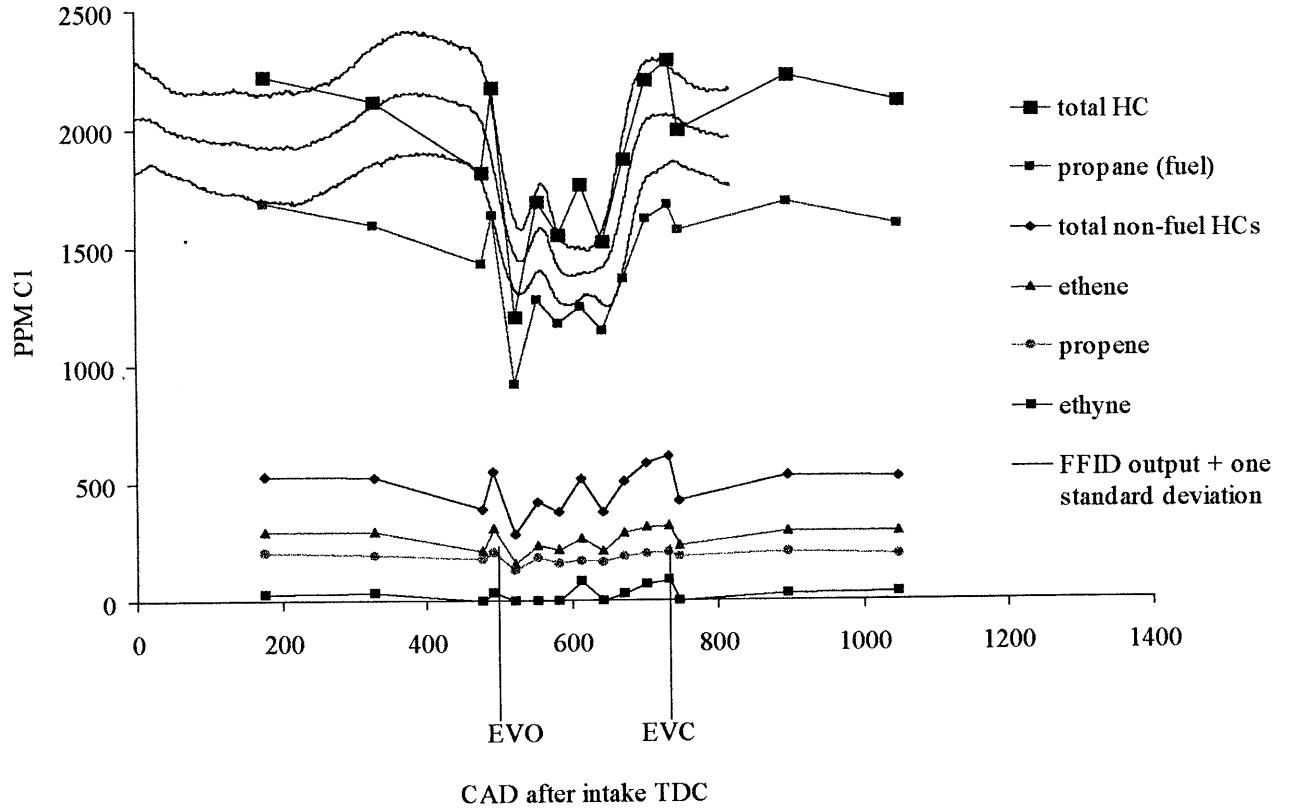

Figure 6.4 HC concentration versus crank angle degree after intake TDC, as measured by sampling unit and FFID. (FFID output scaled due to faulty calibration, for this test only.) Conditions: 900 rpm, relative air/fuel ratio λ = 1.10, load = 2.2 bar IMEP. Sampling location B.

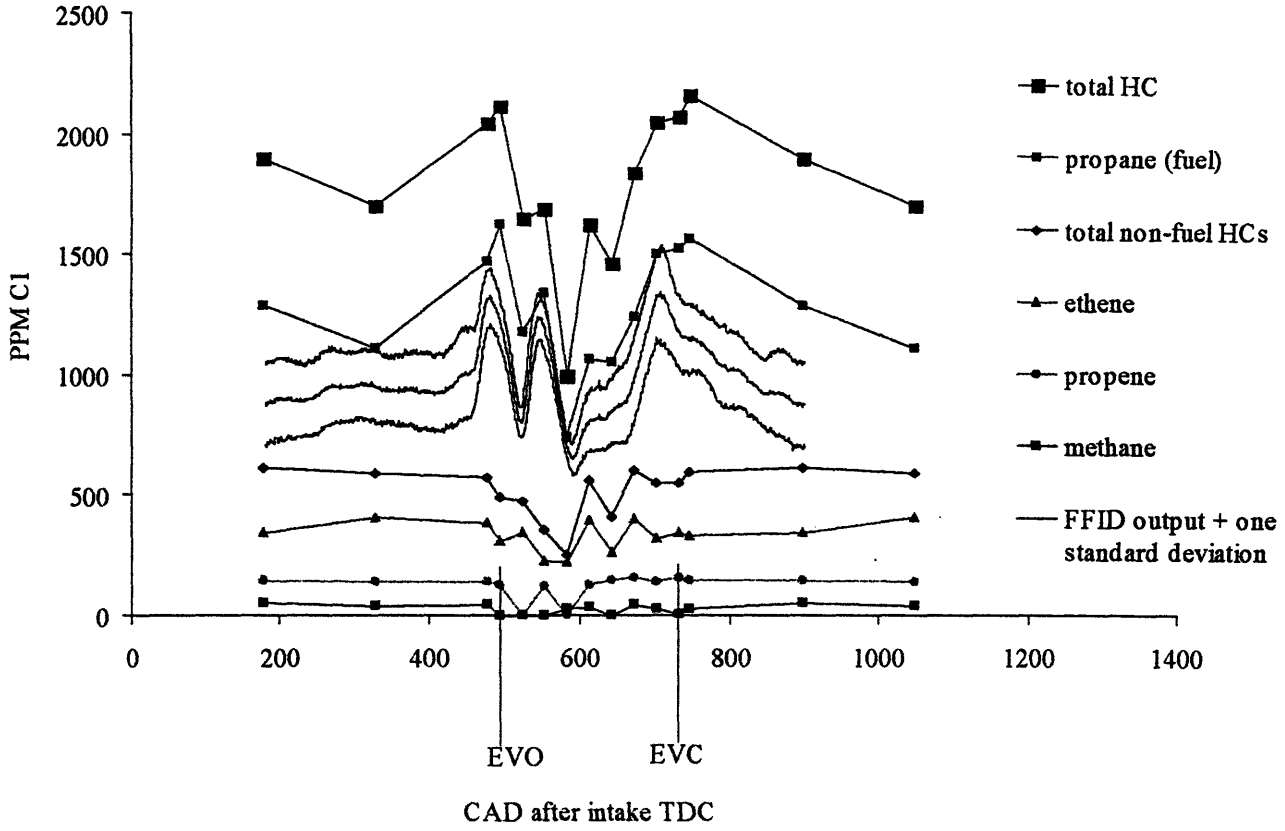

Figure 6.5 HC concentration versus crank angle degree after intake TDC, as measured by sampling unit and FFID. Conditions: 900 rpm, relative air/fuel ratio λ = 1.10, load = 3.75 bar IMEP. Sampling location C.

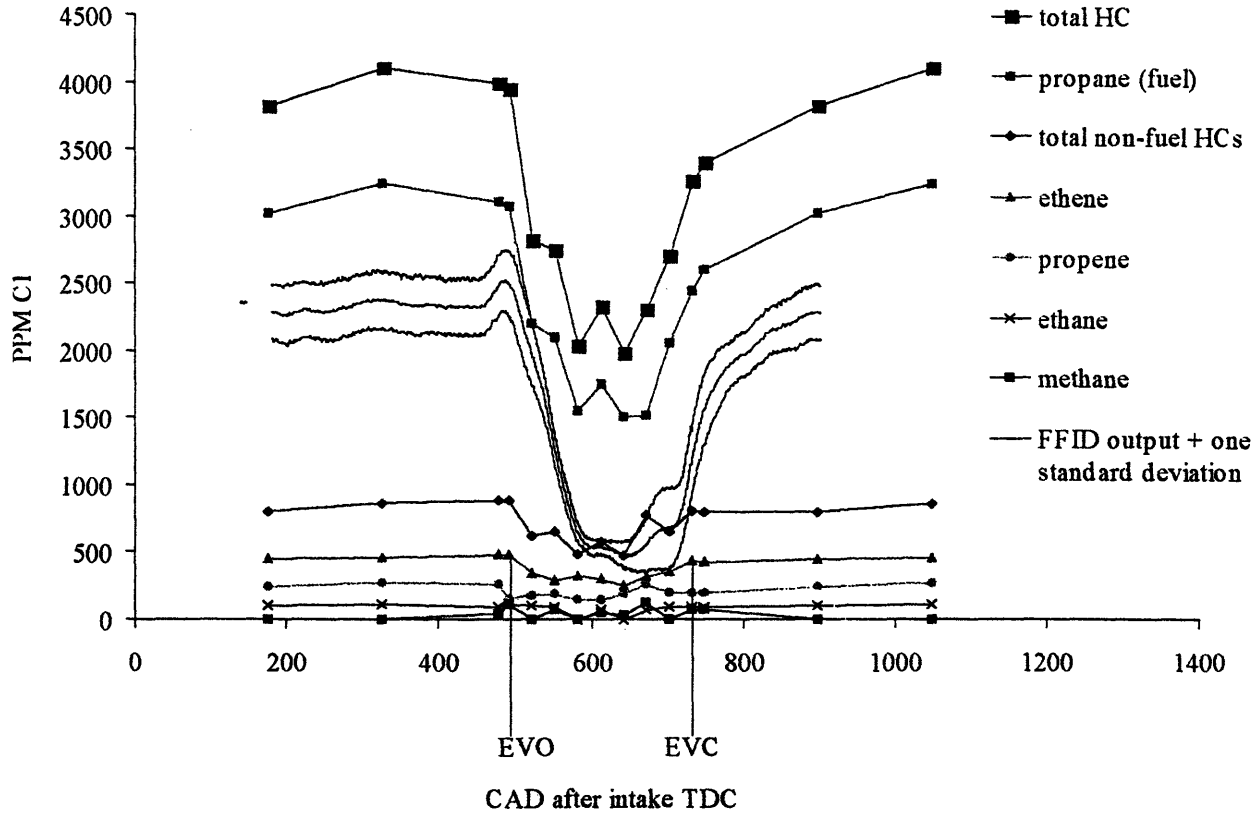

Figure 6.6 HC concentration versus crank angle degree after intake TDC, as measured by sampling unit and FFID. Conditions: 900 rpm, relative air/fuel ratio λ = 1.10, load = 3.75 bar IMEP. Sampling location A.

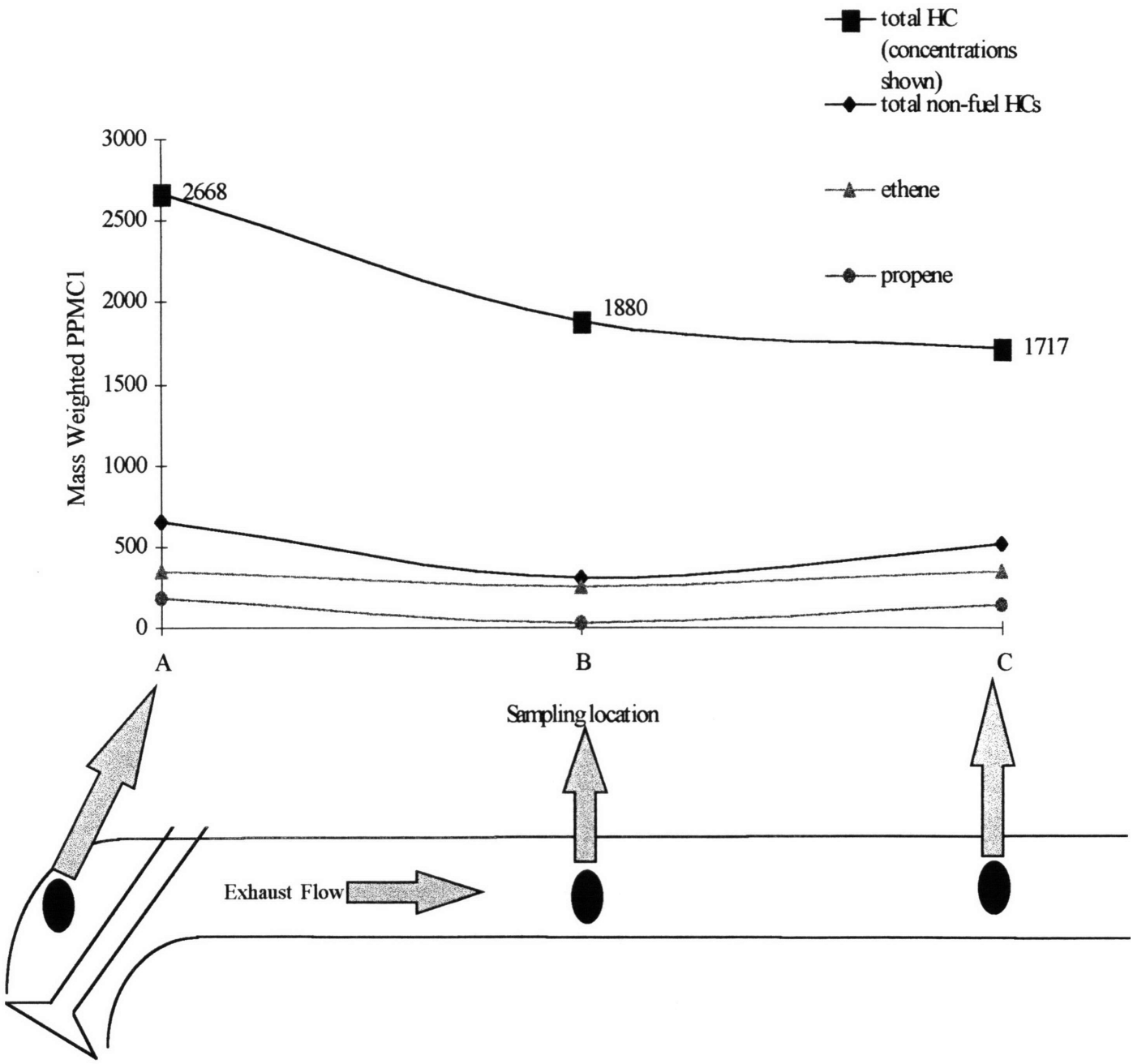

Figure 6.7 Mass weighted concentrations of total HC, total non-fuel HCs, ethene, and propene at three locations along the length of the port/runner. Conditions: 900 rpm, relative air-fuel ratio λ = 1.10, load = 3.75 bar IMEP.

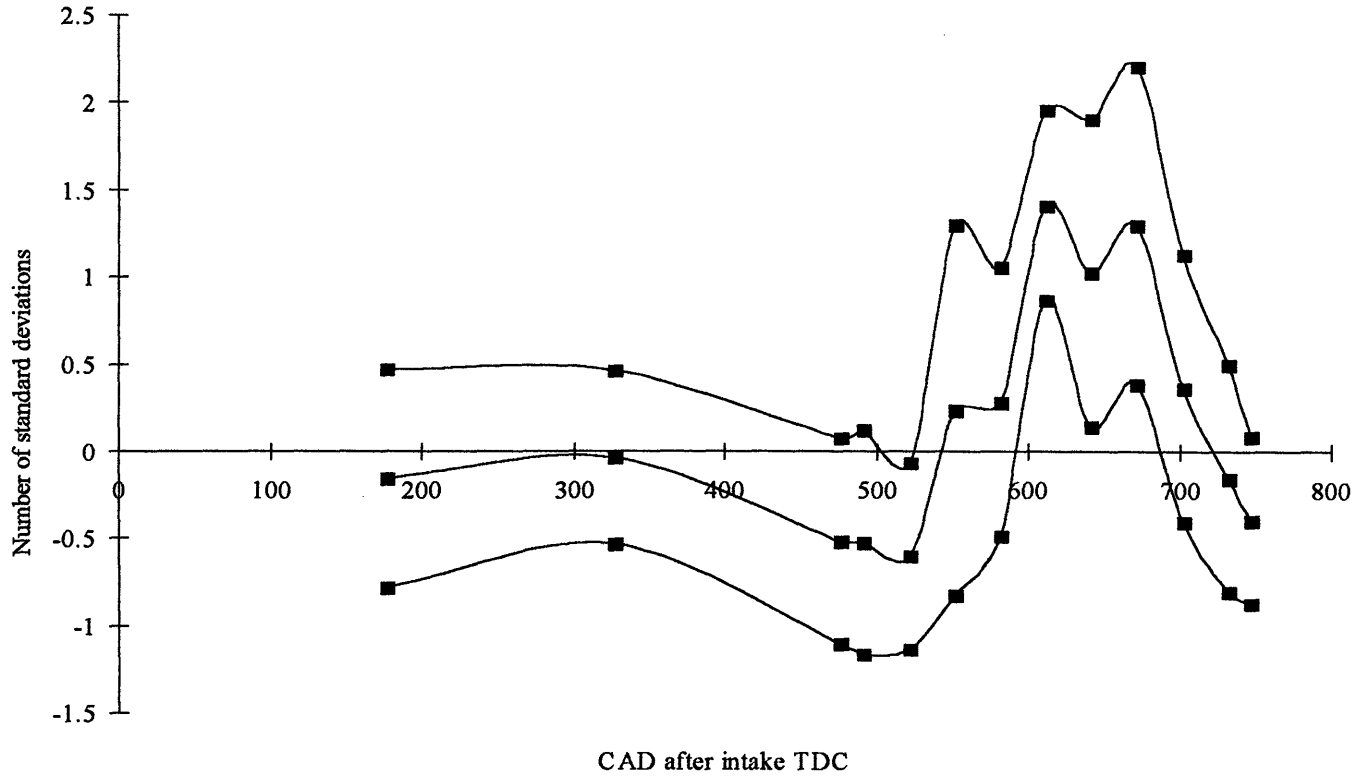

Figure 6.8 Average ratio (plus and minus one standard deviation) of non-fuel HC concentration to fuel HC concentration as a function of crank angle for ten tests, plotted as the number of standard deviations from each test's crank angle averaged value.

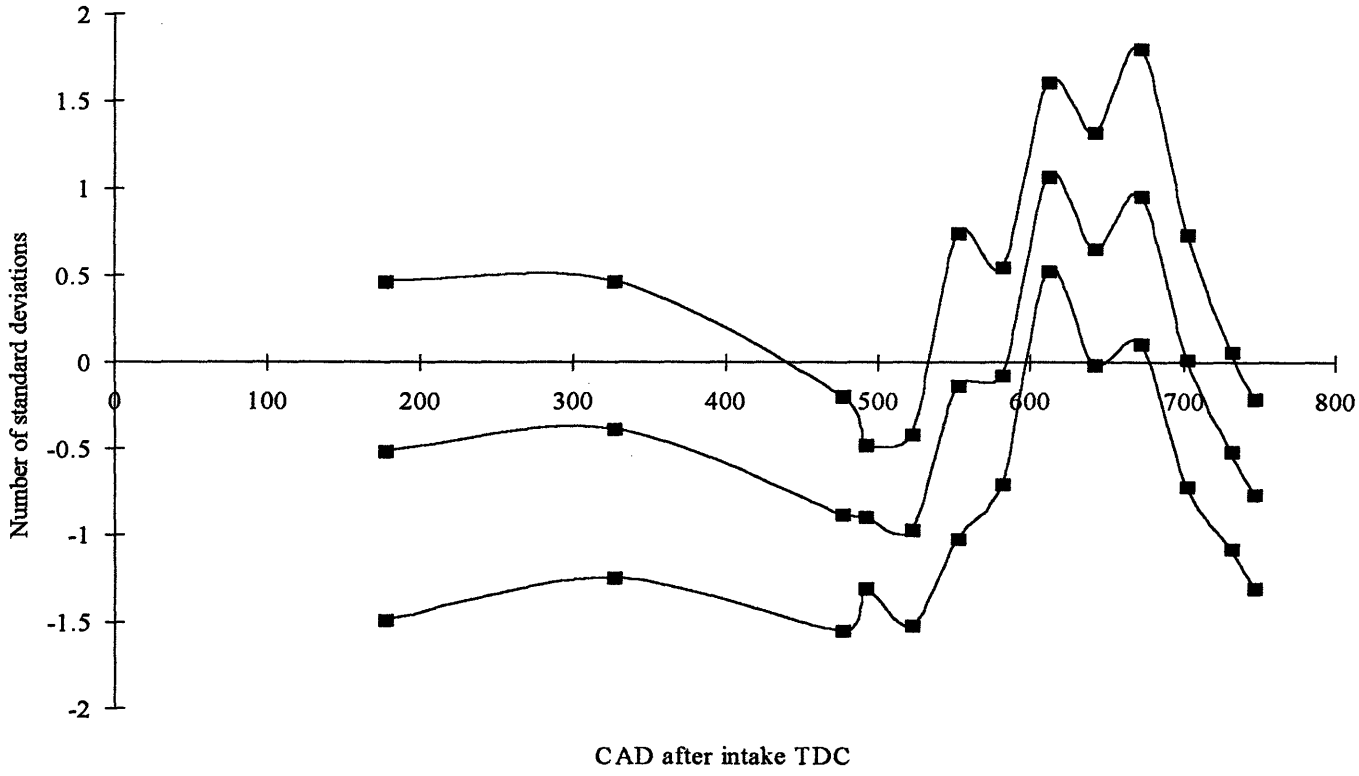

Figure 6.9 Average ratio (plus and minus one standard deviation) of non-fuel HC concentration to fuel HC concentration as a function of crank angle for ten tests, plotted as the number of standard deviations from each test's mass averaged value.

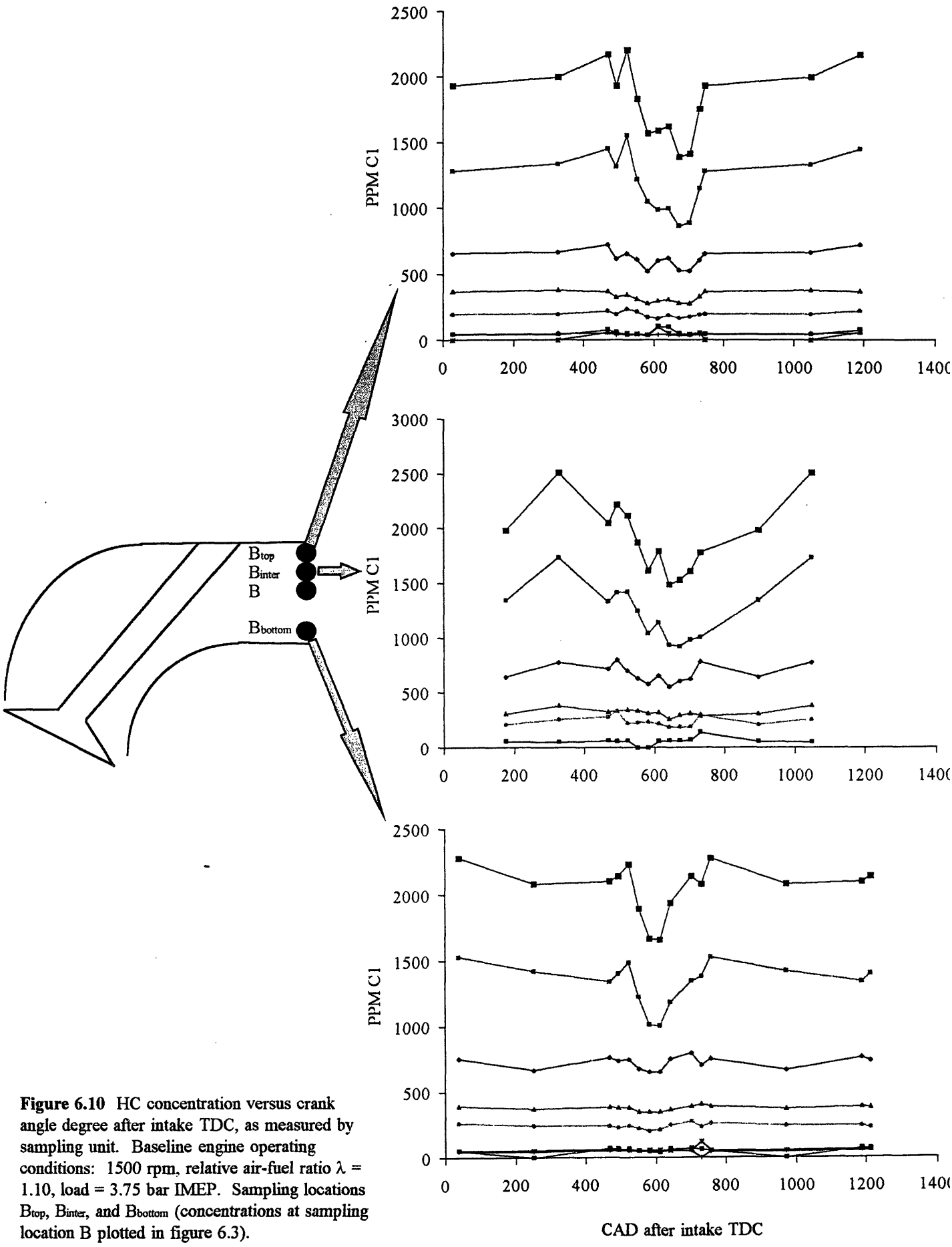

Figure 6.10 HC concentration versus crank angle degree after intake TDC, as measured by sampling unit. Baseline engine operating conditions: 1500 rpm, relative air-fuel ratio λ = 1.10, load = 3.75 bar IMEP. Sampling locations B_{top}, B_{inter}, and B_{bottom} (concentrations at sampling location B plotted in figure 6.3).

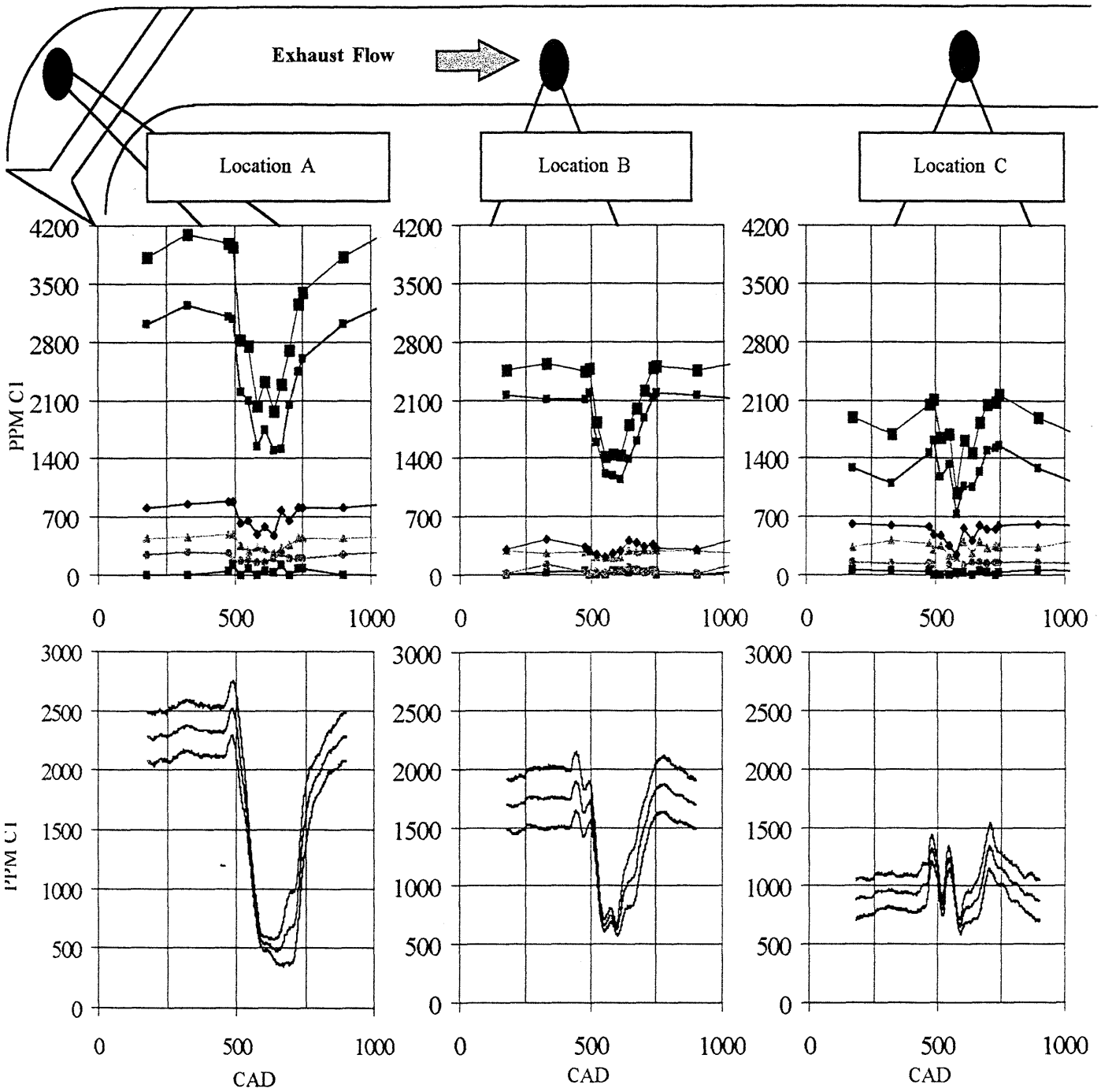

Figure 6.11 HC concentration versus crank angle degree after intake TDC as measured by the sampling unit (top) and FFID (bottom). Symbols represent same variables as in previous figures.
Conditions: 900 rpm, relative air/fuel ratio λ = 1.10, load = 3.75 bar IMEP.

CHAPTER 7

FUEL EFFECTS AT FIXED ENGINE OPERATING CONDITIONS

In addition to tests at different engine operating conditions and sampling locations using propane fuel, a limited number of tests were performed at the baseline conditions using liquid fuels to see if they show the same crank angle resolved trends in species concentrations as does propane. As will be shown in this section, the trends in crank angle resolved speciated concentrations for the liquid fuels are similar to those of propane, and the few differences can be explained in terms of known characteristics of the fuels. Note that liquid fuels have additional mechanisms of unburned HC emission that gaseous fuels do not: liquid fuel can remain as droplets in the cylinder and consequently not undergo complete combustion [5], and liquid fuel can be absorbed into and desorbed from oil layers, while gaseous fuel cannot [6]. As discussed earlier, the fact that the different fuels show similar HC emission trends means that only a limited number of tests need be performed on the liquid fuels, the assumption being that the results of propane tests can be generalized to the liquid fuels as well.

Trends in total and speciated HC concentrations for operation on propane fuel were discussed in section 6.3, but the discussion will be carried one step further here for the sake of comparing to toluene and isooctane emissions. In propane combustion, the intermediate species sampled were ethene, propene, ethyne, methane, and ethane (the former being the most abundant, the latter least). The fractional contribution of each species to the total HC concentration as a function of CA at the baseline operating conditions is shown in figure 7.1. The mass averaged species concentrations measured by the sampling unit at the baseline conditions are shown in figure 7.2. The non-fuel species formed in propane combustion that were measured by the sampling unit are representative of those measured in previous research. In particular, the sampling unit measured the same species in approximately the same relative concentrations as did LoRusso *et al.* and Kaiser *et al.* in tests using propane under similar engine operating conditions [21], [34], with the exception that the author measured ethane while LoRusso *et al.* did not.

Figure 7.3 shows the species concentrations measured in a test in which the engine was fired on toluene fuel at the baseline conditions and in which samples were collected from the base location (B in figure 3.1). As can be seen, toluene exhibits the same trends in total HC concentration as propane. Specifically, near EVO, the total HC concentration in the exhaust decreases; through the exhaust process, the concentration stays low; near EVC, as the rolled-up vortex is being pushed out of the cylinder the concentration increases again; and after the exhaust valve closes, the total HC concentration stays relatively constant until the next time the exhaust valve opens. Unlike propane, however, toluene combustion does not result in a lot of intermediate HCs. In particular, toluene combustion at a lean air-fuel ratio of $\lambda = 1.10$ produces approximately 40 ppmC1 benzene (2% of total HCs) and amounts of methane, ethene, and ethane too small to be measured accurately by the GC. Previous research revealed that toluene combustion does not produce a lot of non-fuel HCs; for example, Kaiser *et al.* sampled the exhaust gas from the runner while operating a similar engine at the same engine operating conditions on toluene fuel and found that the toluene made up 83% of the HCs sampled (on a ppmC1 basis), 6% of the HCs were benzene, and about 1% were methane [21]. The results of the author's experiment were questioned because of the ratio of non-fuel concentration to fuel concentration is quite low relative to that found in previous research. Therefore, samples were taken at a variety of CAs with the engine running rich to see if a larger amount of non-fuel species would be sampled. The results showed that at a relative air-fuel ratio of $\lambda = 0.90$, approximately 91% to 97% of the HCs sampled were toluene, 2% to 5% were benzene, and 1% were methane, ethene, and ethane. It is believed that the difference between the ratio of non-fuel to fuel HCs sampled by the author and by Kaiser *et al.* is due to the fact that the author was sampling from a location very close to the exhaust valve, while Kaiser *et al.* were sampling from a location further downstream in the runner. Hence, the author did not allow as much time for the partial oxidation that occurs in transit through the exhaust port as did Kaiser and thus should not measure as high a ratio of non-fuel to fuel.

Figure 7.4 shows the species concentrations measured at the base location in a test in which the engine was fired on isooctane fuel at the baseline engine operating conditions. As can be seen, isooctane

exhibits the same trends in total HC concentration as do propane and toluene. The most significant difference, however, is that isooctane combustion results in a lot more intermediate HC species than either propane or toluene. Since the intermediate species are too numerous to fit on figure 7.4, concentrations of the non-fuel species sampled at one representative CA, 492° CA corresponding to EVO, are plotted separately in figure 7.5. The most concentrated species sampled — methane, ethene, propene, isobutene, ethyne, and unburned isooctane — are the same as those measured in similar experiments by Kaiser *et al.*, Ninomiya and Golovoy, and Dempster and Shore [21], [22], [23]. The fractional contribution of each HC class (split up by fuel paraffins, non-fuel paraffins, olefins, and acetylenes) to the total HC concentration as a function of CA at the baseline engine operating conditions is shown in figure 7.6. The mass averaged concentrations of each HC family measured by the sampling unit at the baseline conditions are shown in figure 7.7. Non-fuel species contribute 41% to the total HC concentration (on a mass-averaged ppmC1 basis). Kaiser *et al.* found that, when operating on isooctane fuel at similar operating conditions, approximately 50% of the total HC concentration came from non-fuel species [21]. As described above, the difference between these results could perhaps be due to the fact that Kaiser *et al.* sampled further along the runner than the author did and hence allowed more time for partial oxidation of the fuel species.

For all three fuels, the ratio of non-fuel to fuel follows almost the same cyclic trends, although the magnitude of that ratio varies by fuel (as discussed above). Furthermore, for all three fuels, the ratio of non-fuel to fuel at any one CA does not vary significantly from the cycle average. Nonetheless, for all three fuels, the rolled-up vortex (600° CA through EVC) contains slightly more non-fuel than the cycle average. For both propane and isooctane, there is a slightly lower ratio of non-fuel to fuel at EVO than during the bulk flow. Plus, as the exhaust process proceeds and the temperature drops, the ratio of non-fuel to fuel increases. Propane is not absorbed and desorbed from the oil layer, while isooctane and toluene are [6]; yet, no significant difference between the ratio of non-fuel to fuel is noted during the time at which bulk gases escape the cylinder. Consequently, no strong conclusions can be drawn about the amount of partial oxidation undergone by HCs desorbed from the oil layer.

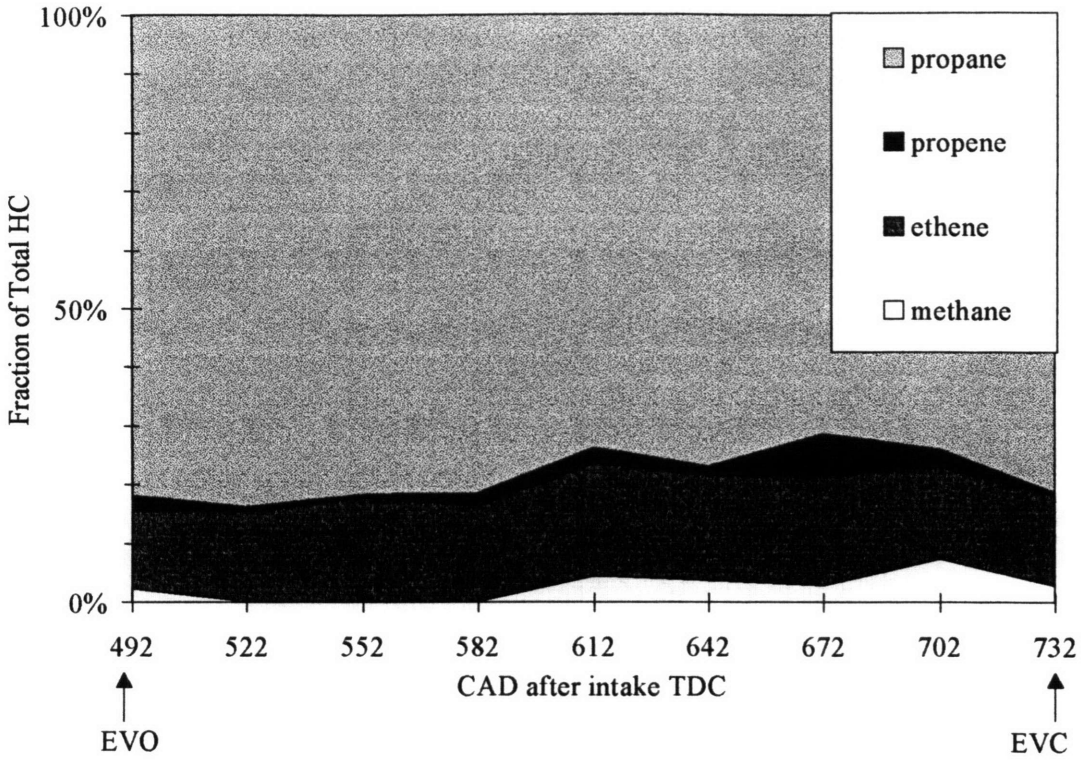

Figure 7.1 Fraction of total HC concentration comprised by each HC species versus crank angle degree after intake TDC. Baseline engine operating conditions, sampling location B.

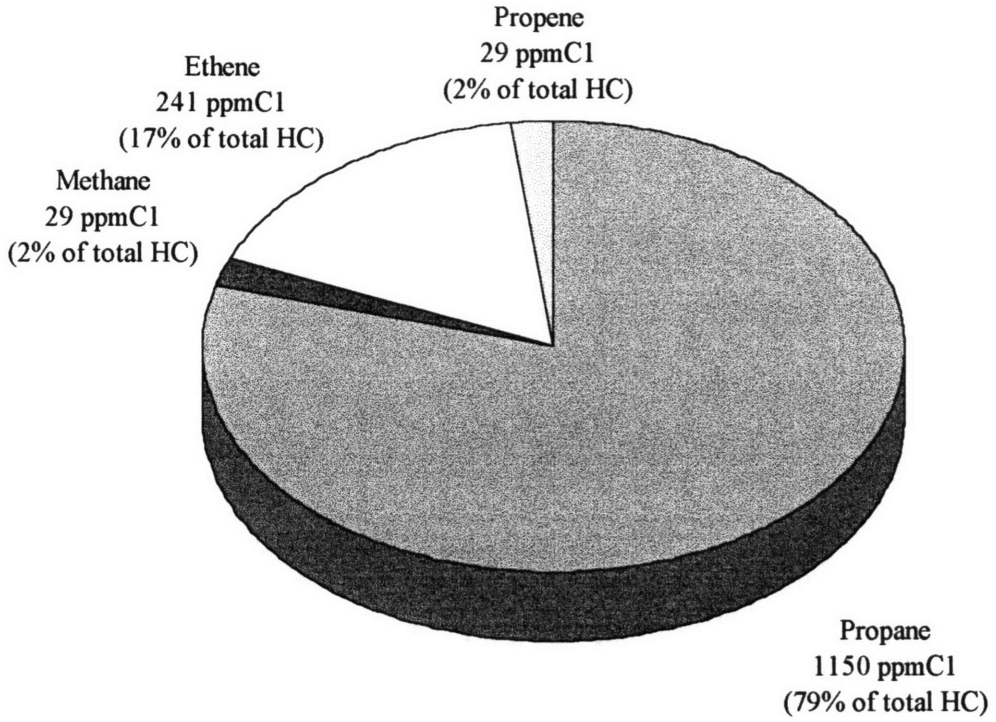

Figure 7.2 Mass averaged species concentrations and fractions of total HC concentration comprised by each HC species. Baseline engine operating conditions, sampling location B.

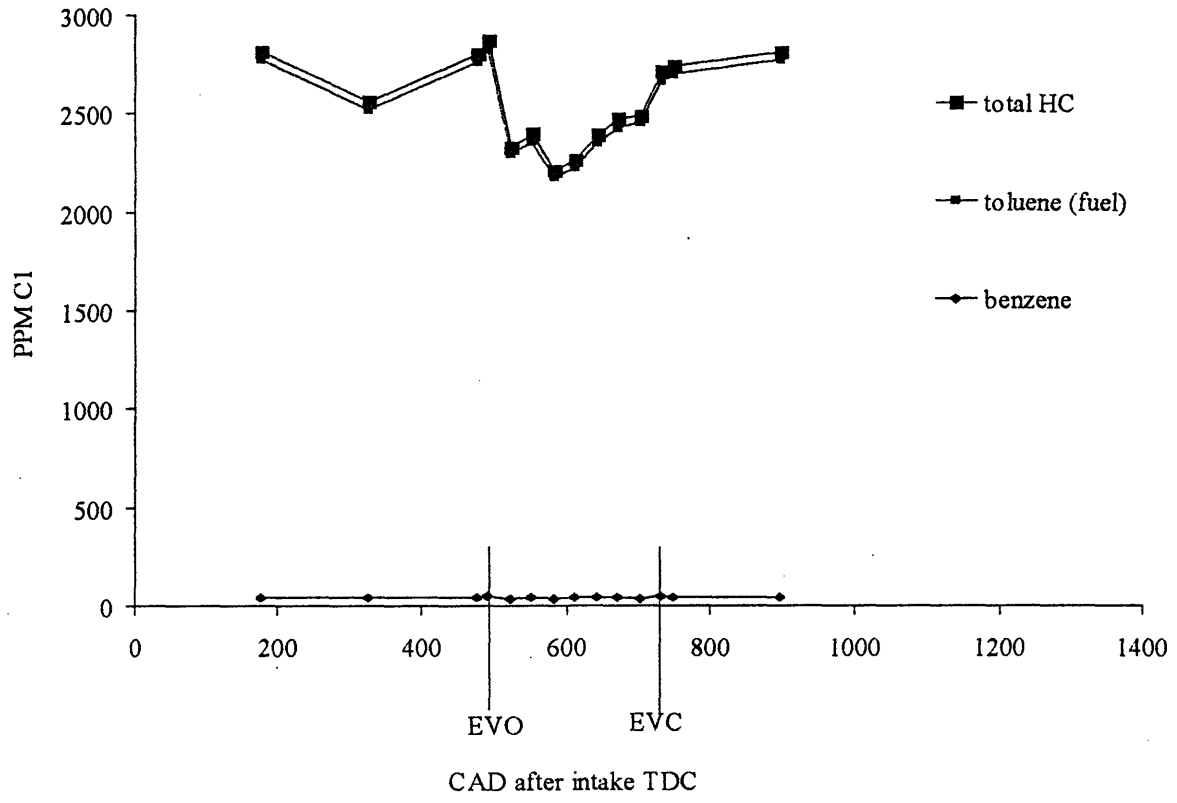

Figure 7.3 HC concentration versus crank angle degree after intake TDC, as measured by the sampling unit in a test using toluene fuel. Baseline engine operating conditions, sampling location B.

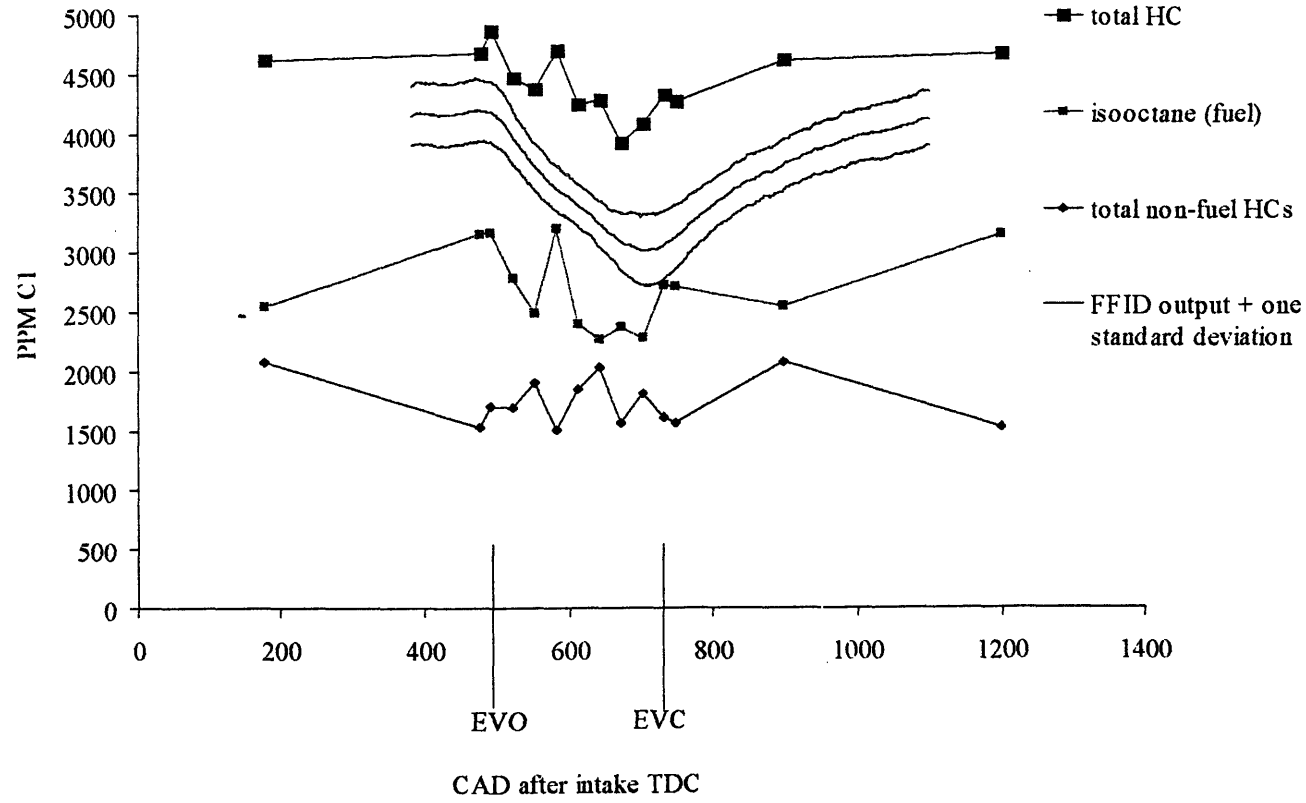

Figure 7.4 HC concentration versus crank angle degree after intake TDC, as measured by the sampling unit in a test using isooctane fuel. Baseline engine operating conditions, sampling location B.

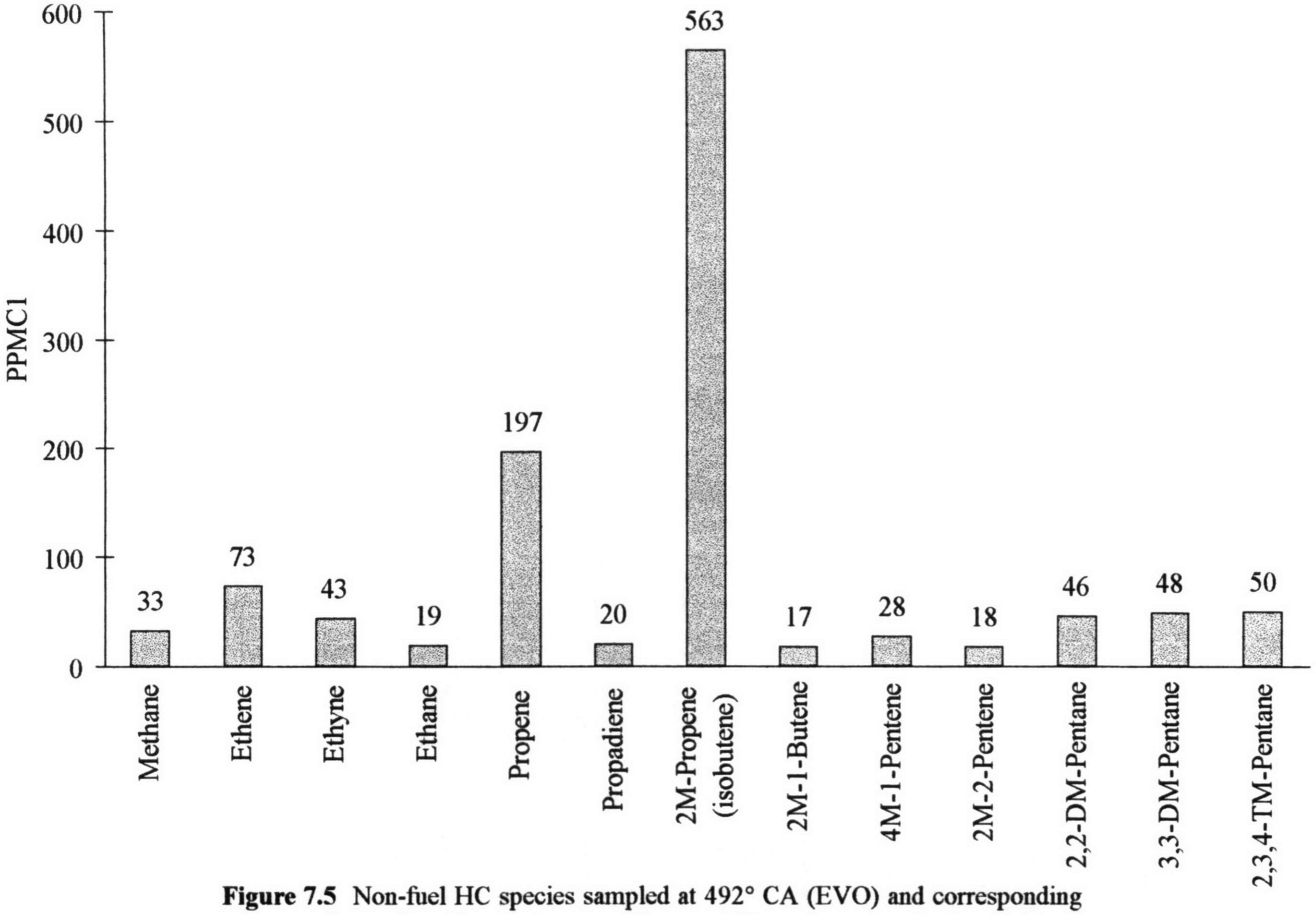

Figure 7.5 Non-fuel HC species sampled at 492° CA (EVO) and corresponding concentrations. Baseline engine operating conditions, isooctane fuel, sampling location B.

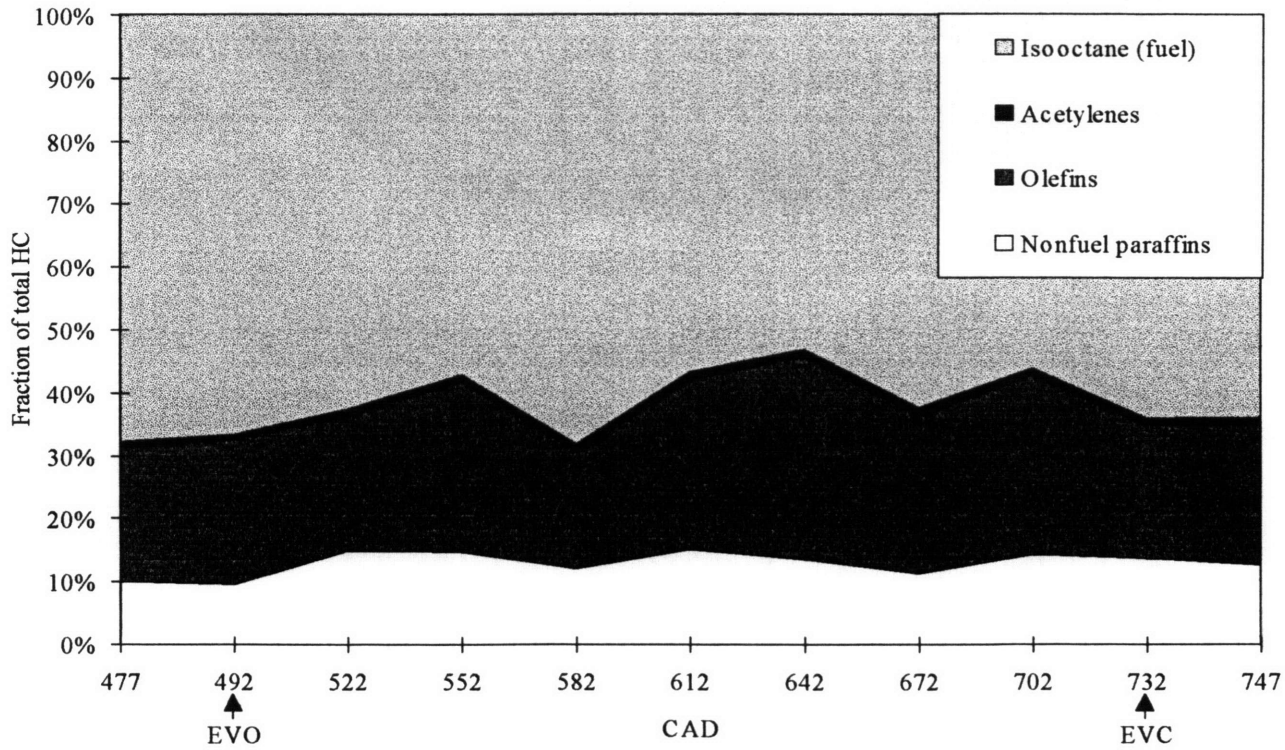

Figure 7.6 Fraction of total HC concentration comprised by each HC class (paraffins separated into fuel and non-fuel components). Baseline engine operating conditions, isooctane fuel, sampling location B.

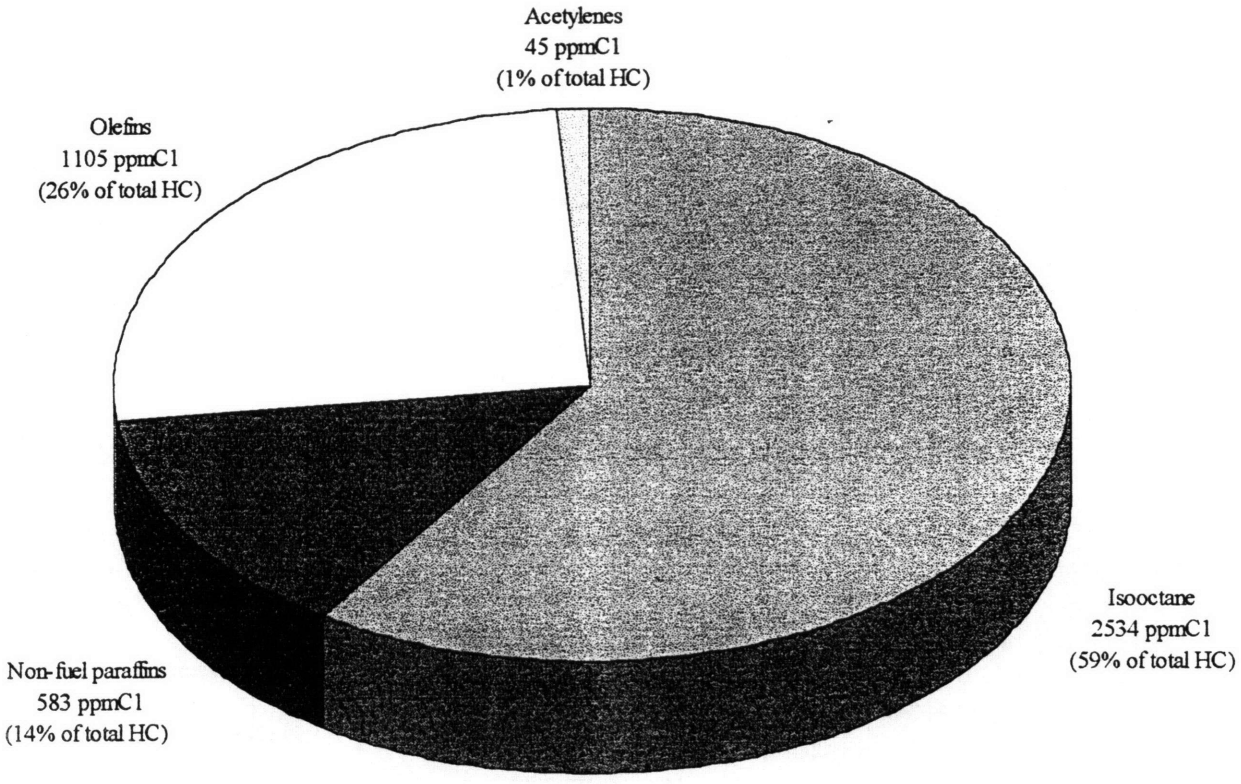

Figure 7.7 Mass averaged concentrations of each HC class (paraffins divided into fuel and non-fuel) and corresponding fraction of total HC mass. Baseline engine operating conditions, isooctane fuel, sampling location B.

CHAPTER 8

EFFECT OF ENGINE OPERATING CONDITIONS USING PROPANE FUEL

This section details trends in HC concentration with respect to engine operating conditions such as speed, load, and air-fuel ratio, focusing on the trends in CA-resolved total HC and speciated HC concentrations as well as mass averaged HC concentrations.

8.1 Engine Speed

The following is a comparison of total HC concentrations at two speeds and comparison of these results to those of previous researchers. Data taken by the sampling unit from the base location in the port (location B) shows a 4.2% to 4.6% decrease in total HC concentration per 100 rpm increase in engine speed, based on an average of the concentration changes at individual CAs. (Comparison between the CA-resolved total HC concentration at speeds of 900 rpm and 1500 rpm measured at location B is shown in figure 8.1.) Similarly, data taken by the sampling unit from the base location in the port shows a 4.3% to 4.7% decrease in total HC concentration per 100 rpm increase in engine speed, based on a weighting of CA-resolved data by the exhaust mass flowrate at those CAs, as described in section 5.3. Drobot found that the change in total HC concentration is approximately 5% to 7% per 100 rpm [18]. Thompson and Wallace found that the change in total HC concentration is approximately 3% per 100 rpm [7]. These data are consistent with the explanation that increased engine speed allows a decreased time for heat transfer and hence increased exhaust gas temperatures, which in turn lead to increased rates of HC oxidation [7].

Next, comparison is made of the trends in non-fuel HC concentrations with respect to engine speed. Using the sampling unit, it has been found that changes in engine speed produce no statistically significant decrease in total non-fuel HC concentrations based on either changes at individual CAs or based on a mass average. (Comparison between the CA-resolved total non-fuel HC concentration at speeds of 900 rpm and 1500 rpm is shown in figure 8.2.) More specifically, for individual species, the

same holds: changes in speed produce no statistically significant drop in individual species concentration either at individual CAs or on a mass averaged basis, although some variations do occur at individual CAs (for example, see figure 8.3 for comparison of CA-resolved ethene concentration at 900 rpm and 1500 rpm). These data are consistent with the explanation that, as the engine speed increases and temperatures increase, intermediate species become more likely to react and form CO and CO_2, but the fuel species also becomes more like to react and replenish the non-fuel species. Note that, because total HC concentration decreases as engine speed increases, while non-fuel HC concentrations (both total and individual species) stay constant, the non-fuel HCs' percent contribution to total HC concentration increases as speed increases.

8.2 Engine Load

The effect of engine load on port HC concentrations is weaker than that of engine speed. When comparing data at individual CAs, the average increase in total HC concentration per bar IMEP increase in load is 2.7% at 900 rpm and 3.1% at 1500 rpm. (Comparison of the CA-resolved total HC concentration at two loads is shown in figure 8.4.) When comparing the data on a mass weighted basis, the increase in total HC concentration per bar IMEP increase in load is 7.7% at 900 rpm and 8.3% at 1500 rpm. The difference between the CA resolved trends and the mass averaged trends is consistent with the fact that the greatest increases in HC concentration per bar IMEP increase in load occur at the later crank angles, i.e. from about 600°CA to EVC, when the mass flow is the largest. Comparison between data taken via the sampling unit and that taken by other researchers is difficult because the trends in HC concentration with respect to load are so weak that the simple difference in engine types is sufficient to explain those differences: Drobot measured roughly a 3.5% increase in total HC concentration per bar IMEP increase in load when firing on propane [18], while Thompson and Wallace measured a 10% decrease per bar increase in load when firing on methane [7]. It is worth noting that, like the data shown in figure 8.4, Thompson and Wallace's CA resolved HC concentrations show higher plateau HC

concentrations and more pronounced drops in concentration during the exhaust process at higher loads [7]. This trend is consistent with the fact that, at lower loads, the larger backflow during the valve overlap period tends to carry back into the cylinder more of the gas with high HC concentration emitted at the end of the exhaust process, thus decreasing the plateau HC level and increasing the cylinder's residual fraction, thereby leading to worse combustion and higher HC concentrations in the bulk gas [7].

Intermediate HC concentrations drop off sharply as the load is increased. When comparing data at individual CAs, the average decrease in non-fuel concentration per bar increase in IMEP is 21% at 900 rpm and 20% at 1500 rpm. (Comparison of the CA-resolved non-fuel concentration at two loads is shown in figure 8.5.) When comparing the data on a mass weighted basis, the decrease in non-fuel HC concentration per bar IMEP increase in load is 17% at 900 rpm and 21% at 1500 rpm.

8.3 Air-fuel ratio

Tests using the sampling unit show that as the relative air-fuel ratio (λ) is increased, the HC concentration decreases, as would be expected due to increased availability of oxygen for oxidation reactions [7]. When λ is increased by 0.1 (from 0.9 to 1.0 or from 1.0 to 1.1), the CA-resolved and mass averaged total HC concentrations decrease by approximately 20%. (Comparison of total HC concentrations as a function of CA at three relative air-fuel ratios is shown in figure 8.6. Comparison of total HC concentrations as a function of air-fuel ratio at four CAs is shown in figure 8.7.)

This trend compares favorably with that measured by previous researchers. Drobot's data shows roughly a 19% decrease in cylinder exit total HC concentration per 0.1 increase in λ using propane fuel [18]. Min's data shows a 29% decrease in mass averaged HC concentration per 0.1 increase in λ using propane fuel [12].

Intermediate species exhibit varied concentration trends with respect to air-fuel ratio. (Non-fuel species concentrations as a function of air-fuel ratio are plotted at four CAs in figures 8.8 through 8.11.) Like the fuel species, intermediate species ethyne and methane tend to become less concentrated as the

air-fuel ratio is increased. However, as the air-fuel ratio is increased, the concentration of olefins such as propene and ethene remain constant or even increase. This trend was also observed by Kaiser *et al.* and Dempster and Shore [21], [23]. One possible explanation for the increase in olefin concentration with increasing air-fuel ratio is that as the air-fuel ratio is increased, the greater oxygen concentration facilitates decomposition of the fuel species into intermediate species including olefins, but that olefins simply cannot be oxidized on the time scale of their residence in the engine, even when the oxygen concentration is high. Consequently, as the air-fuel ratio is increased, the amount of fuel transformed into olefins increases more than the amount of olefins that can be transformed into carbon monoxide. The driving factor behind this trend, the incomplete combustion in the cylinder during flame passage, has been demonstrated by LoRusso *et al* [34].

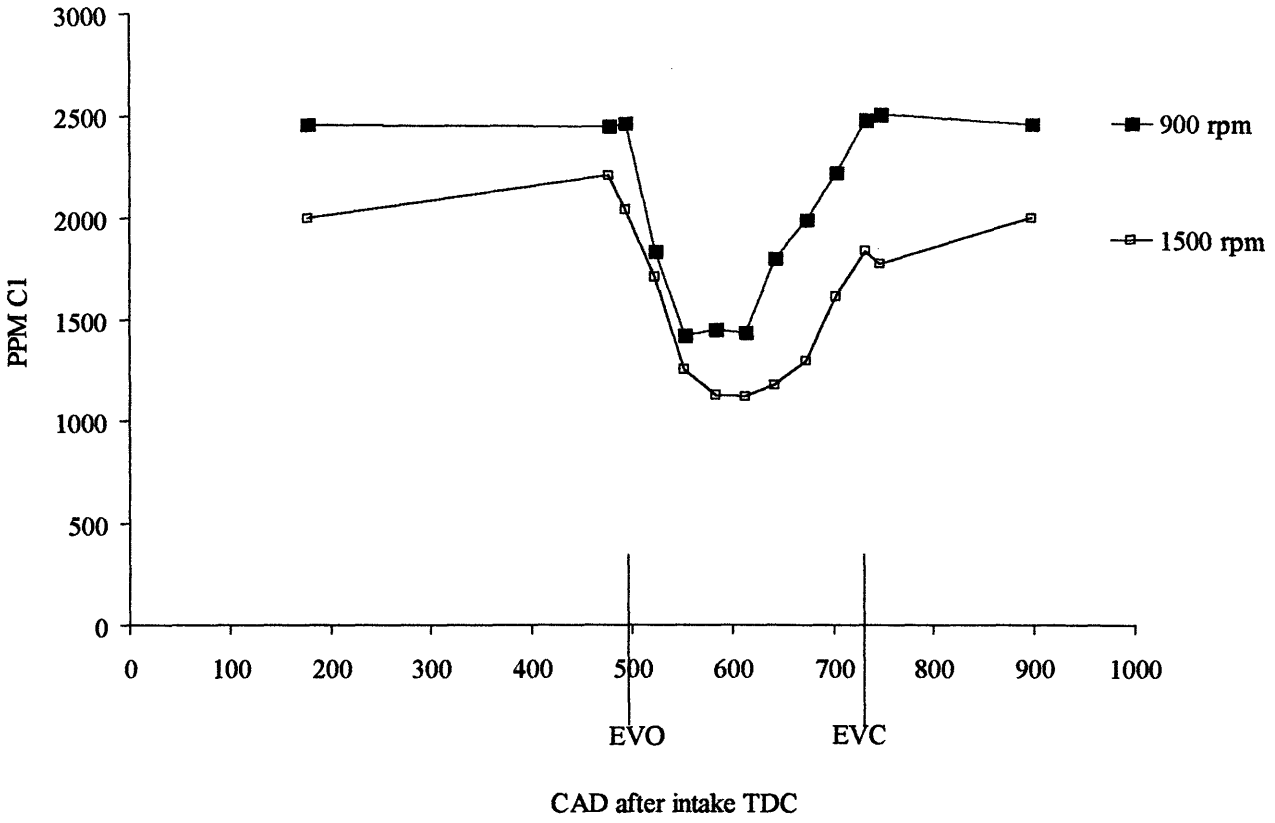

Figure 8.1 Total HC concentration versus crank angle at two engine speeds as measured by the sampling unit. Conditions: 900 and 1500 rpm, relative air-fuel ratio λ = 1.10, load = 3.75 bar IMEP, sampling location B.

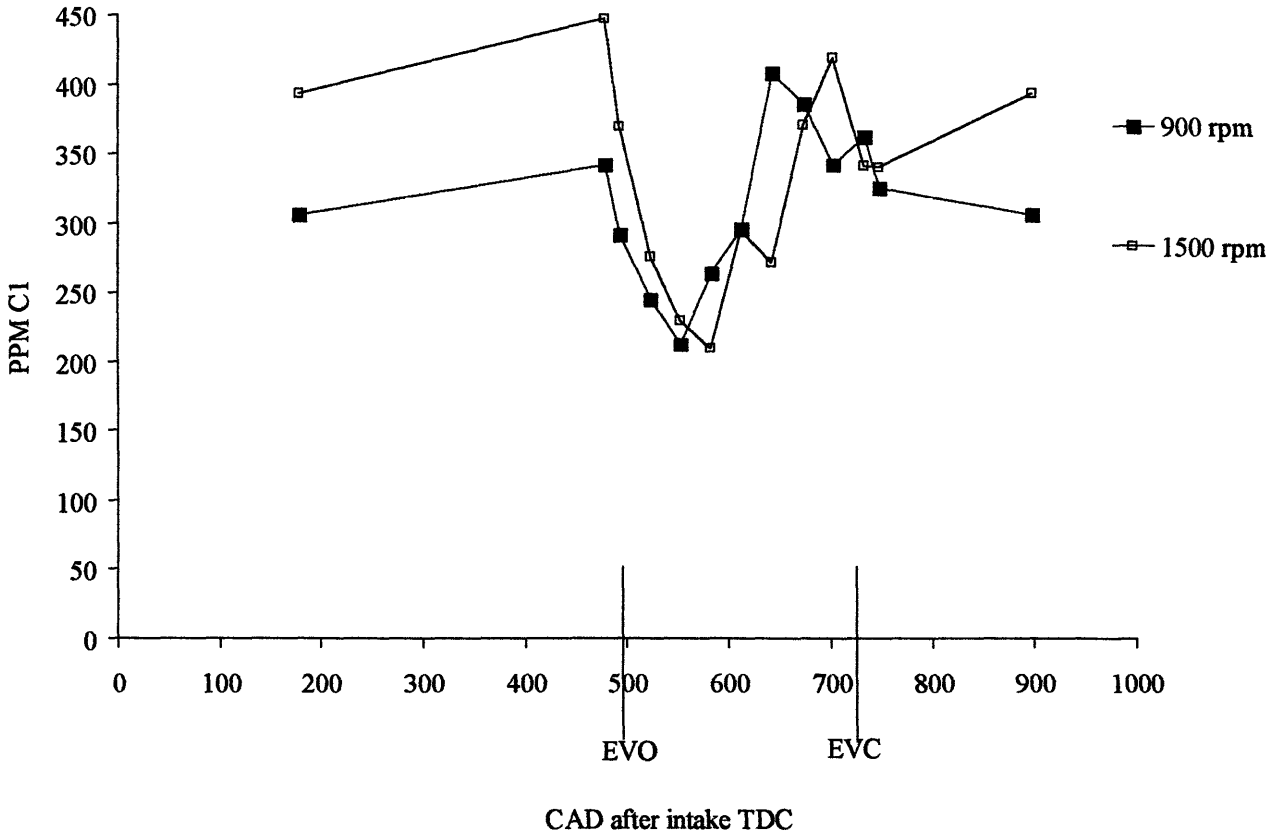

Figure 8.2 Non-fuel HC concentration versus crank angle at two engine speeds as measured by the sampling unit. Conditions: 900 and 1500 rpm, relative air-fuel ratio λ = 1.10, load = 3.75 bar IMEP, sampling location B.

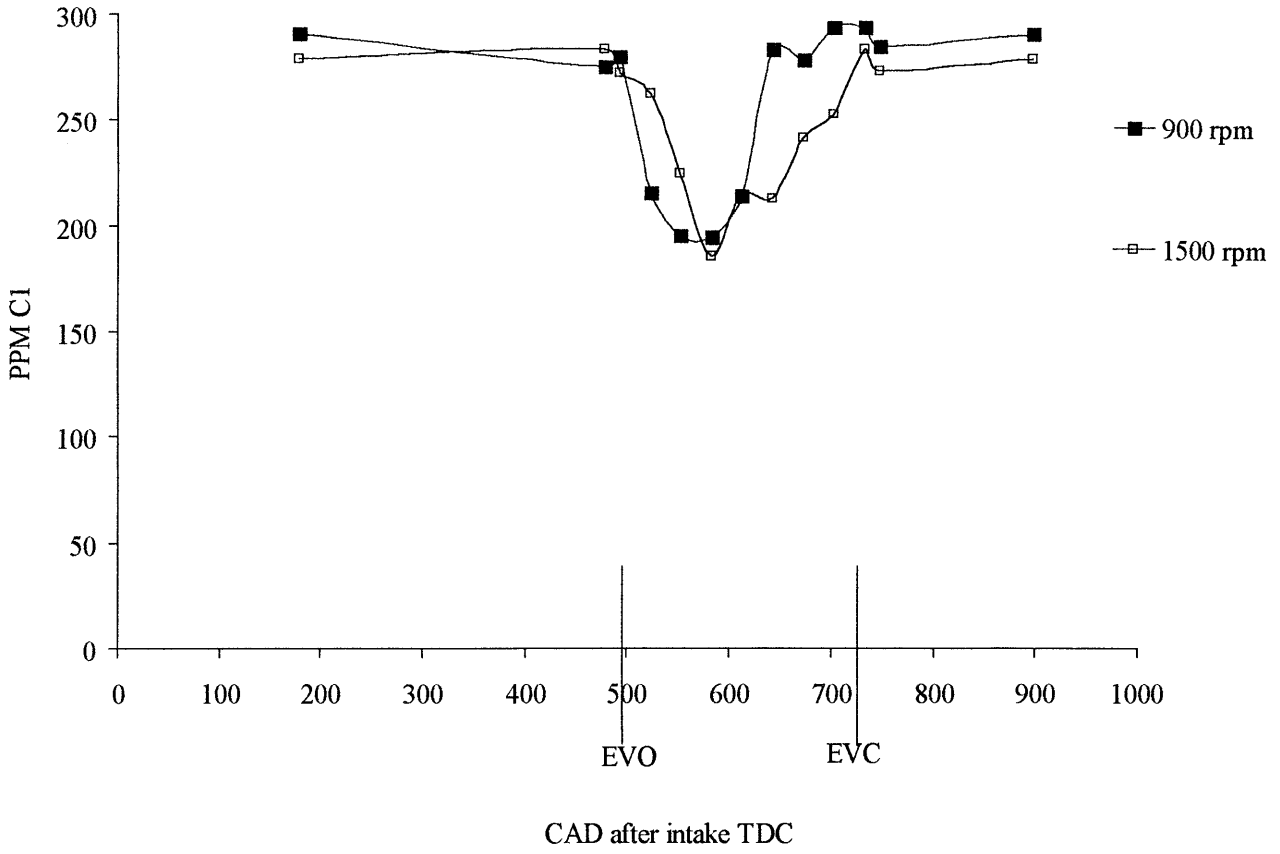

Figure 8.3 Ethene concentration versus crank angle at two engine speeds as measured by the sampling unit. Conditions: 900 and 1500 rpm, relative air-fuel ratio λ = 1.10, load = 3.75 bar IMEP, sampling location B.

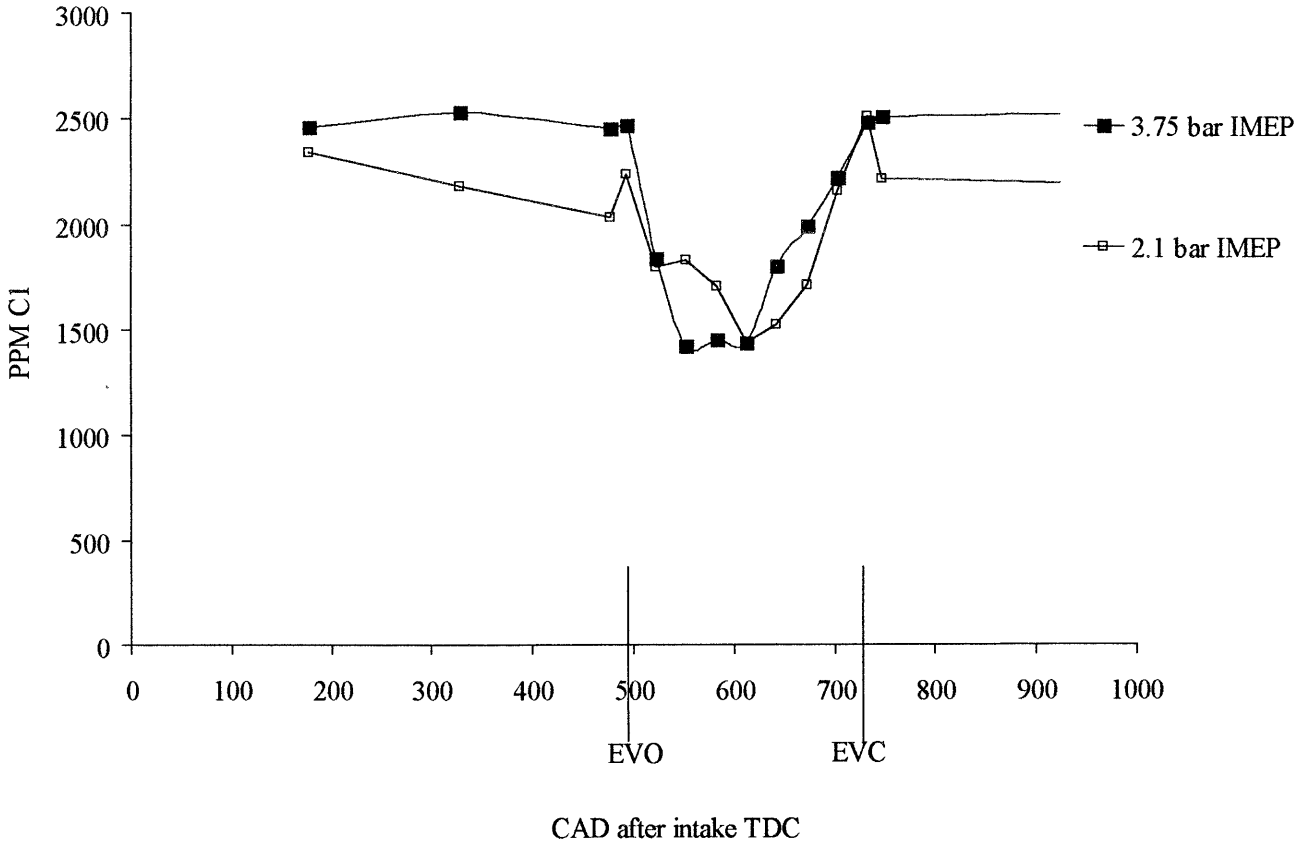

Figure 8.4 Total HC concentration versus crank angle at two engine loads as measured by the sampling unit. Conditions: 900 rpm, relative air-fuel ratio λ = 1.10, loads = 2.1 and 3.75 bar IMEP, sampling location B.

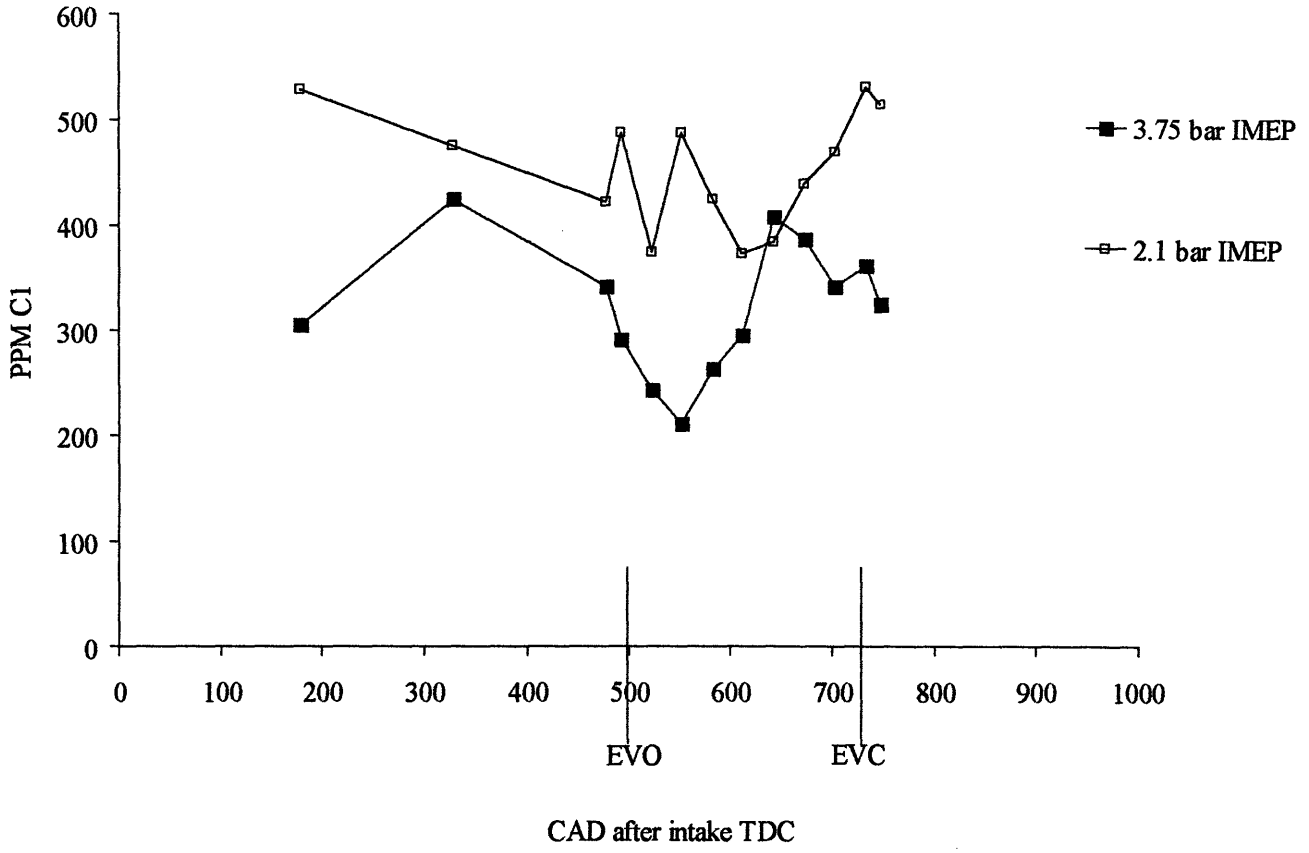

Figure 8.5 Non-fuel HC concentration versus crank angle at two engine loads as measured by the sampling unit. Conditions: 900 rpm, relative air-fuel ratio λ = 1.10, loads = 2.1 and 3.75 bar IMEP, sampling location B.

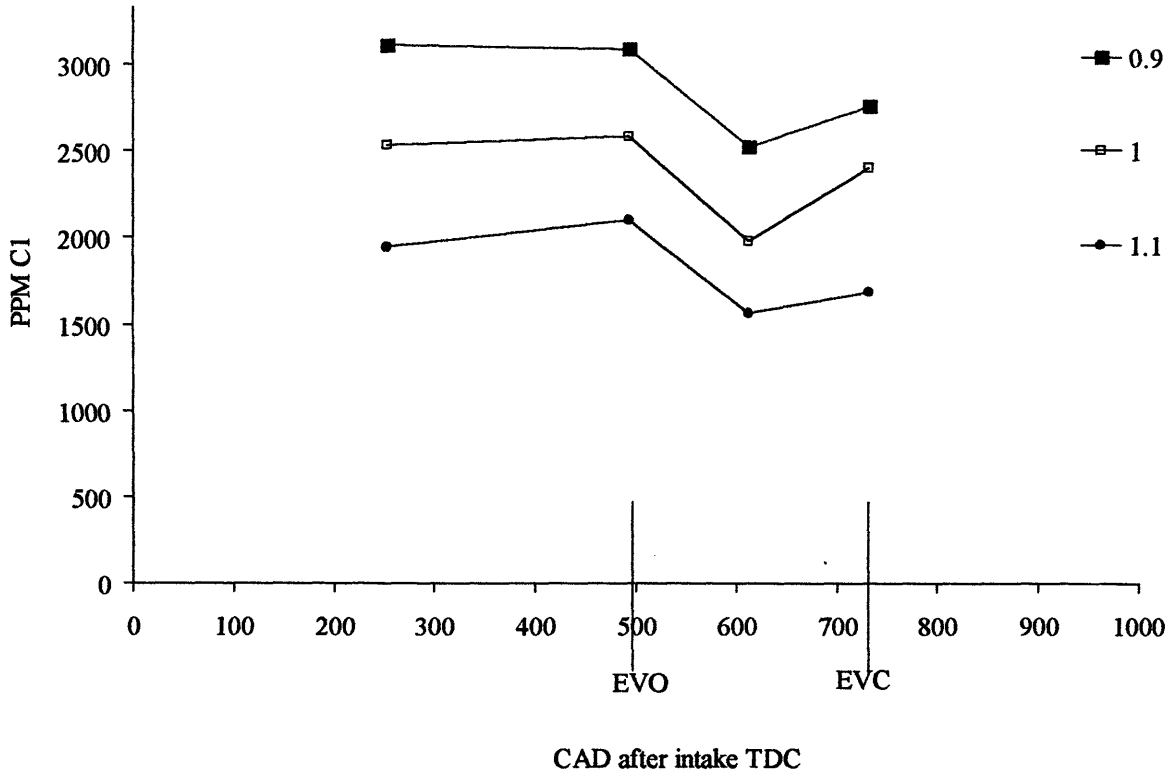

Figure 8.6 Total HC concentration versus crank angle at three relative air-fuel ratios (λ) as measured by the sampling unit. Conditions: 1500 rpm, relative air-fuel ratio λ = 0.90, 1.00, 1.10, load = 3.75 bar IMEP, sampling location B.

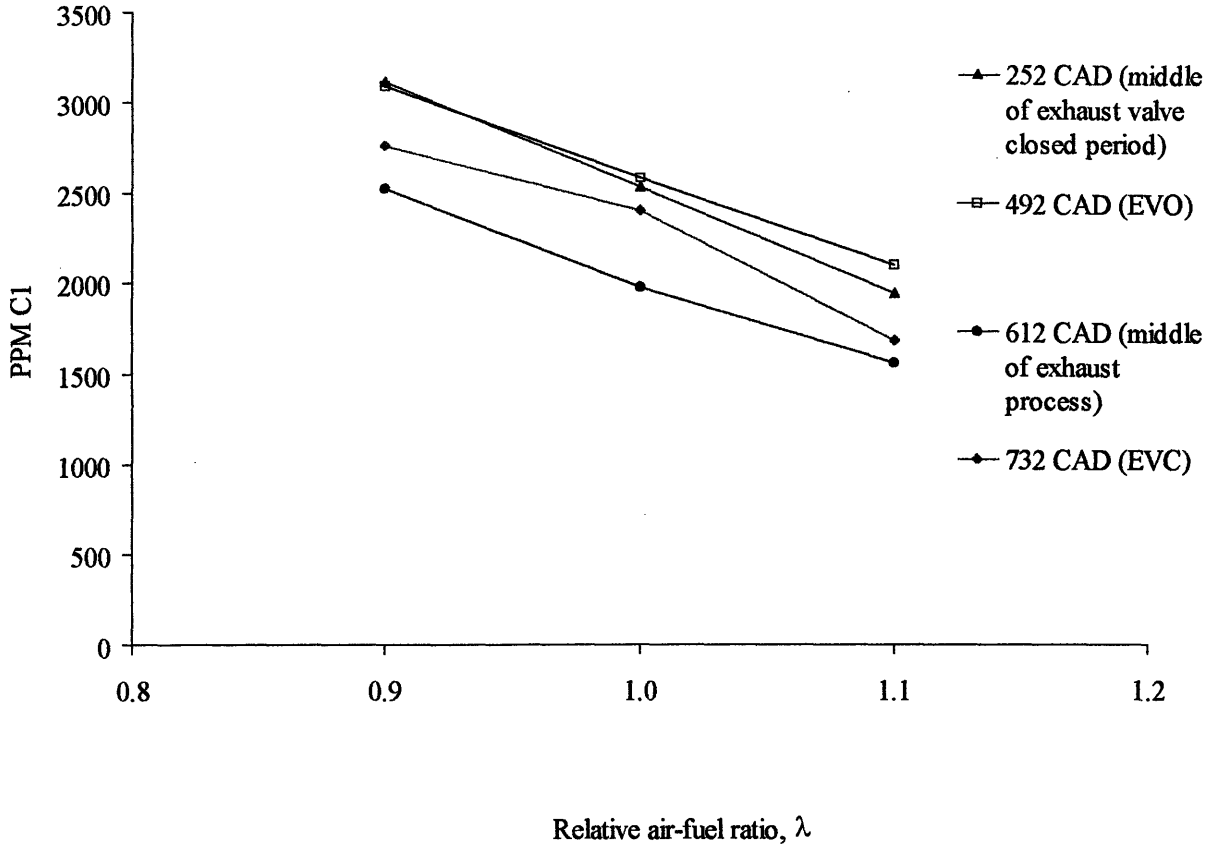

Figure 8.7 Total HC concentration versus relative air-fuel ratio (λ) at four crank angles as measured by the sampling unit. Conditions: 1500 rpm, relative air-fuel ratio λ = 0.90, 1.00, 1.10, load = 3.75 bar IMEP, sampling location B.

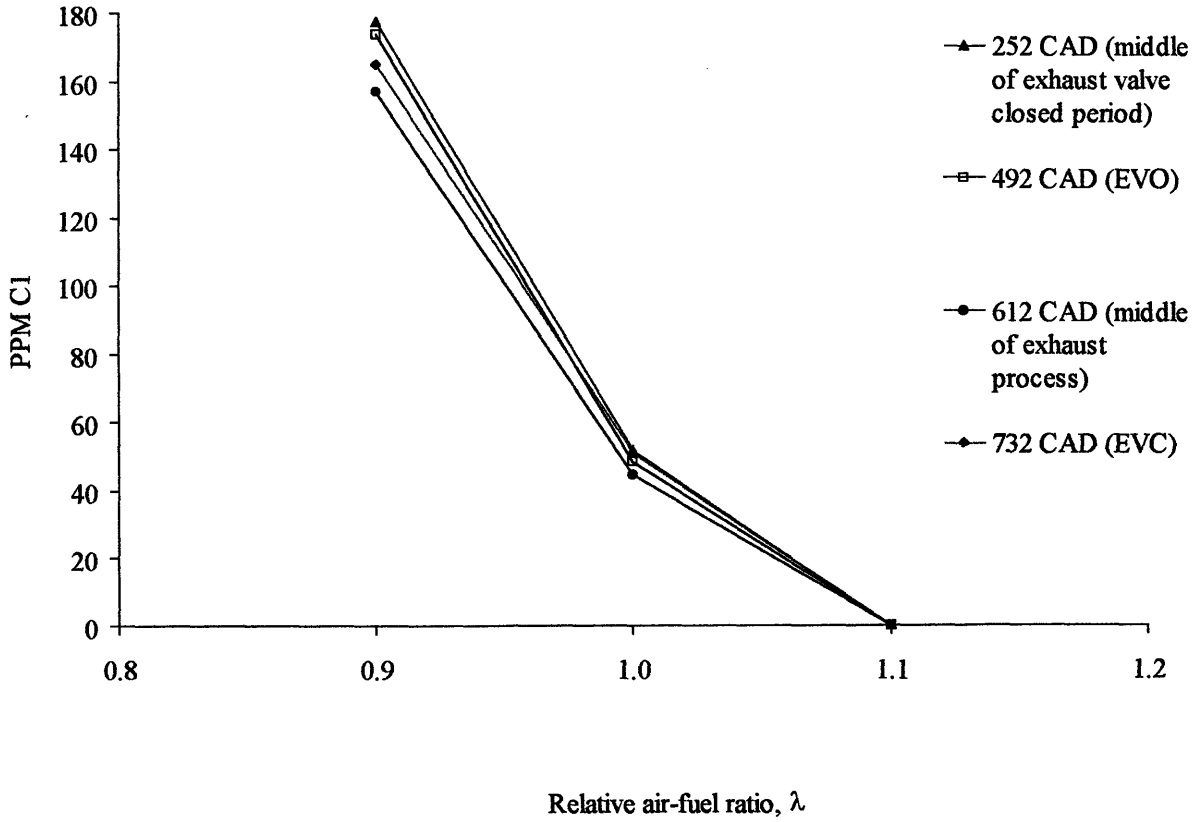

Figure 8.8 Methane concentration versus relative air-fuel ratio (λ) at four crank angles as measured by the sampling unit. Conditions: 1500 rpm, relative air-fuel ratio λ = 0.90, 1.00, 1.10, load = 3.75 bar IMEP, sampling location B.

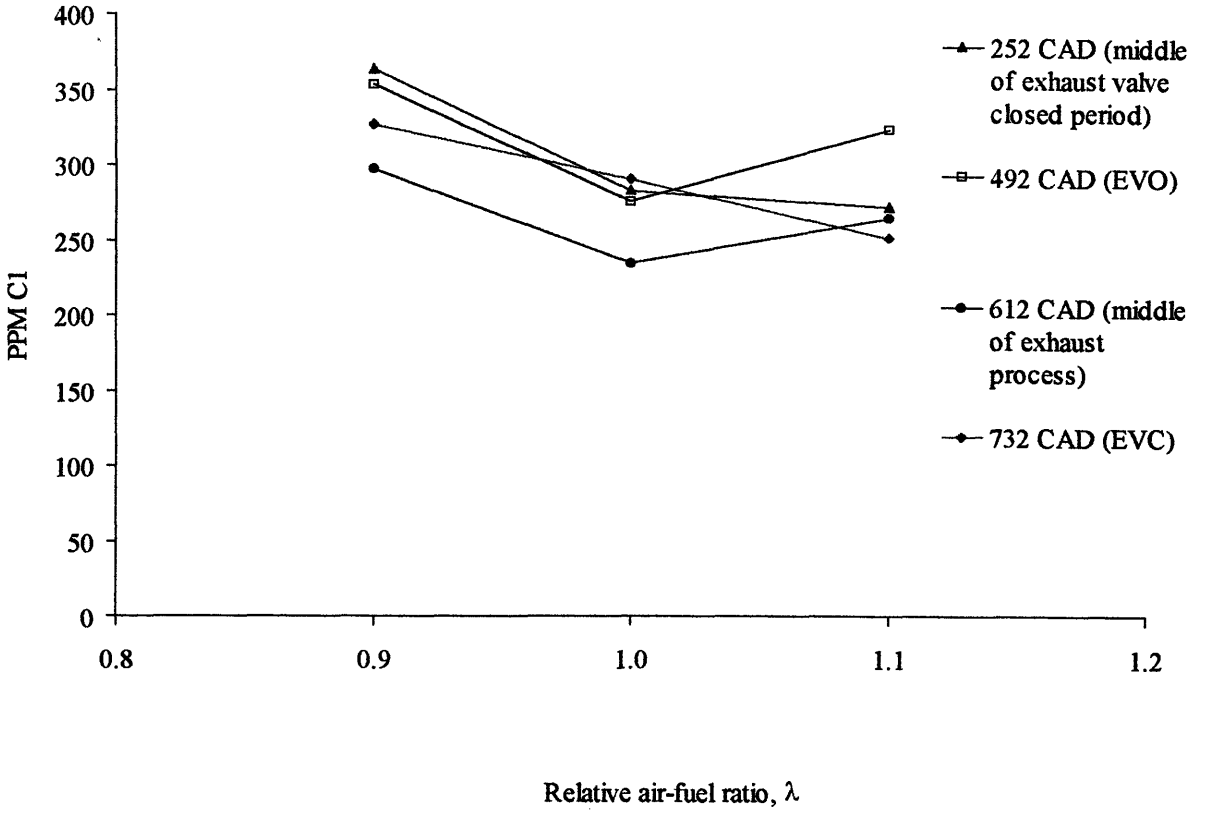

Figure 8.9 Ethene concentration versus relative air-fuel ratio (λ) at four crank angles as measured by the sampling unit. Conditions: 1500 rpm, relative air-fuel ratio λ = 0.90, 1.00, 1.10, load = 3.75 bar IMEP, sampling location B.

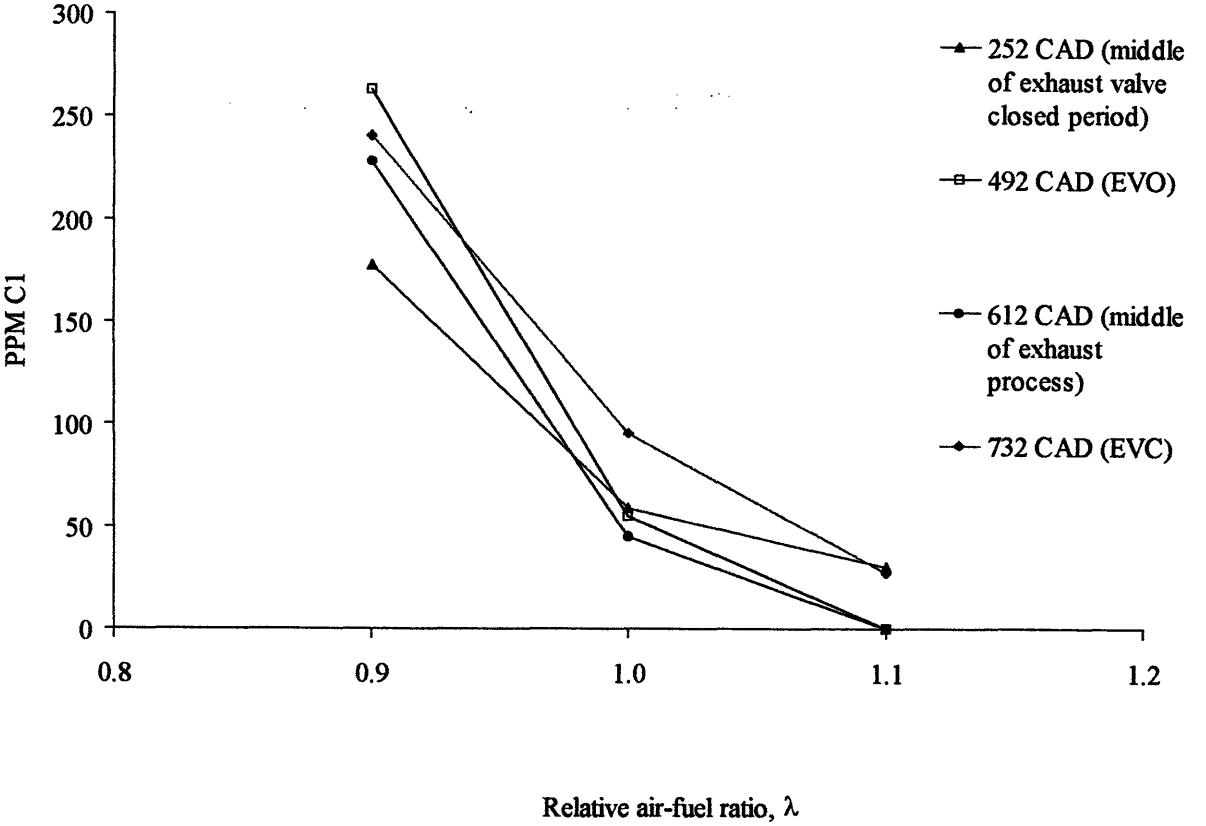

Figure 8.10 Ethyne concentration versus relative air-fuel ratio (λ) at four crank angles as measured by the sampling unit. Conditions: 1500 rpm, relative air-fuel ratio λ = 0.90, 1.00, 1.10, load = 3.75 bar IMEP, sampling location B.

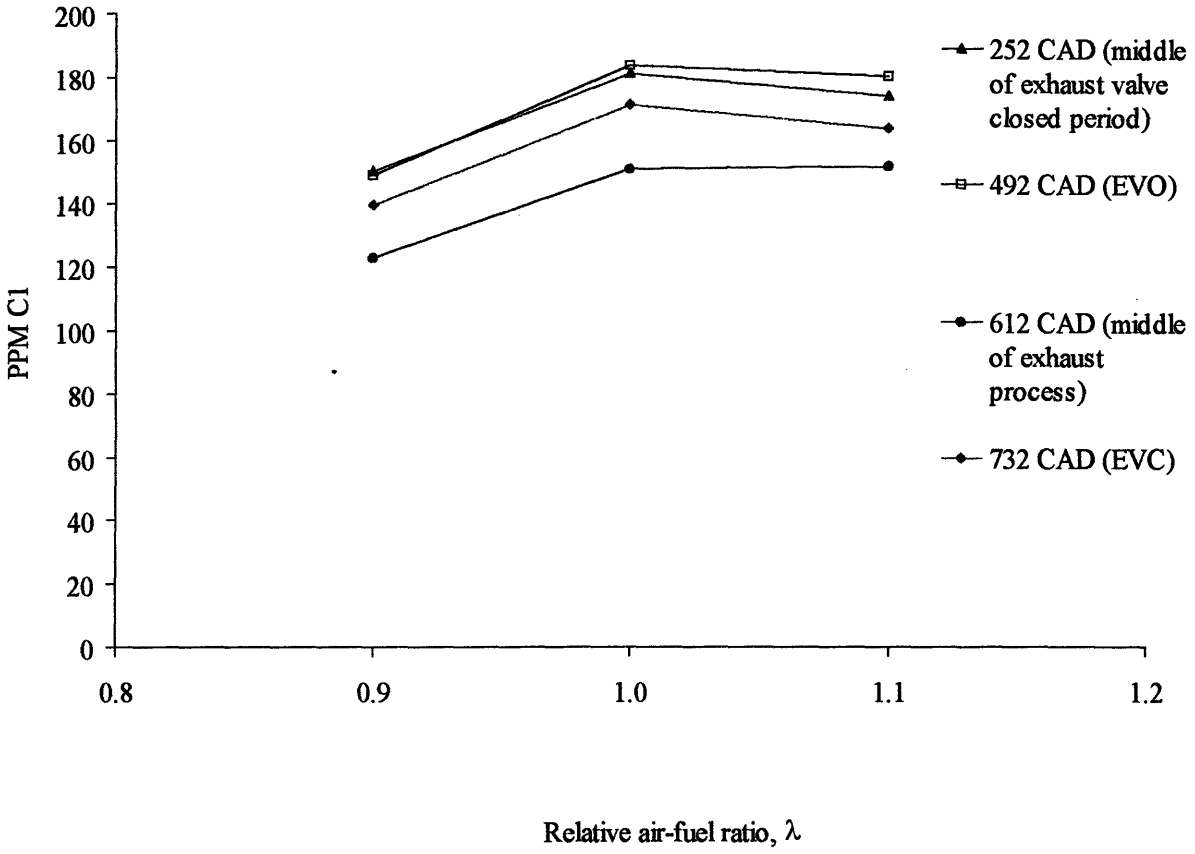

Figure 8.11 Propene concentration versus relative air-fuel ratio (λ) at four crank angles as measured by the sampling unit. Conditions: 1500 rpm, relative air-fuel ratio λ = 0.90, 1.00, 1.10, load = 3.75 bar IMEP, sampling location B.

CHAPTER 9

CONCLUSIONS

Prior to the work in this paper, questions abounded regarding the nature of HCs emerging from the cylinder. In the course of these experiments, a sampling unit combining the features of a FFID and wall mounted sampling valves was designed and built in order to enable crank angle resolved, spatially resolved, speciated measurements of engine-out HC concentrations. Results of the experiments show that:

1. The sampling unit has the space resolving capability of a FFID and the speciating capability of wall-mounted sampling valves. The unit's observed resolution is approximately 15°CA at 900 rpm.
2. Measurements made by the sampling unit over a period on the order of 1000 cycles compare well to cycle averaged measurements made by the FFID, the only difference being a multiplicative scaling factor error in the FFID measurements due to imprecise calibration.
3. Spatial resolution of the exhaust port by the sampling unit reveals no significant concentration gradients across the radius of the port, most likely due to strong mixing during the exhaust event. Significant mixing and oxidation occurs as the flow progresses along the length of the port. In particular, total HC concentrations decrease by 36% to 50% across the length of the port, while non-fuel HC concentrations decrease by 17% to 23%, therefore indicating significant amounts of partial oxidation.
4. CA resolved trends in the speciated data show that, as the exhaust process progresses and temperatures drop, the ratio of non-fuel HC mass to fuel HC mass in the exhaust increases.
5. Comparison of speciated results with propane, toluene, and isooctane shows that, although the ratio of non-fuel ppmC1 to fuel ppmC1 changes from fuel to fuel (from less than 10% for toluene, to approximately 20 to 30% for propane, to greater than 40% for isooctane), the crank angle resolved trends in non-fuel ppmC1 to fuel ppmC1 do not change significantly. Consequently, it is believed that the trends observed in HC concentrations versus engine operating conditions and port location from propane tests can be qualitatively generalized to the liquid fuels.

6. For propane, the major non-fuel HCs formed are ethene, propene, ethyne, methane, and ethane. For toluene, most of the non-fuel HCs is benzene, with trace amounts of methane, ethene, and ethane. For isooctane, the major non-fuel HCs formed are isobutene, propene, ethene, ethyne, methane, as well as various di- and trimethylpentanes.
7. When firing on propane, the total HC concentration decreases by 4.5% $\pm$ 0.3% per 100 rpm increase in engine speed (either on a crank angle averaged or a mass averaged basis). However, the non-fuel HC concentrations do not change significantly with changes in engine speed, indicating that at higher speeds the increased of non-fuel oxidation is countered by an increased of non-fuel formation through partial oxidation of fuel molecules.
8. When firing on propane, the increase in total HC concentration per bar IMEP increase in load is 2.9% $\pm$ 0.2% on a crank angle averaged basis and 8.0% $\pm$ 0.3% on a mass averaged basis. The decrease in non-fuel HC concentration per bar IMEP increase in load is 20% $\pm$ 3% on either a crank angle or a mass averaged basis.
9. When firing on propane, the total HC concentration (on either a crank angle averaged or mass averaged basis) decreases by roughly 20% to 22% when the relative air-fuel ratio (λ) is increased from 0.90 to 1.00 or from 1.00 to 1.10. As air-fuel ratio is increased, exhaust concentrations of propane, ethyne, and methane decrease, while concentrations of propene and ethene can stay constant or even increase.

REFERENCES

[1] Seinfeld, J. H., Atmospheric Chemistry and Physics of Air Pollution, John Wiley & Sons, New York, pp. 58, 61 (1986).

[2] McNeill, E., *Clean Air Act*, EESC Issue Paper (1992).

[3] Pelz, N., Dempster, N. M., Hundleby, G. E., Shore, P. R., "The Composition of Gasoline Engine Hydrocarbon Emissions - An Evaluation of Catalyst and Fuel Effects," *SAE Paper No. 902074* (1990).

[4] Owen, K., Coley, T., Automotive Fuels Reference Book, 2nd ed., Society of Automotive Engineers, Inc., Warrendale, PA, p. 648 (1995).

[5] Cheng, W. K., Hamrin, D., Heywood, J. B., Hochgreb, S., Min, K., Norris, M., "An Overview of Hydrocarbon Emissions Mechanisms in Spark-Ignition Engines," *SAE Paper No. 932708* (1993).

[6] Gatellier, B., Trapy, J., Herrier, D., Quelin, J. M., Galliot, F., "Hydrocarbon Emissions of SI Engines as Influenced by Fuel Absorption-Desorption in Oil Films," *SAE Paper No. 920095* (1992).

[7] Thompson, N. D., Wallace, J. S., "Effect of Engine Operating Variables and Piston and Ring Parameters on Crevice Hydrocarbon Emissions," *SAE Paper No. 940480* (1994).

[8] Drobot, K., "Hydrocarbon Oxidation in the Exhaust Port and Runner of a Spark Ignition Engine," MSME Thesis, Massachusetts Institute of Technology (1994).

[9] Caton, J. A., Heywood, J. B., "Models for Heat Transfer, Mixing and Hydrocarbon Oxidation in a Exhaust Port of a Spark-Ignited Engine," *SAE Paper No. 800290* (1980).

[10] Mendillo, J. V., Heywood, J. B., "Hydrocarbon Oxidation in the Exhaust Port of a Spark Ignition Engine," *SAE Paper No. 810019* (1981).

[11] Finlay, I. C., Boam, D. J., Bingham, J. F., Clark, T. A., "Fast Response FID Measurement of Unburned Hydrocarbons in the Exhaust Port of a Firing Gasoline Engine," *SAE Paper No. 902165* (1990).

[12] Min, K., "The Effects of Crevices on the Engine-Out Hydrocarbon Emissions in Spark Ignition Engines," Ph.D. Thesis, Massachusetts Institute of Technology (1994).

[13] Woods, W. A., Brown, P. G., Sogut, O. S., "A Comparison of Hydrocarbon Measurements With A Fast Response Flame Ionization Detector And A Rapid Acting Sampling Valve," IMechE Proceedings, Paper C448/023 (1992).

[14] Tabaczynski, R. J., Heywood, J. B., Keck, J. C., "Time-Resolved Measurements of Hydrocarbon Mass Flowrate in the Exhaust of a Spark-Ignition Engine," *SAE Paper No. 720112* (1972).

[15] Heywood, J. B., Internal Combustion Engine Fundamentals, McGraw Hill, Inc., New York, pp. 375, 579, 679-680 (1988).

[16] LoRusso, J. A., Lavoie, G. A., Kaiser, E. W., "An Electrohydraulic Gas Sampling Valve with Application to Hydrocarbon Emissions Studies," *SAE Paper No. 800045* (1980).

[17] Brown, P. G., Woods, W. A., "Measurements of Unburnt Hydrocarbons in a Spark Ignition Combustion Engine during the Warm-Up Period," *SAE Paper 922233* (1992).

[18] Drobot, K., "Hydrocarbon Oxidation in the Exhaust Port and Runner of a Spark Ignition Engine," M.S. Thesis, Massachusetts Institute of Technology (1994).

[19] Kaiser, E., Siegl, W. O., Trinker, F. H., Cotton, D. F., Cheng, W. K., Drobot, K., "Effect of Engine Operating Parameters on Hydrocarbon Oxidation in the Exhaust Port and Runner of a Spark Ignition Engine," *SAE Paper 950159* (1995).

[20] Namazian, M., Heywood, J. B., "Flow in the Piston-Cylinder-Ring Crevices of a Spark-Ignition Engine: Effect on Hydrocarbon Emissions, Efficiency and Power," *SAE Paper 820088* (1988).

[21] Kaiser, E. W., Siegl, W. O., Henig, Y. I., Anderson, R. W., Trinker, F. H., "Effect of Fuel Structure on Emissions from a Spark-Ignited Engine," *Environmental Science and Technology*, vol. 25, pp. 2005-2012 (1991).

[22] Ninomiya, J. S., Golovoy, A., "Effects of Air-Fuel Ratio on Composition of Hydrocarbon Exhaust from Isooctane, Diisobutylene, Toluene, and Toluene-n-Heptane Mixture," *SAE Paper 690504* (1969).

[23] Dempster, N. M., Shore, P. R., "An Investigation into the Production of Hydrocarbon Emissions from a Gasoline Engine Tested on Chemically Defined Fuels," *SAE Paper 900354* (1990).

[24] Kaiser, E. W., Siegl, W. O., Henig, Y. I., Anderson, R. W., Trinker, F. H., "Effect of Fuel Structure on Emissions from a Spark-Ignited Engine. 3. Olefinic Fuels," *Environmental Science and Technology*, vol. 27, pp. 1440-1447 (1993).

[25] Rhee, K. T., Myers, P. S., Uyehara, O. A., "Time- and Space- Resolved Species Determination in Diesel Combustion Using Continuous Flow Gas Sampling," *SAE Paper 780226* (1978).

[26] Jensen, T. E., Siegl, W. O., Richert, J. F. O., Loo, J. F., Prostak, A., Sigsby, J. E., Lipari, F., "Advanced Emission Speciation Methodologies for the Auto/Oil Air Quality Improvement Research Program - I. Hydrocarbons and Ethers," *SAE Paper No. 920320* (1992).

[27] Westbrook, C. K., Dryer, F. L., "Simplified Reaction Mechanisms for the Oxidation of Hydrocarbon Fuels in Flames," *Comb. Sci. and Tech.*, vol. 27, pp. 31-43 (1981).

[28] Cambustion Ltd., *Sample Tube Flow Analysis Package, Single Tube Version (SATFLAP1)*, version 1.23, Cambridge, U. K. (1994).

[29] Nisbet, J., calculations using CFD code FIRE from AVL, 1995.

[30] Cambustion Ltd., *Sample Tube Flow Analysis Package, CP System (SATFLAP3)*, version 1.19, Cambridge, U. K. (1994).

[31] Woschni, G., "Universally Applicable Equation for the Instantaneous Heat Transfer Coefficient in the Internal Combustion Engine," *SAE Paper 670931* (1967).

[32] Chun, K. M., Heywood, J. B., "Estimating Heat-Release and Mass-of-Mixture Burned from Spark-Ignition Engine Pressure Data," *Combustion Science and Technology*, vol. 54, pp. 133-144 (1987).

[33] Peckham, M., personal correspondance, 28 February 1996.

[34] LoRusso, J. A., Kaiser, E. W., Lavoie, G. A., "In-Cylinder Measurements of Wall Layer Hydrocarbons in a Spark Ignited Engine," *Combustion Science and Technology*, vol. 33, pp. 75-112 (1983).

APPENDIX 1

ESTIMATION OF CRANK ANGLE RESOLUTION

Optimum resolution corresponds to sampling gas that emerged from the cylinder during as small a crank angle interval as possible. As discussed in section 4.1.1, the crank angle that the sampling unit resolves is estimated by superimposing an assumed velocity field for gas within the sampling unit on an assumed sampled volume and estimating the range of crank angles to which gas in the volume corresponds. First, the size and shape of the assumed sampled volume will be discussed, followed by a discussion of two assumed gas velocity fields and the crank angle resolution computed using each field.

Sampled volume:

An experiment was performed in which the sampling unit's reservoir pressure was monitored before and after opening the solenoid valve for 0.6 milliseconds a fixed number of times. This pressure data, combined with the known volume of the reservoir and known gas temperature, gave the mass trapped by the valve. The result of the experiment was a number of data relating the mass sampled per valve opening to the initial pressure drop across the valve. A linear fit was applied to the data via a least squared-error technique; in the pressure range of interest, the mass sampled per 0.6 ms valve opening is:

$$m_{sampled} = 7.8\times10^{-8} kg \cdot \Delta p(bar) + 9.3\times10^{-8} kg \qquad \text{(A1.1)}$$

The pressure drop used for these calculations is 0.3 bar, the pressure drop at the beginning of the sampling process, since that is when the sampled volume is the largest so resolution is the worst. At the pressure drop of 0.3 bar, $m_{sampled}$ = 1.2 x 10^{-7} kg. This mass corresponds to 3.3 x 10^{-7} m^3 at the pressure and temperature in the vacuum chamber (~0.3 bar and ~300 K).

Based upon the sampled volume, one can decide what shape the sampled volume must take. Assuming essentially inviscid flow, the possibilities are, from geometric considerations, the following: a half torus (Fig. A1.1a), a hemisphere (Fig. A1.1b), or a distorted hemisphere (Fig. A1.1c). Given that the separation between the solenoid valve face and the opposite edge of the vacuum chamber is 1.9 mm, the

sampled volume must correspond to a distorted hemisphere. Then, assuming that the sizes a and b (Fig A1.1c) are about equal, those sizes are approximately 7 millimeters.

Velocity fields:

The velocity field from the transfer tube exit to the solenoid valve face inside the vacuum chamber is neither that of a line source located along the center line nor that of a point source located at the center of the transfer tube exit; however, the field has characteristics of both. Hence, approximation of the crank angle resolution will be made using both approximations to the velocity field, the assumption being that the real crank angle resolution will lie somewhere between those calculated using the two velocity fields.

Line source — One assumption regarding the velocity field in the vacuum chamber is that it resembles a line source. That is, the flow from the transfer tube spreads out in the vacuum chamber as if it were emanating from a line source located at the axis of symmetry (see figure A1.2). Then, at any radius r > 0,

$$v(r) = \frac{Q_{tt}}{2\pi \cdot r \cdot h} \tag{A1.2}$$

where Q_{tt} is the volume flowrate leaving the transfer tube (calculated from *SATFLAP1* [28], see Appendix 4) and h is the "height" of the line source, i.e., the distance from the transfer tube exit to the face of the solenoid valve. Because velocity in the transfer tube is much greater than the average velocity in the vacuum chamber, the time it takes a particle to pass from point 1 to point 2 (see Fig. A1.3) is negligible (~ 10^{-5} seconds) compared to the time it takes to pass from 3 to 4 (~ 10^{-3} seconds). Thus, for this velocity field, the time window resolved by the sampling unit is essentially the time it takes a particle to leave the center line and reach r = 7 mm (= b in figure A1.1c):

$$\Delta t = \int_0^{r=a} \frac{dr}{v(r)} = \int_0^{r=a} \frac{dr}{\frac{1}{r}\frac{Q_{tt}}{2\pi \cdot h}} = \frac{\pi \cdot a^2 \cdot h}{Q_{tt}}. \tag{A1.3}$$

And the crank angle resolution is:

$$\Delta CA = \Delta t \cdot \omega_{engine} = \frac{\pi \cdot a^2 \cdot h}{Q_{tt}} \cdot \frac{N}{60\,\text{sec}} \cdot \frac{360° CA}{1 rev} \tag{A1.4}$$

where ω_{engine} is the engine speed in crank angle degrees per second and N is the engine speed in rpm. The above formulae for the line source velocity field yield a crank angle resolution $\Delta CA = 30°$ at 900 rpm.

Point source — The other assumption regarding the velocity field in the vacuum chamber is that it resembles a point source emanating from the center of the transfer tube exit (see Fig. A1.4). Then, at any radius $r > r_{tt}$, the velocity is given by:

$$v(r) = \frac{Q_{tt}}{2\pi \cdot r^2}. \tag{A1.5}$$

Note that there is a singularity at the transfer tube exit, so only points outside the transfer tube exit (radius greater than r_{tt}) are considered.

For this velocity field, the time window resolved by the sampling unit is essentially the time it takes a particle to go from radius r_{tt} to r such that the particle reaches point * (see Fig. A1.5), again neglecting the time spent in the transfer tube.

At point *, the radius is:

$$r^* = \sqrt{b^2 + h^2} = 4.5 \text{ mm} \tag{A1.6}$$

where b and h were defined in figures A1.1 and A1.2 respectively.

Then the time resolution is:

$$\Delta t = \int_{r_{tt}}^{r=r^*} \frac{dr}{v(r)} = \int_{r_{tt}}^{r^*} \frac{dr}{\frac{1}{r^2}\frac{Q_{tt}}{2\pi}} = \frac{2\pi}{3Q_{tt}} \cdot \left(r^{*3} - r_{tt}^3\right). \tag{A1.7}$$

And the crank angle resolution is:

$$\Delta CA = \Delta t \cdot \omega_{engine} = \frac{2\pi}{3Q_{tt}} \cdot \left(r^{*3} - r_{tt}^3\right) \cdot \frac{N(rpm)}{60\,sec} \cdot \frac{360° CA}{1 rev}. \tag{A1.8}$$

The above formulae for the point source velocity field yield a crank angle resolution $\Delta CA = 18°$ at 900 rpm. In summary, the result of the estimate is that the crank angle resolution is somewhere between 18° and 30° crank angle at 900 rpm.

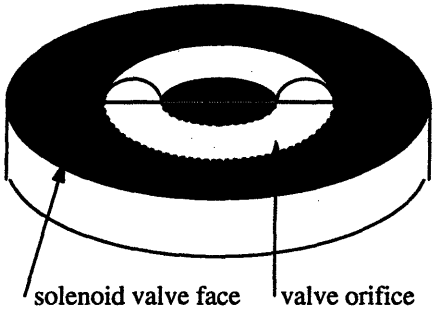

(a) Half torus if the radius of the sampled volume is less than that of valve orifice

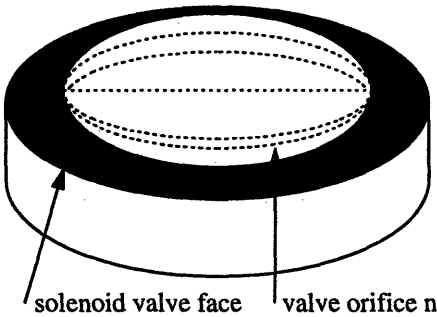

(b) Hemisphere if the radius of the sampled volume is greater than that of valve orifice

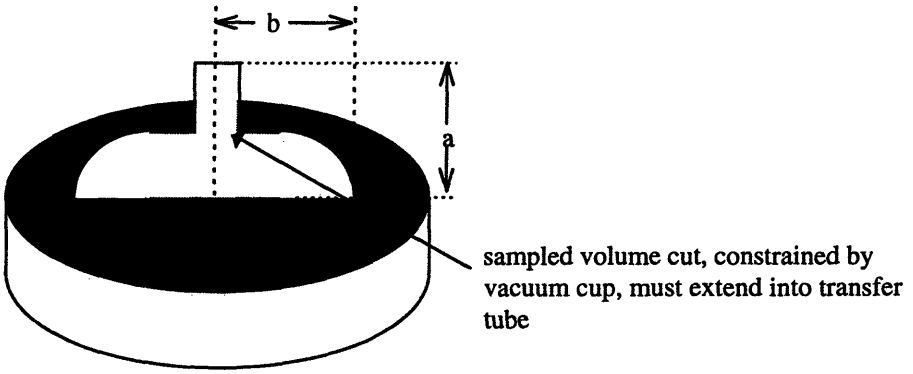

(c) Distorted hemisphere if sampled volume would be a hemisphere but has dimensions too great to fit into vacuum chamber

Figure A1.1 Potential shapes of sampled volumes and geometric constraints for each

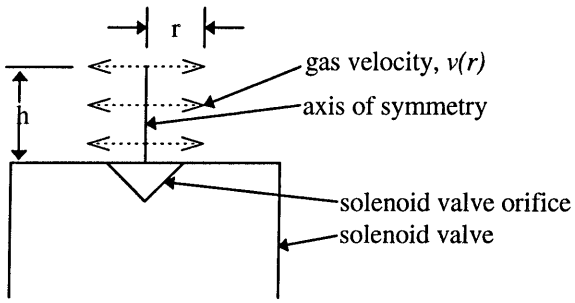

Figure A1.2 Schematic of line source velocity profile. Height of source, h, equals distance from transfer tube outlet to solenoid valve face.

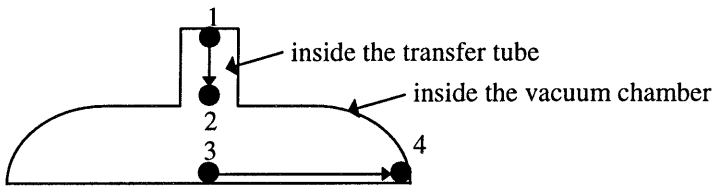

Figure A1.3 Sampled volume with points of reference. Point 1 is the furthest point within the transfer tube that is sampled by the solenoid valve. Point 2 is the outlet of the transfer tube. Point 3 is right next to the solenoid valve orifice, at r = 0. Point 4 is the furthest point within the vacuum chamber sampled by the solenoid valve, r = b.

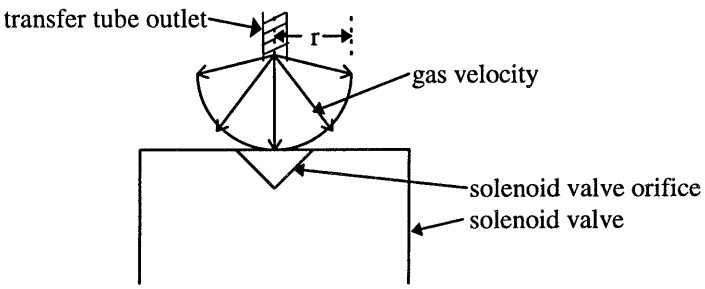

Fig. A1.4 Schematic of point source velocity profile.

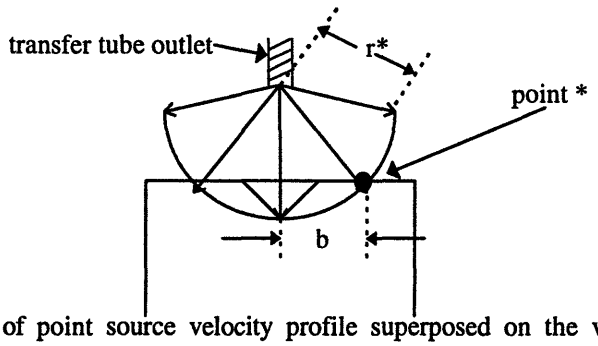

Fig. A1.5 Schematic of point source velocity profile superposed on the vacuum chamber geometry showing the definition of r*: the radius at which the bottom edge of the sampled volume extends a length "b" away from the valve orifice center, where "b" is defined in Fig. A1.1(c) above.

APPENDIX 2

ESTIMATION OF FRACTIONAL OXIDATION WITHIN TRANSFER TUBE

In order to approximate the fraction of each HC species oxidized within the transfer tube, the following steps are taken. For each species, the rate of oxidation (in moles/m^3s) is calculated using rate expressions tabulated by Westbrook and Dryer [27]. The rates considered are for the following transformation:

$$C_nH_m + (\tfrac{n}{2} + \tfrac{m}{4})O_2 \rightarrow nCO + \tfrac{m}{2} H_2O. \qquad \text{(A2.1)}$$

The temperature of gas within the transfer tube used for the rate calculations is estimated to be the temperature of a nearby thermocouple, approximately 900 K. (Note that the port gas temperatures calculated using FIRE are less than 900 K, but 900 K will be used as for the worst case estimate.) The calculated rates of oxidation are divided by the molar concentration and multiplied by the transit time through the transfer tube to give the fraction of the species oxidized in transit.

Tables A2.1 and A2.2, at the end of Appendix 2, are the conditions at which the reaction rates are estimated and the molar fractions of each species, respectively. The mole fractions of each species that are used in calculations are mole fractions representative of the those found via the sampling unit. Note that use of these mole fractions in the rate calculations assumes that the fraction reacted in the transfer tube is small; this assumption will be verified in this appendix.

The reaction rate in mole/m^3s is calculated from:

$$\text{Rate} = A \cdot exp\left(-E_a/RT\right) \cdot [C_nH_m]^a [O_2]^b = A \cdot exp\left(-E_a/RT\right) \cdot X_{C_nH_m}^a \cdot X_{O_2}^b \cdot \left(\frac{p}{R_{universal}T}\right)^{a+b} \qquad \text{(A2.2)}$$

where [s] is the concentration of species s in mole/ m^3 and X_s is the molar fraction of species s (unitless). Note $X_s = \dfrac{[s]}{(p/R_{universal}T)}$. The constants A, E_a, a, and b are tabulated by Westbrook and Dryer [27]. Then, the fraction oxidized is approximately $\dfrac{Rate \cdot transit\ time}{initial\ concentration}$. Using these formulae, the parameters in tables A2.1 and A2.2, and the constants tabulated by Westbrook and Dryer, the estimated reaction rates

and fractions oxidized can be calculated; the results are listed in table A2.3. As can be seen from table A2.3, the fraction of total HCs (weighted by mass) oxidized in the transfer tube is less than one percent. Note that, even if the gas temperature were 200°C hotter, the net fraction oxidized in the transfer tube would be only 2%.

Table A2.1 Conditions at which rates are estimated

Conditions:	
Temperature (estimated via a nearby thermocouple)	~900 K
Pressure (taken at inlet of transfer tube)	1 atm
Transit time (within transfer tube)	4 milliseconds

Table A2.2 Species mole fractions used in the estimation of reaction rates.

Species	Mole Fraction
Isooctane	0.00056
Toluene	0.00036
Propane	0.0011
Propene	0.0001
Ethene	0.0002
Methane	0.00002
Oxygen	0.018
Carbon Monoxide	~0

Table A2.3 Reaction rates and fractions of each species oxidized in transit.

Species	Rate of concentration decrease (mole/m^3s)	Fraction oxidized
Isooctane	2.0E-7	0.01%
Toluene	2.0E-7	0.02%
Propane	6.1E-7	0.02%
Propene	6.6E-7	0.2%
Ethene	1.2E-6	0.2%
Methane	8.5E-6	13%
Total (weighted)		0.1%

APPENDIX 3

ESTIMATION OF FRACTIONAL OXIDATION IN STORAGE UNIT AND VERIFICATION VIA EXPERIMENT

Theoretical estimation of fraction oxidation:

In the case of HCs oxidized in the storage unit, the long residence time is the culprit, not the high temperature. However, this appendix treats the estimation of fractional oxidation similar to that in the previous appendix: a rate expression from Westbrook and Dryer [27] is used to approximate the initial rate of oxidation, then the total fraction of each species oxidized is approximately the residence time multiplied by the initial rate of oxidation (in moles/m^{3}s) divided by the initial concentration. Note that using the initial rate of oxidation should overestimate actual oxidation. Further note that worst case values of parameter conditions (temperature and residence time) and species concentrations were chosen for use in the following calculations; that is, the combination of conditions chosen should produce the largest estimated amount of reaction. These conditions are listed in tables A3.1 and A3.2.

The reaction rate in mole/m^{3}s is calculated using the following formula:

$$\text{Rate} = A \cdot exp\left(-E_a/RT\right) \cdot [C_nH_m]^a [O_2]^b = A \cdot exp\left(-E_a/RT\right) \cdot X_{C_nH_m}^a \cdot X_{O_2}^b \cdot \left(\frac{p}{R_{universal}T}\right)^{a+b} \qquad \text{(A3.1)}$$

where symbols are defined in Appendix 2. The fraction oxidized is approximately $\frac{Rate \cdot residence\ time}{initial\ concentration}$. Reaction rates and fractions oxidized, estimated from the above formulae and parameters listed in tables A3.1 and A3.2, are listed in Table A3.3. As can be seen from table A3.3, the weighted fraction of total HCs estimated to oxidize during storage is far less than one percent.

Experimental verification of fraction oxidized:

A number of experiments were run to verify that little oxidation occurs while samples are in storage. In one experiment, a gas of known HC concentration was stored in a number of different storage loops and analyzed over a two day period. Samples were stored at room temperature (as per procedure for

analyzing gaseous samples, detailed in the Experimental Design section). Results show that approximately 5.6% of the total HCs oxidize per day, which is 1% per four and a half hours (the length of analysis for tests using propane fuel). Note that, over a period of two days, small leaks in the sampling loops may become significant and may result in decreased HC concentrations, so 1% is the upper bound on oxidation observed in this test. Another experiment was run in which samples of the engine's exhaust gas were taken in fifteen storage loops and analyzed over a four and a half hour period in order to see if measurable reaction occurred. All samples were taken during the same crank angle interval and with the engine at the same operating conditions, so sample compositions should all be the same, assuming no drift in engine operating conditions. The maximum observed decrease in total HC concentration is 9%. Figure A3.1 shows the results of this test; one may observe that the sample-to-sample variability (perhaps due to fluctuations in engine operating conditions) is on the same order of magnitude as the estimated amount of oxidation. Consequently, the measured 9% oxidation rate per four and a half hours incorporates the effect of sample-to-sample variability and, therefore, should be taken as an upper bound to the amount oxidized in storage during this test.

Table A3.1 Conditions at which rates are estimated (worst case scenario).

Conditions:	
Temperature (controlled by heating unit)	100 °C
Pressure (storage pressure equals pressure after dilution)	1 atm
Residence time (maximum time in storage unit)	14 hours

Table A3.2 Species mole fractions used in the estimation of reaction rates (worst case scenario).

Species	Mole Fraction (after dilution)
Isooctane	0.00026
Toluene	0.00007
Propane	0.00024
Propene	0.00002
Ethene	0.00004
Methane	0.000004
Oxygen	0.004
Carbon Monoxide	~0

Table A3.3 Reaction rates and fractions of each species oxidized in the storage unit.

Species	Rate of concentration decrease (mole/m^3s)	Fraction oxidized
Isooctane	2.8E-11	0.004%
Toluene	6.1E-11	0.03%
Propane	1.0E-10	0.01%
Propene	1.4E-10	0.02%
Ethene	2.6E-10	0.02%
Methane	5.6E-19	~0
Total (weighted)		0.01%

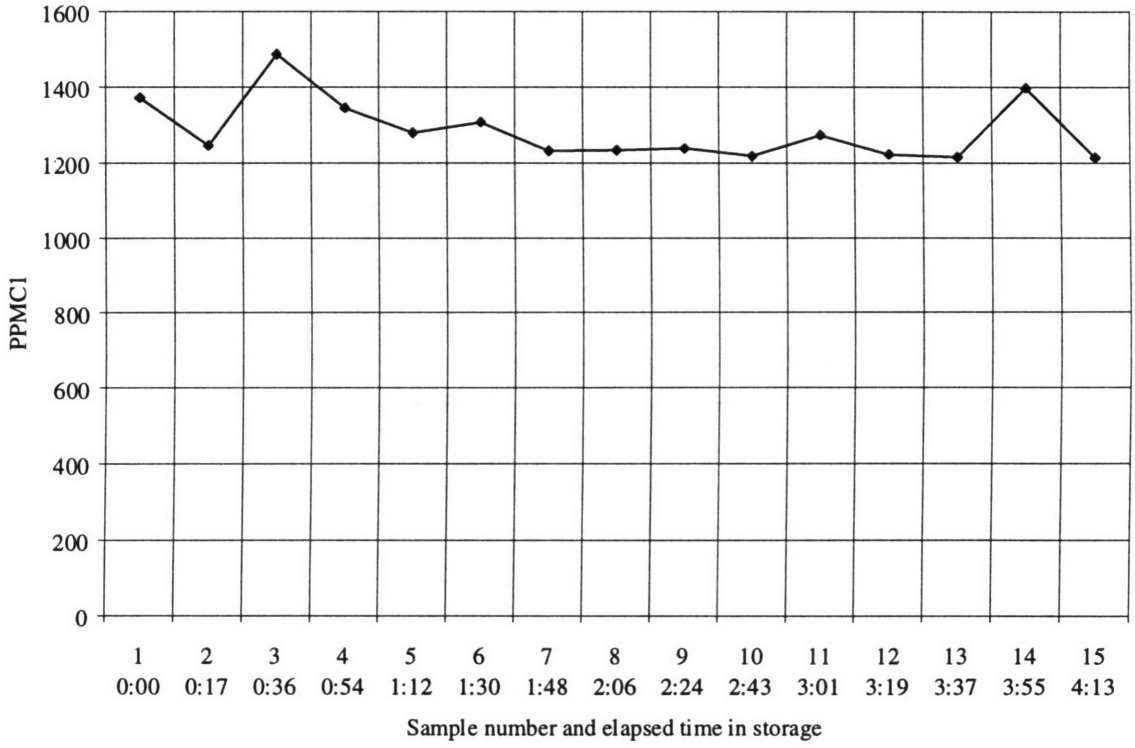

Figure A3.1 Total HC concentration of 15 samples taken from exhaust port of engine by the sampling unit, and the time elapsed (hours:minutes) between the start of GC analysis and the time when each particular sample enters the GC. Conditions: 1500 rpm, load = 3.6 bar IMEP, relative air-fuel ratio λ = 1.10. Sampling location B_{bottom}.

APPENDIX 4

CALCULATION OF TRANSIT TIME IN SAMPLING UNIT

Calculation of the transit time from the exhaust valve through the sampling unit, which was discussed briefly in section 5.2, will be discussed more fully in this appendix, followed by a discussion of the uncertainty in the transit time. The transit time consists of three parts, each of which will be discussed separately:

1. transit time from the cylinder exit (i.e., the exhaust valve plane) to the transfer tube inlet
2. transit time from the transfer tube inlet to the transfer tube outlet
3. transit time from the transfer tube outlet to the solenoid valve inlet (i.e., through the vacuum chamber).

The total transit time is the sum of the three individual times. The transit time is most useful when expressed in crank angle degrees, which equals transit time in seconds times engine speed in CAD per second, since both the input to the solenoid valve's control unit and the desired sampling time are expressed in crank angle degrees.

1. Transit time from the cylinder exit to the transfer tube inlet:

The transit time from the exhaust valve plane to the transfer tube inlet is taken to be the distance from the center of the exhaust valve plane to the transfer tube inlet divided by the estimated cycle averaged velocity of the exhaust gas. Dr. Jonny Nisbet at Volvo Corporation performed CFD calculations of the gas velocities in the exhaust port [29]; from these calculations, the cycle averaged velocity was estimated as roughly 13 m/s.

2. Transit time from the transfer tube inlet to the transfer tube outlet:

The transit time through the transfer tube is calculated using the program *SATFLAP1* from Cambustion [28]. Inputs to *SATFLAP1* are the listed in table A4.1. Note that *SATFLAP1* works for the section of the transfer tube from the port, through the three-way valve, and to the vacuum chamber

because the diameter is almost entirely uniform. On the other hand, *SATFLAP1* and *SATFLAP3* are not reliable for the section of the transfer tube from the port, through the three-way valve, and through the FFID transfer tube because each of those tubes has a significantly different diameter, while *SATFLAP1* and *SATFLAP3,* whose output is extremely sensitive to tube diameter, work only for uniform diameter tubing [30].

3. Transit time from the transfer tube outlet to the solenoid valve inlet:

The transit time from the transfer tube outlet to the solenoid valve inlet (i.e., the time for gas to travel through the vacuum chamber) is calculated using a conservation of mass on the control volume shown in Fig. A4.2. The assumption used in this calculation is that the flow spreads radially outward from the transfer tube outlet, as if from a point source of mass. In reality, this is probably not true, but errors incurred in this transit time contribute little to the total error because this transit time is about one-eighth of the other transit times.

Taking a control volume as shown in Fig. A4.2 and applying the conservation of mass, noting that the gas is at approximately constant pressure (thus constant density), gives the gas velocity at any radius r:

$$v_{in} \cdot \pi \cdot r_{tt}^2 = v_{out}(r) \cdot 2\pi \cdot r^2 . \qquad \text{(A4.1)}$$

Note that only radii larger than that of the transfer tube are considered in order to avoid a singularity at the transfer tube exit. Since $v_{out} = {}^{dr}/_{dt}$ for a gas particle, the transit time is:

$$\tau = \int_{r_{tt}}^{h} \frac{dr}{v_{out}(r)} \qquad \text{(A4.2)}$$

where h is the distance from the transfer tube outlet to the solenoid valve face (1.9 mm) and r_{tt} is the radius of the transfer tube.

Uncertainty in the transit time

Uncertainty in the calculated transit time comes from uncertainty in the calculation of the cycle averaged velocity from the cylinder exit to the transfer tube inlet and uncertainty in transit times through the transfer tube resulting from uncertainty in the inputs to *SATFLAP1*. Calculations using extreme values of cycle averaged port velocities show that the velocity can affect the transit time by about 2%. The greatest uncertainty in the inputs to *SATFLAP1* is the transfer tube's inlet pressure because fluctuations in port pressure alter the transfer tube inlet pressure. Highly sensitive measurements of the port pressure show that port pressure fluctuates less than 0.1 bar. Use of the extreme port pressures results in transit times that differ by at most 8%. Consequently, the total uncertainty in transit times through the sampling unit is on the order of 8%.

Table A4.1 Inputs to *SATFLAP1*

Input name	Input value	Note
Tube diameter	22.5 thousandths of an inch	equals diameter of tubing, not diameter of three-way valve, since transfer tube is almost entirely composed of the 22.5 thousandths of an inch tubing
Tube length	varies for each sampling location	length of in-port section of tube ① plus lengths ② and ③inside three-way valve plus length of tube connecting three-way valve to vacuum chamber ④ (see Fig A4.1 for numbers)
Tube temperature	375°C	average of transfer tube outlet temperature (room temperature) and transfer tube inlet (assumed equal to temperature of thermocouple placed nearby in exhaust flow)
Sample pressure	1 bar, absolute	corresponds to transfer tube inlet pressure
FID pressure	0.3 bar, absolute	corresponds to vacuum chamber or transfer tube outlet pressure
Atm pressure	1.01 bar, absolute	

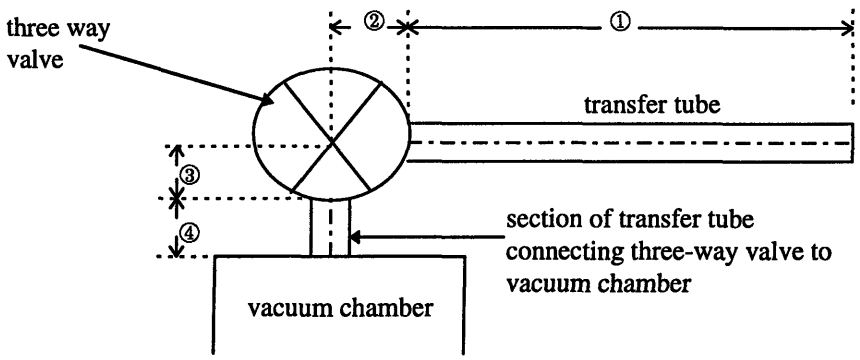

Figure A4.1 Lengths of tubing used for *SATFLAP1* input.

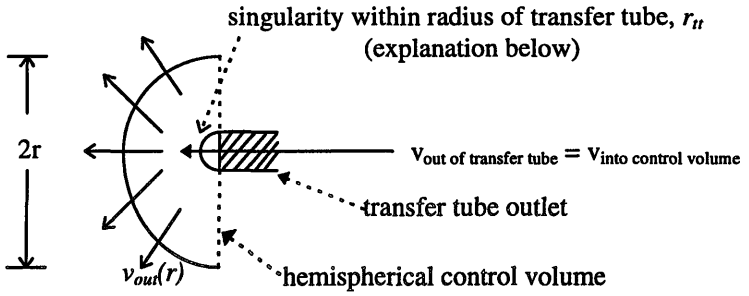

Figure A4.2 Control volume used in calculation of transit time through vacuum chamber.

APPENDIX 5

CONCENTRATION DATA FOR SELECTED EXPERIMENTS

Fuel: Propane
Engine Speed: 900 rpm
Engine Load: 2.2 bar IMEP
Relative air-fuel ratio, λ: 1.10
Sampling location: B

Crank Angle Degree after intake TDC	Methane (ppmC1)	Ethene (ppmC1)	Ethyne (ppmC1)	Ethane (ppmC1)	Propene (ppmC1)	Propane (ppmC1)	Total HCs (ppmC1)	Total Nonfuel (ppmC1)
177	0	295	31	0	207	1689	2222	533
327	0	295	33	0	197	1590	2115	525
477	0	214	0	0	178	1427	1819	392
492	0	306	33	0	207	1630	2177	546
522	0	156	0	0	128	921	1205	285
552	0	237	0	0	182	1272	1691	419
582	0	217	0	0	161	1172	1550	378
612	0	267	81	0	172	1245	1765	520
642	0	209	0	0	165	1146	1521	375
672	0	289	29	0	188	1361	1867	506
702	0	311	72	0	202	1618	2203	586
732	0	321	86	0	205	1675	2286	611
747	0	235	0	0	188	1569	1991	422

Fuel: Propane
Engine Speed: 900 rpm
Engine Load: 2.1 bar IMEP
Relative air-fuel ratio, λ: 1.10
Sampling location: B

Crank Angle Degree after intake TDC	Methane (ppmC1)	Ethene (ppmC1)	Ethane (ppmC1)	Propene (ppmC1)	Propane (ppmC1)	Total HCs (ppmC1)	Total Nonfuel (ppmC1)
177	81	409	0	39	1810	2338	528
327	62	351	0	63	1702	2177	475
477	94	282	0	45	1610	2031	422
492	44	366	0	77	1747	2235	487
522	60	294	0	21	1421	1796	375
552	47	315	0	126	1338	1826	488
582	51	295	0	79	1279	1704	425
612	55	299	0	18	1067	1439	372
642	47	325	0	13	1138	1522	384
672	54	316	0	69	1270	1709	439
702	58	354	0	57	1686	2155	469
732	60	390	0	80	1975	2506	531
747	65	345	0	104	1700	2214	514

(No ethyne measured in this test.)

Fuel: Propane
Engine Speed: 1500 rpm
Engine Load: 2.1 bar IMEP
Relative air-fuel ratio, λ: 1.10
Sampling location: B

Crank Angle Degree after intake TDC	Methane (ppmC1)	Ethene (ppmC1)	Ethane (ppmC1)	Propene (ppmC1)	Propane (ppmC1)	Total HCs (ppmC1)	Total Nonfuel (ppmC1)
177	57	356	0	52	1237	1702	465
327	125	370	0	33	1279	1807	528
492	72	362	0	11	1084	1528	445
522	43	344	0	42	1069	1498	430
552	0	353	0	45	943	1341	398
582	41	271	0	43	794	1148	354
612	64	330	0	82	811	1287	476
642	60	331	0	16	726	1132	407
672	46	334	0	11	821	1210	390
702	56	356	0	56	1091	1559	468
747	49	353	0	75	1276	1753	477

Fuel: Propane
Engine Speed: 1500 rpm
Engine Load: 3.75 bar IMEP
Relative air-fuel ratio, λ: 1.10
Sampling location: B

Crank Angle Degree after intake TDC	Methane (ppmC1)	Ethene (ppmC1)	Ethane (ppmC1)	Propene (ppmC1)	Propane (ppmC1)	Total HCs (ppmC1)	Total Nonfuel (ppmC1)
177	44	279	0	70	1601	1994	394
477	40	284	0	123	1764	2211	446
492	44	273	0	52	1672	2041	369
522	0	263	0	13	1433	1708	275
552	0	225	0	4	1027	1256	229
582	0	186	0	23	918	1126	209
612	48	215	0	30	825	1119	294
642	41	213	0	17	908	1179	271
672	37	242	0	92	929	1299	370
702	119	253	0	46	1195	1613	418
732	51	284	0	6	1494	1835	341
747	40	273	0	26	1436	1776	340

(No ethyne measured in these tests.)

Fuel: Propane
Engine Speed: 900 rpm
Engine Load: 3.75 bar IMEP
Relative air-fuel ratio, λ: 1.10
Sampling location: B

Crank Angle Degree after intake TDC	Methane (ppmC1)	Ethene (ppmC1)	Ethane (ppmC1)	Propene (ppmC1)	Propane (ppmC1)	Total HCs (ppmC1)	Total Nonfuel (ppmC1)
177	0	291	0	15	2155	2461	306
327	34	266	0	124	2109	2533	424
477	41	276	0	25	2109	2451	342
492	0	281	0	11	2177	2468	291
522	0	216	0	28	1595	1840	244
552	0	196	0	17	1211	1423	212
582	46	195	0	24	1187	1451	264
612	41	215	0	39	1142	1437	295
642	30	284	0	95	1394	1802	408
672	43	279	0	65	1608	1994	386
702	38	294	0	9	1878	2220	342
732	40	294	0	28	2120	2482	362
747	0	286	0	39	2185	2509	325

Fuel: Propane
Engine Speed: 900 rpm
Engine Load: 3.75 bar IMEP
Relative air-fuel ratio, λ: 1.10
Sampling location: A

Crank Angle Degree after intake TDC	Methane (ppmC1)	Ethene (ppmC1)	Ethane (ppmC1)	Propene (ppmC1)	Propane (ppmC1)	Total HCs (ppmC1)	Total Nonfuel (ppmC1)
177	0	449	108	247	3015	3818	803
327	0	463	119	275	3240	4098	857
477	38	481	98	265	3102	3985	883
492	115	481	120	163	3069	3948	879
522	0	348	101	175	2193	2819	625
552	76	297	93	190	2090	2746	656
582	0	331	0	152	1548	2031	483
612	53	305	69	149	1743	2319	576
642	28	254	0	193	1500	1974	475
672	123	323	75	260	1517	2298	781
702	0	359	94	201	2048	2703	655
732	78	446	94	196	2440	3254	814
747	75	436	90	201	2594	3396	802

(No ethyne measured in these tests.)

Fuel: Propane
Engine Speed: 900 rpm
Engine Load: 3.75 bar IMEP
Relative air-fuel ratio, λ: 1.10
Sampling location: C

Crank Angle Degree after intake TDC	Methane (ppmC1)	Ethene (ppmC1)	Ethane (ppmC1)	Propene (ppmC1)	Propane (ppmC1)	Total HCs (ppmC1)	Total Nonfuel (ppmC1)
177	55	342	68	147	1288	1901	613
327	42	409	0	140	1107	1697	590
477	48	387	0	140	1472	2047	575
492	0	310	55	126	1622	2112	490
522	0	346	129	0	1171	1646	475
552	0	230	0	124	1335	1689	354
582	30	221	0	0	740	991	251
612	36	399	0	126	1065	1626	561
642	0	262	0	146	1051	1460	409
672	47	400	0	155	1237	1840	603
702	29	322	57	141	1501	2051	550
732	3	344	49	155	1523	2075	552
747	28	332	92	146	1564	2162	597

(No ethyne measured in this test.)

Fuel: Propane
Engine Speed: 1500 rpm
Engine Load: 3.75 bar IMEP
Relative air-fuel ratio, λ: 1.10
Sampling location: C

Crank Angle Degree after intake TDC	Methane (ppmC1)	Ethene (ppmC1)	Ethyne (ppmC1)	Ethane (ppmC1)	Propene (ppmC1)	Propane (ppmC1)	Total HCs (ppmC1)	Total Nonfuel (ppmC1)
327	0	298	44	64	202	592	1156	564
477	70	350	55	58	216	956	1651	695
492	61	311	60	51	208	928	1559	631
522	0	320	58	71	214	798	1404	606
552	57	333	64	53	266	583	1292	710
582	55	310	64	60	181	540	1145	605
612	115	312	62	76	193	590	1285	695
642	32	298	52	36	182	466	1014	549
672	60	311	47	0	202	643	1216	573
702	92	306	49	56	187	764	1405	640
732	100	356	56	54	250	1014	1774	760
747	50	296	51	42	187	727	1302	575

Fuel: Propane
Engine Speed: 1500 rpm
Engine Load: 3.75 bar IMEP
Relative air-fuel ratio, λ: 1.10
Sampling location: A

Crank Angle Degree after intake TDC	Methane (ppmC1)	Ethene (ppmC1)	Ethyne (ppmC1)	Ethane (ppmC1)	Propene (ppmC1)	Propane (ppmC1)	Total HCs (ppmC1)	Total Nonfuel (ppmC1)
177	49	373	64	82	395	2158	3057	899
327	73	491	85	107	325	3067	4062	996
462	54	460	0	71	228	2072	2885	814
492	56	390	72	62	250	2185	2943	758
522	63	363	74	89	229	1898	2642	744
552	175	402	0	73	223	1907	2779	872
582	57	308	91	0	182	1435	1981	547
612	52	327	62	72	215	1597	2263	666
642	79	353	55	72	236	1930	2671	740
672	56	325	56	57	235	1637	2309	672
702	82	325	58	62	261	1643	2372	729
732	84	357	79	85	253	1919	2697	778

Fuel: Propane
Engine Speed: 1500 rpm
Engine Load: 3.75 bar IMEP
Relative air-fuel ratio, λ: 1.10
Sampling location: Binter

Crank Angle Degree after intake TDC	Methane (ppmC1)	Ethene (ppmC1)	Ethyne (ppmC1)	Ethane (ppmC1)	Propene (ppmC1)	Propane (ppmC1)	Total HCs (ppmC1)	Total Nonfuel (ppmC1)
177	58	307	55	62	213	1343	1983	640
327	53	386	56	86	254	1734	2513	779
467	65	326	53	48	279	1332	2049	717
492	61	338	57	62	340	1415	2216	801
522	63	345	55	71	222	1418	2120	702
552	0	339	55	67	225	1243	1875	632
582	0	315	50	30	235	1039	1619	580
612	56	322	63	55	218	1138	1790	652
642	66	264	48	36	188	935	1488	554
672	66	295	58	61	187	920	1530	609
702	68	316	57	57	186	983	1610	627
732	139	291	51	49	300	1003	1783	779

Fuel: Propane
Engine Speed: 1500 rpm
Engine Load: 3.75 bar IMEP
Relative air-fuel ratio, λ: 1.10
Sampling location: B_{top}

Crank Angle Degree after intake TDC	Methane (ppmC1)	Ethene (ppmC1)	Ethyne (ppmC1)	Ethane (ppmC1)	Propene (ppmC1)	Propane (ppmC1)	Total HCs (ppmC1)	Total Nonfuel (ppmC1)
327	45	380	0	48	194	1331	1999	667
467	79	371	58	56	219	1448	2172	724
492	57	328	47	41	194	1315	1936	620
522	37	343	49	43	233	1549	2206	657
552	46	312	44	44	212	1217	1832	615
582	36	278	40	35	170	1050	1570	520
612	104	298	99	39	160	987	1588	601
642	95	306	48	40	183	999	1623	624
672	47	281	42	36	165	864	1393	529
702	40	279	44	32	175	888	1415	526
732	49	329	55	40	189	1149	1755	606
747	45	369	0	45	197	1281	1937	656

Fuel: Propane
Engine Speed: 1500 rpm
Engine Load: 3.75 bar IMEP
Relative air-fuel ratio, λ: 1.10
Sampling location: B_{bottom}

Crank Angle Degree after intake TDC	Methane (ppmC1)	Ethene (ppmC1)	Ethyne (ppmC1)	Ethane (ppmC1)	Propene (ppmC1)	Propane (ppmC1)	Total HCs (ppmC1)	Total Nonfuel (ppmC1)
252	0	377	55	45	245	1421	2087	667
467	74	390	62	55	243	1342	2104	763
492	67	385	62	59	229	1403	2143	740
522	67	386	59	54	241	1483	2231	748
552	51	352	55	47	224	1224	1898	674
582	50	349	59	47	206	1016	1668	651
612	40	352	59	49	212	1008	1661	653
642	67	372	53	68	247	1187	1940	754
702	73	394	57	50	280	1346	2143	797
732	61	408	123	0	234	1380	2084	703
757	52	392	56	48	263	1526	2282	755

Fuel: Toluene
Engine Speed: 1500 rpm
Engine Load: 3.75 bar IMEP
Relative air-fuel ratio, λ: 1.10
Sampling location: B

Crank Angle Degree after intake TDC	Benzene (ppmC1)	Toluene (ppmC1)	Total HCs (ppmC1)
177	44	2775	2819
327	39	2526	2564
477	42	2770	2812
492	46	2832	2878
522	35	2298	2333
552	42	2362	2403
582	36	2182	2218
612	40	2231	2270
642	41	2353	2394
672	43	2435	2478
702	37	2458	2495
732	47	2673	2719
747	43	2703	2747

Fuel: Isooctane
Engine Speed: 1500 rpm
Engine Load: 3.75 bar IMEP
Relative air-fuel ratio, λ: 1.10
Sampling location: B

Crank Angle Degree after intake TDC	Methane (ppmC1)	Ethene (ppmC1)	Ethyne (ppmC1)	Ethane (ppmC1)	Propene (ppmC1)	Propadiene (ppmC1)	Isobutene (ppmC1)
177	33	73	45	21	195	19	534
477	34	76	44	21	204	22	590
492	33	73	43	19	197	20	563
522	34	74	44	21	201	21	570
552	32	74	47	20	196	0	518
582	34	75	45	20	200	20	538
612	33	76	47	20	199	0	524
642	32	73	45	19	193	19	535
672	33	75	43	20	202	22	567
702	32	73	46	19	193	0	532
732	33	74	43	20	199	20	551
747	34	76	47	21	204	19	569

Crank Angle Degree after intake TDC	2M-1-Butene (ppmC1)	4M-1-Pentene (ppmC1)	2M-2-Pentene (ppmC1)	2,2-DM-Pentane (ppmC1)	3,3-DM-Pentane (ppmC1)	Isooctane (ppmC1)
177	16	17	17	45	44	2547
477	17	30	18	47	50	3156
492	17	28	18	46	48	3169
522	17	30	17	45	50	2783
552	13	0	17	46	42	2485
582	0	0	17	47	36	3196
612	13	17	0	46	40	2396
642	16	27	16	43	46	2264
672	17	32	17	44	51	2368
702	16	19	17	45	44	2273
732	15	0	17	47	46	2727
747	17	23	17	46	46	2707

Crank Angle Degree after intake TDC	2,3,4-TM-Pentane (ppmC1)	Toluene (ppmC1)	Octene (ppmC1)	M-Octane (ppmC1)	3,5-DM-Heptane (ppmC1)	Total HCs (ppmC1)	Total Nonfuel (ppmC1)
177	60	286	579	0	0	4623	2075
477	0	275	26	0	36	4688	1532
492	50	252	183	0	0	4869	1700
522	99	226	23	186	0	4478	1696
552	106	394	357	0	0	4384	1899
582	160	270	23	0	0	4707	1510
612	105	389	308	0	0	4247	1850
642	138	297	489	0	0	4292	2028
672	61	217	19	0	0	3927	1560
702	92	348	296	0	0	4085	1812
732	189	249	24	0	0	4337	1610
747	105	281	24	0	0	4276	1569

7637-35